Electronic Supplementary Material (ESI) for Journal of Materials Chemistry C.

Supporting Information For:

A Superhydrophobic MOF Facilitating Efficient Solvent-Free Catalytic Chemical Fixation of CO_2 and Oxidation of Hydrocarbons and MOF@Cotton@Starch Composite Based Selective Sensing of an Herbicide

Subhrajyoti Ghosh,[a†] *Srijan Mukherjee,*[a†] *Veerappan Karthik,*[b] *Priti Bera,*[a] *Amarajothi Dhakshinamoorthy,**[bc] *and Shyam Biswas**[a]

[a] Department of Chemistry, Indian Institute of Technology Guwahati, 781039 Assam, India

[b] School of Chemistry, Madurai Kamaraj University, Madurai, Tamil Nadu, 625021, India.

[c] Departamento de Química, Universitat Politècnica de València, Camino de Vera s/n, Valencia 46022, Spain

[†] Equal Contribution

*Corresponding author. Tel: 91-3612583309, Fax: 91-3612582349

E-mail address: sbiswas@iitg.ac.in, admguru@gmail.com

Materials and Characterization Methods:

All the reagents, starting materials and solvents were procured from commercial sources and used without purification, except the 2-(perfluorobenzamido)terephthalic acid linker. The linker was synthesized according to the below mentioned procedure (Scheme S1) and its purity was verified by the ATR-IR, ^{1}H NMR, ^{19}F NMR,^{13}C NMR and mass spectrometric analysis (Figures S1-S4). The notations used for characterization of the bands are broad (br), strong (s), very strong (vs), medium (m), weak (w) and shoulder (sh). PXRD patterns were collected by using Rigaku Smartlab X-ray diffractometer with Cu-*K*α radiation (l = 1.54056 Å), 40 kV of operating voltage and 125 mA of operating current. The Attenuated Total Reflectance Infrared (ATR-IR) spectra were recorded using PerkinElmer UATR Two at ambient condition in the region 500-4000 cm^{-1}. Thermogravimetric analysis (TGA) was carried out with a PerkinElmer TGA 4000 thermogravimetric analyser in the temperature range of 30-700 °C in an O_2 atmosphere at the rate of 4 °C min^{-1}. N_2 sorption isotherms were recorded by using Quantachrome Autosorb iQ-MP volumetric gas adsorption equipment at -196 °C. Before the sorption analysis, the degassing of the compound was carried out at 100 °C under a high vacuum for 24 h. FE-SEM images were captured with a Zeiss (Zemini) scanning electron microscope. A Bruker Avance III 400 NMR spectrometer was used for recording ^{1}H NMR and ^{19}F NMR spectra at 400 MHz. Fluorescence lifetimes were measured using Picosecond Time-resolved and Steady State Luminescence Spectrometer on an Edinburg Instruments Lifespec II & FSP 920 instrument. Fluorescence sensing studies were performed with a HORIBA JOBIN YVON Fluoromax-4 spectrofluorometer. Pawley refinement was carried out using Materials Studio software. The DICVOL program incorporated within STOE's WinXPow software package was used to determine the lattice parameters.

Synthesis Procedure of the 2-(Perfluorobenzamido)Terephthalic Acid Linker:

For the synthesis of the 2-(perfluorobenzamido)terephthalic acid linker, in a two-neck round bottom flux (containing 15 mL of dry THF), 182 mg (1 mmol) of 2-aminoterephthalic acid was added and it was dissolved by sonication. Thereafter, 255 µL (1.1 mmol) of 2,3,4,5,6-pentafluorobenzoyl chloride was dropwise added to the aforementioned mixture under stirring conditions at room temperature. After the injection of 255 µL of 2,3,4,5,6-pentafluorobenzoyl chloride, the mixture was stirred for 2 h at room temperature under N_2 atmosphere (Scheme S1). After 2 h, a white colour precipitate appeared. Then, the solvent was evaporated and the obtained white colour product was dried for 12 h in an 80 °C oven. Yield: 360 mg (0.93 mmol, 96%). ^{1}H NMR (500 MHz, DMSO-d_6): δ = 11.73 (s, 1H), 8.98 (s, 1H), 8.10 (d, 1H), 7.80 (d, 1H) ppm. ^{13}C NMR (125 MHz, DMSO-d_6): δ = 169.53, 168.93, 166.73, 156.55, 151.63, 145.24, 145.18, 145.12, 143.59, 143.53, 143.47, 141.87, 141.77, 140.23, 140.13, 139.30, 139.21, 135.78, 131.85, 125.19, 122.15, 118.03, 115.98, 113.01, 110.04, 109.92, 109.08 ppm. ^{19}F NMR -141.57, -151.32, -160.95. MALDI-TOF (m/z): 398.196 for $(M+Na)^{+}$ ion (M = mass of 2-(perfluorobenzamido)terephthalic acid linker). In Figures S1-S4, the NMR and mass spectra of the 2-(perfluorobenzamido)terephthalic acid linker are shown.

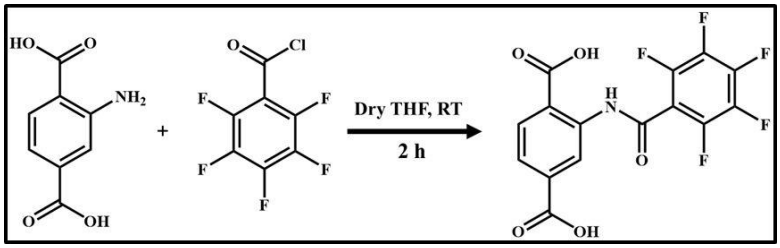

Scheme S1. Reaction scheme for the preparation of 2-(perfluorobenzamido)terephthalic acid linker.

Experimental Procedure for Catalytic Cycloaddition of CO_2:

In a typical catalytic cycloaddition procedure, **1′** or UiO-66-NH_2 or UiO-66 or H_2L or $ZrCl_4$ (10 mg) was taken as a catalyst in a round-bottom flask and epoxides (20 mmol) and TBAB (0.1 – 4 mol%) were added. This heterogeneous slurry was purged three times with CO_2 and finally a CO_2 balloon was connected. This reaction set up was heated at 80 °C for 24 h. Progress of the reaction was monitored by measuring ^{1}H NMR spectrum of the reaction mixture after separation of the catalyst.

Experimental Procedure for Catalytic Oxidation of Hydrocarbons:

In a typical experiment, **1′** or UiO-66-NH_2 (10 mg) was taken in a pressure tube. To this tube, hydrocarbon (1 mmol), TBHP (15 µL) and acetonitrile (2.5 mL) were added. To this heterogeneous slurry, O_2 gas was purged through balloon. This reaction set up was kept at 60 °C for 24 h. The reaction was monitored by analysing the reaction mixture periodically. Agilent 5977B GC-MS was used to characterize the oxidation products and reaction mixture. Internal standard method was used to determine the conversion of a substrate. A similar procedure was used to perform reusability tests.

Preparation of MOF (1′) Suspension for the Fluorescence Sensing Experiments:

The probe **1′** (4 mg) was taken in a 5 mL glass vial containing 4 mL of methanol. Then, the suspension was sonicated for 15 min and kept it for overnight to make the suspension stable. During the fluorescence experiment, 200 µL of above-mentioned suspension of **1′** was added to 3000 µL of mixture of methanol and deionized water (volume ration of water and methanol is 1:2) in a quartz cuvette. All the fluorescence spectra were collected in the range of 370-600 nm by exciting the suspension at 350 nm. For competitive experiments, the solutions of the different competitive analytes (concentration = 10 mM) were added to the suspension of **1′** and spectra were collected in the same range.

Fabrication of MOF@Starch@Cotton Composite:

To fabricate the composite, initially, 300 mg of starch was heated under stirring condition in 10 mL of water at 140 °C until the solution become clear. After preparing this homogeneous

starch solution, 200 mg of solid MOF was added to it and sonicated for 30 min to disperse the MOF particles homogeneously in the polymeric solution. After that, ten pieces (1 ×1 cm^2) of cotton fabric were dipped into that suspension and then it was dried in 120 °C oven. This process was repeated three times to coat the polymeric solution uniformly.

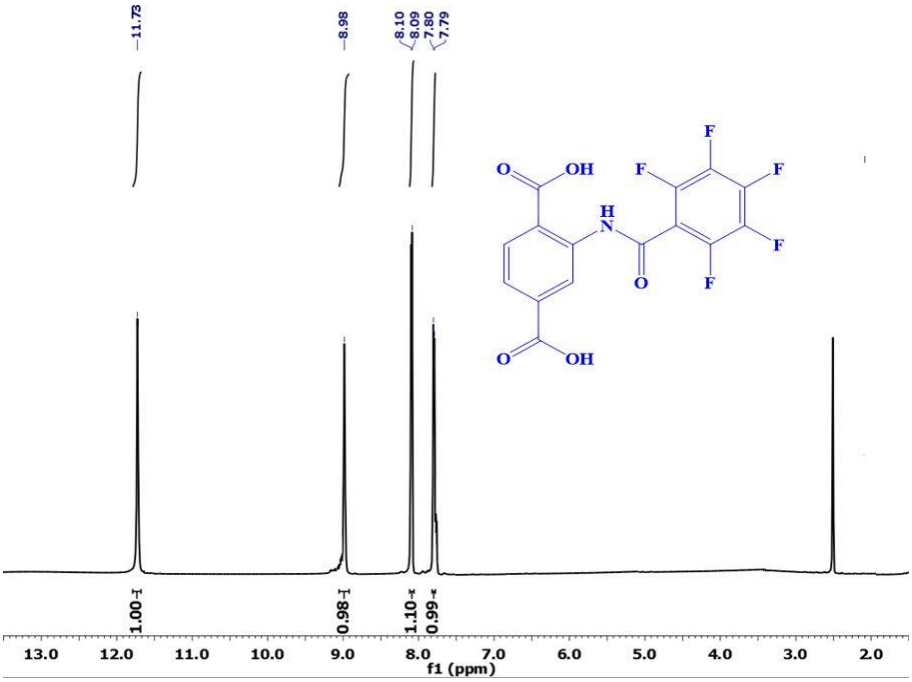

Figure S1. ^{1}H NMR spectrum of 2-(perfluorobenzamido)terephthalic acid linker in DMSO-d_6.

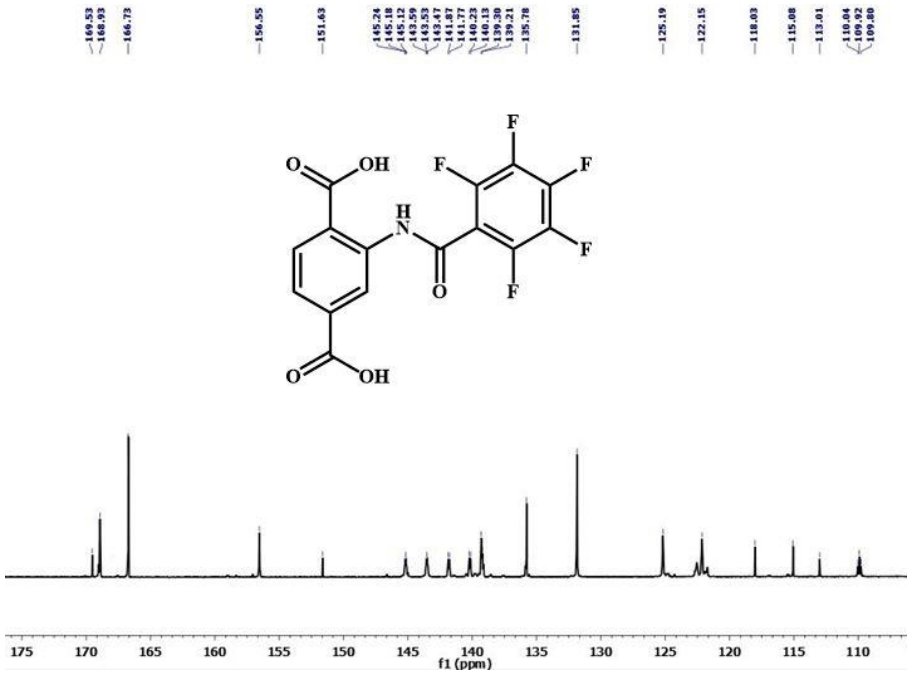

Figure S2. ^{13}C NMR spectrum of 2-(perfluorobenzamido)terephthalic acid linker in DMSO-d_6.

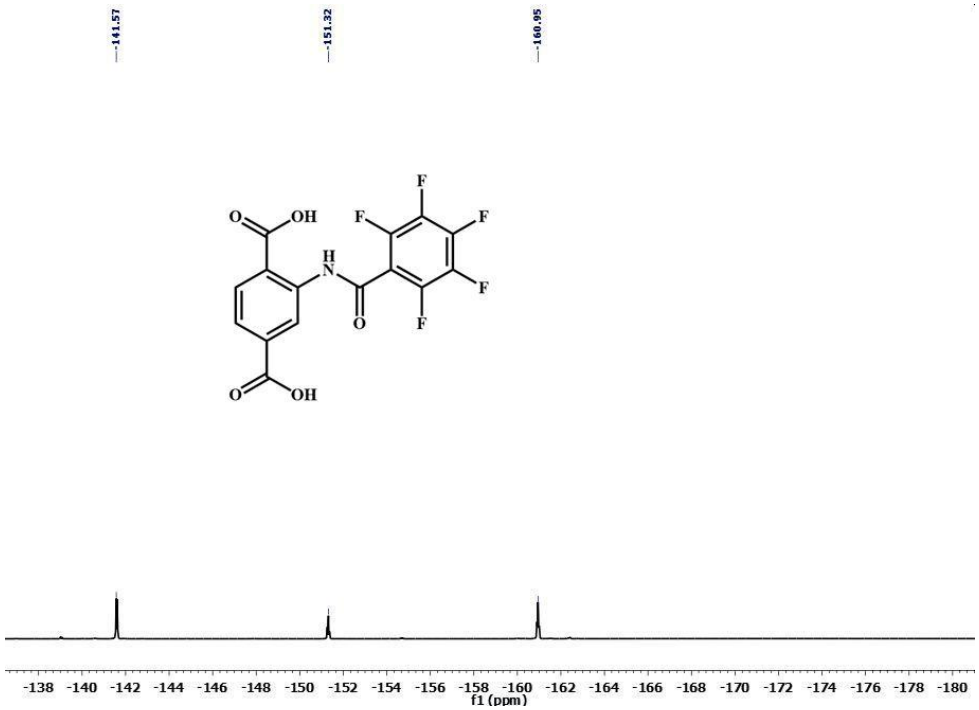

Figure S3. ^{19}F NMR spectrum of 2-(perfluorobenzamido)terephthalic acid linker in DMSO-d_6.

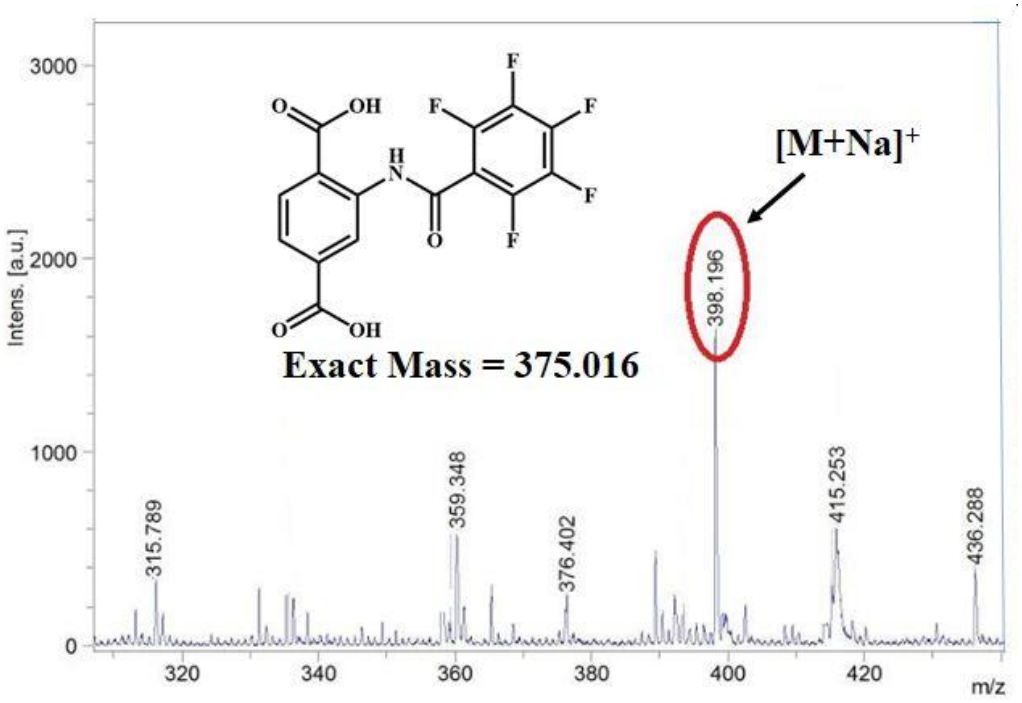

Figure S4. MALDI-TOF mass spectrum of 2-(perfluorobenzamido)terephthalic acid linker measured in methanol. The spectrum shows m/z peak at 398.198, which corresponds to $(M+Na)^+$ ion (M = mass of 2-(perfluorobenzamido)terephthalic acid linker).

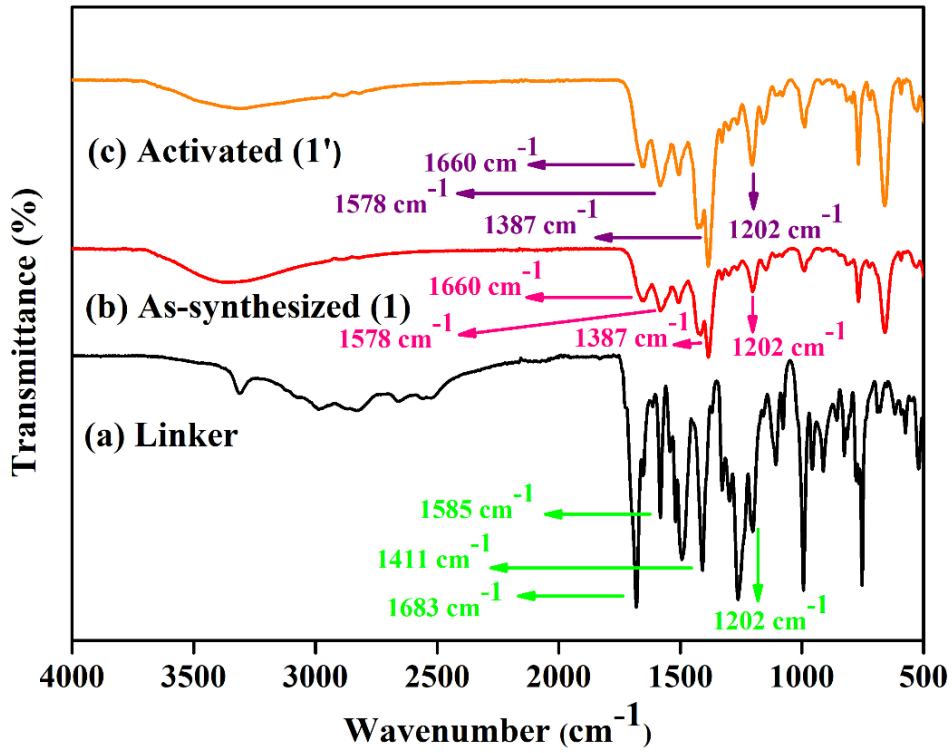

Figure S5. ATR-IR spectra of (a) 2-(perfluorobenzamido)terephthalic acid linker, (b) **1** (as-synthesized) and (c) **1′** (activated).

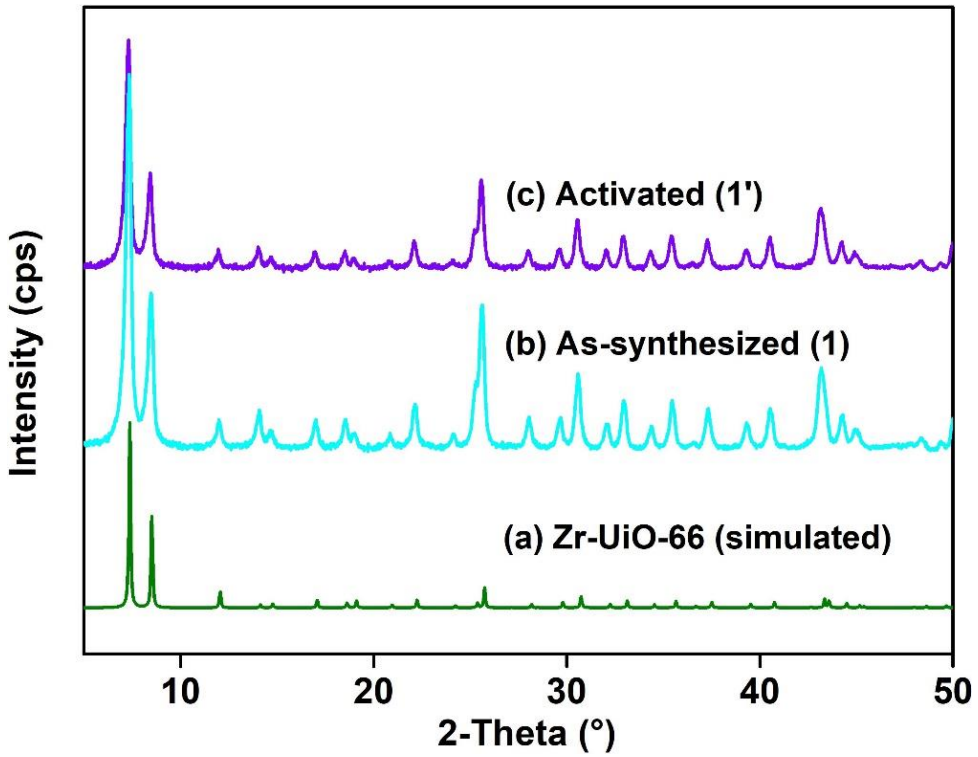

Figure S6. PXRD patterns of (a) simulated Zr-UiO-66 (green), (b) as-synthesized **1** (clay) and (c) activated **1′** (violet).

Table S1. Unit cell parameters of **1′** obtained by indexing its PXRD data. The obtained values have been compared with parent UiO-66 MOF.

Compound Name	**1′**	UiO-66
Crystal System	cubic	cubic
a = b = c (Å)	20.745 (4)	20.7004 (2)
V ($Å^3$)	8927.7 (27)	8870.3 (2)

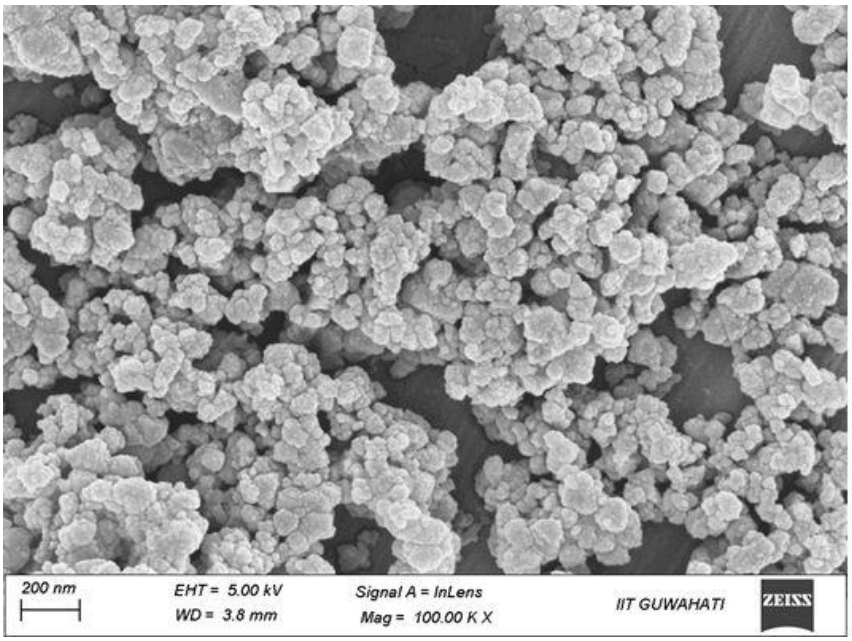

Figure S7. FE-SEM image of as-synthesized **1′**.

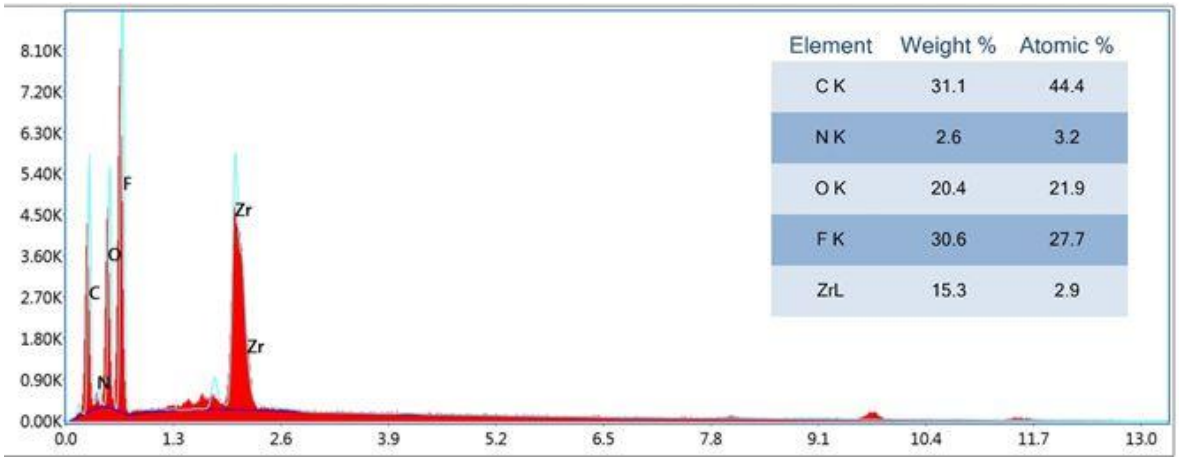

Figure S8. EDX spectrum of **1′**.

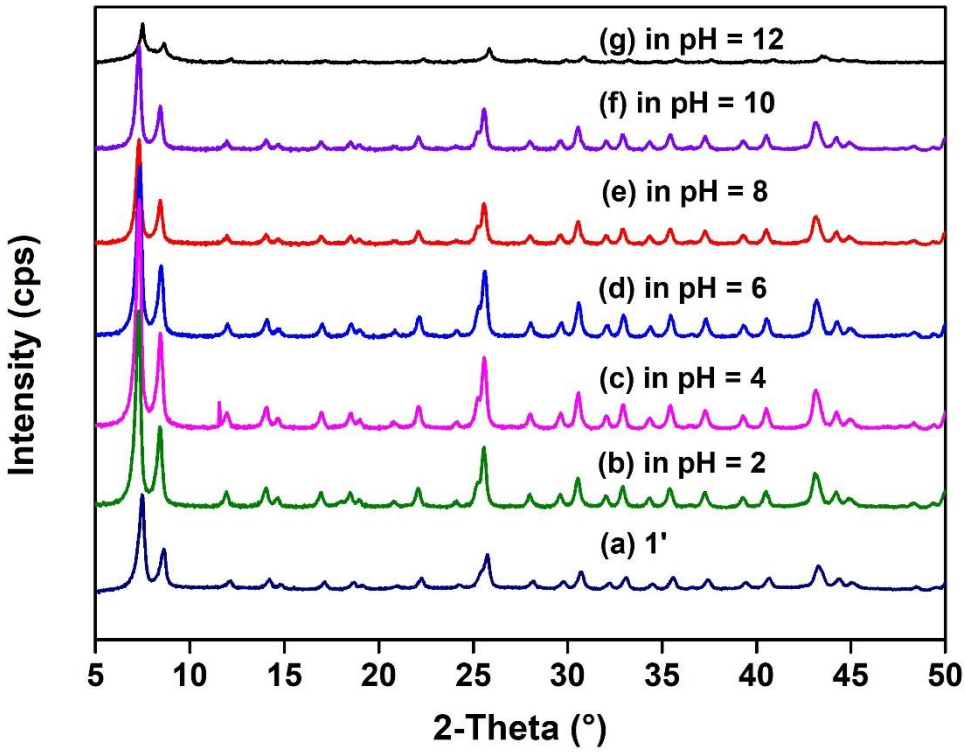

Figure S9. PXRD patterns of **1′** in different forms: (a) activated **1′**, after stirred with (b) pH = 2, (c) pH = 4 (d) pH = 6, (e) pH = 8, (f) pH = 10 and (g) pH = 12.

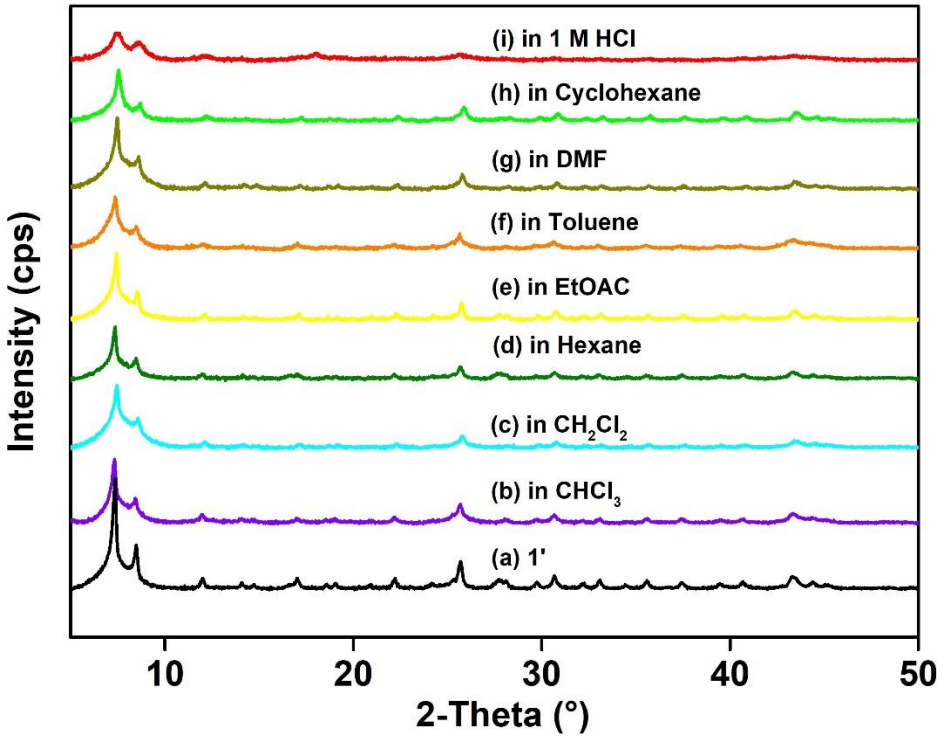

Figure S10. PXRD patterns of **1′** in different forms: (a) activated **1′**, after stirred with (b) $CHCl_3$, (c) CH_2Cl_2, (d) hexane, (e) EtOAc, (f) toluene, (g) DMF, (h) cyclohexane and (f) 1 M HCl.

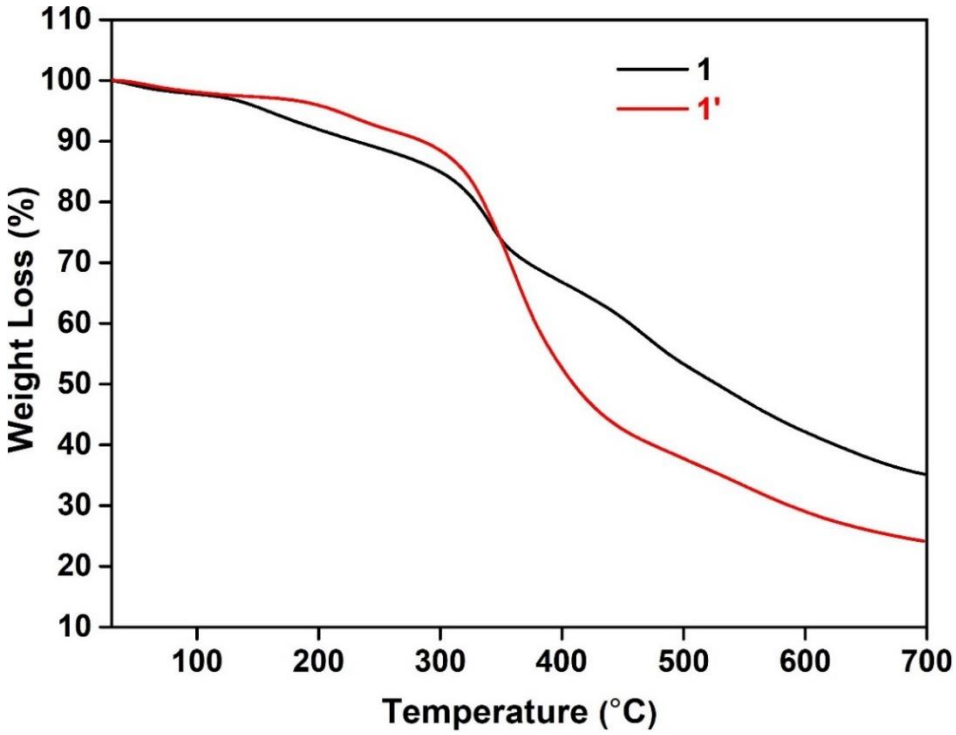

Figure S11. Thermogravimetric analysis curves of as-synthesized **1** (black) and thermally activated **1′** (red) recorded under O_2 atmosphere in the temperature range of 30-700 °C with a heating rate of 4 °C min^{-1}.

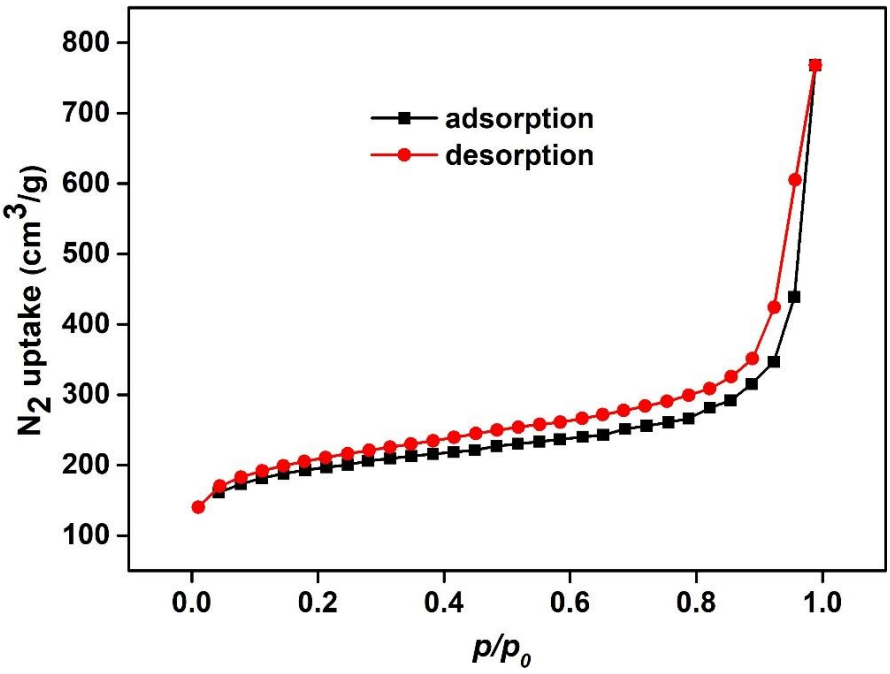

Figure S12. N_2 adsorption (black squares) and desorption (red circles) isotherms of thermally activated **1′** recorded at –196 °C.

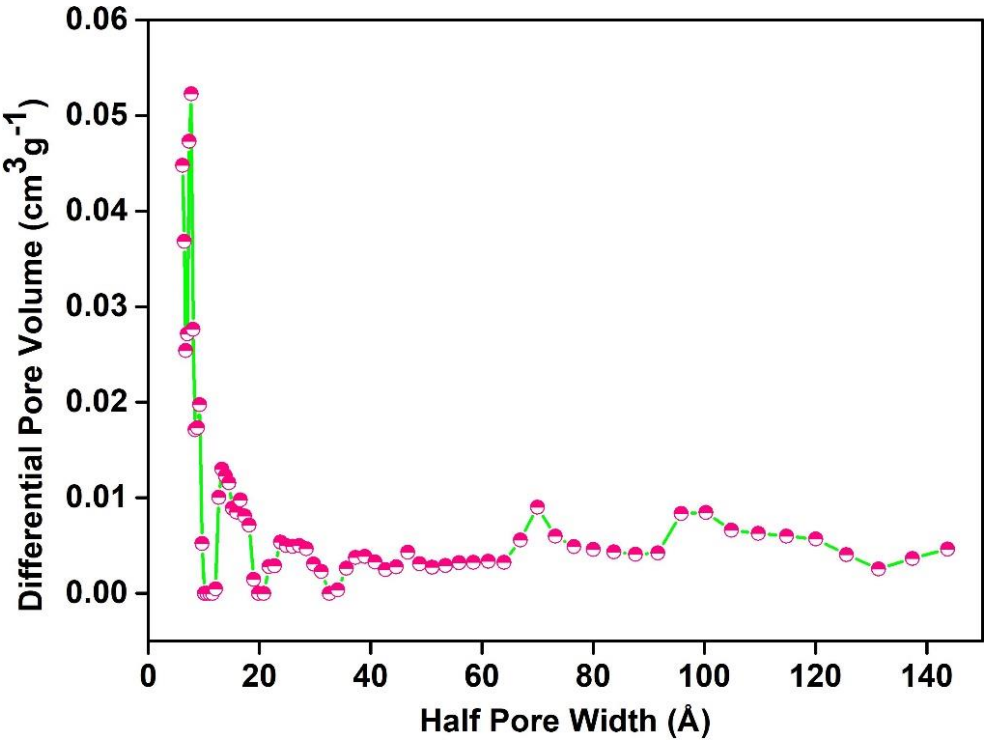

Figure S13. Density functional theory pore-size distribution of compound **1′** as determined from its N_2 adsorption isotherms at -196 °C.

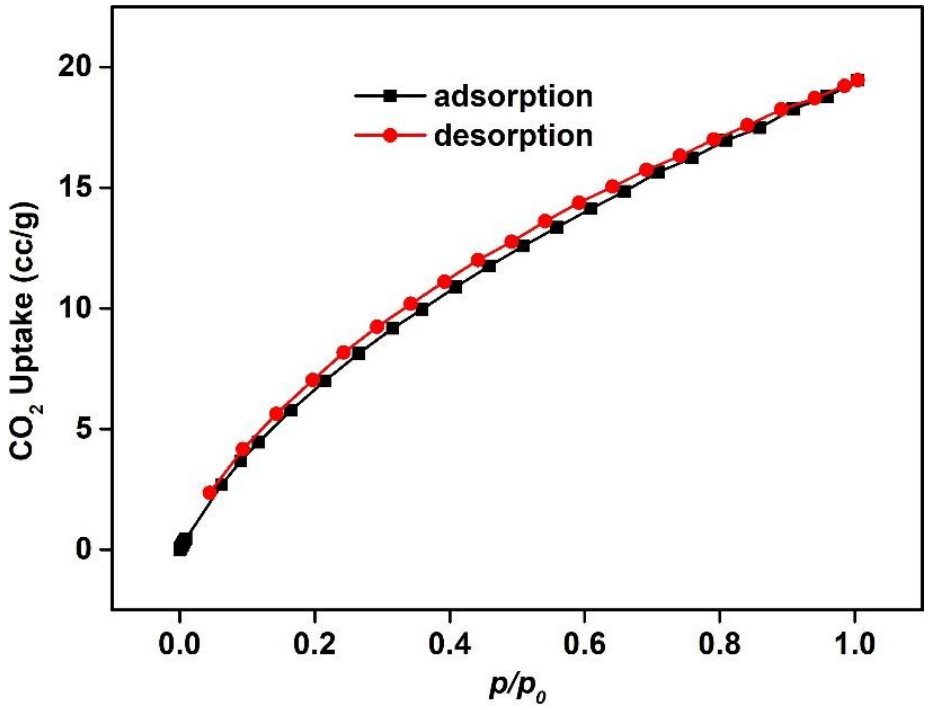

Figure S14. CO_2 uptake measurement of **1′** at room temperature.

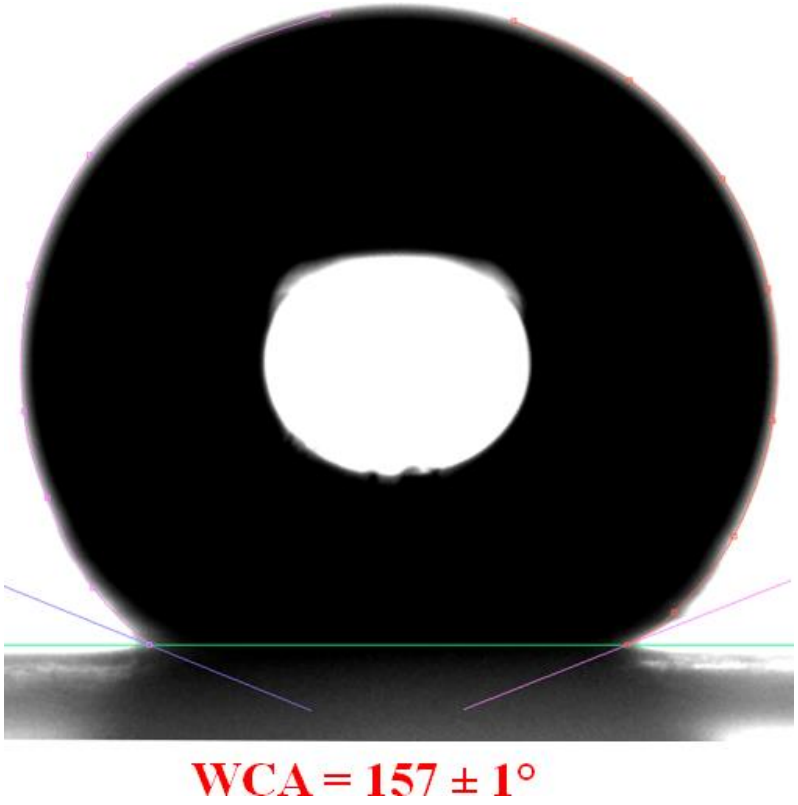

Figure S15. Water contact angle (WCA) of **1′**.

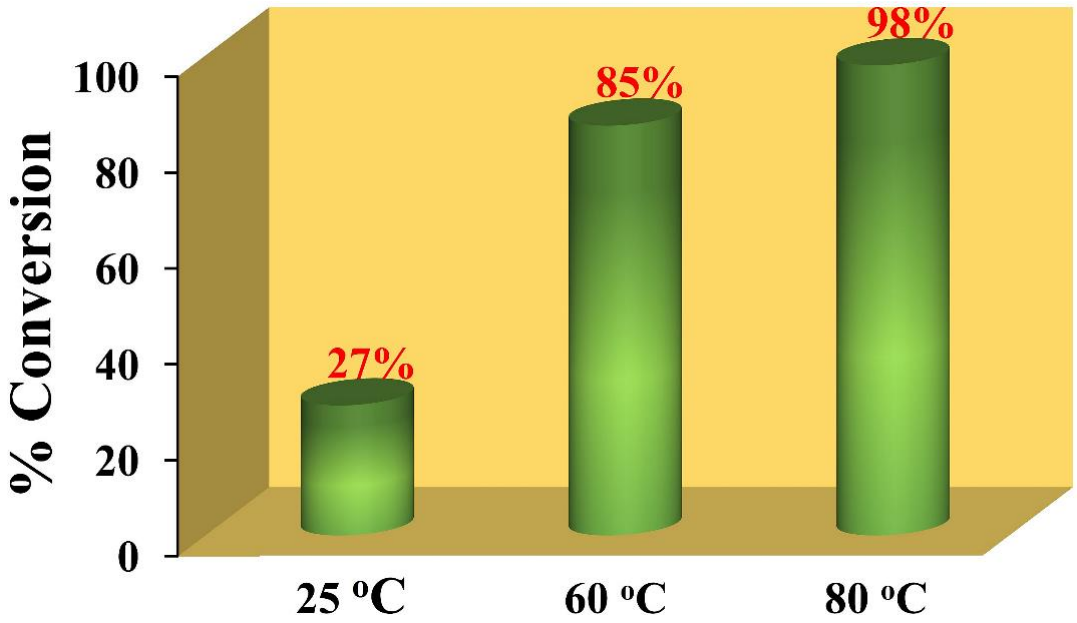

Figure S16. Effect of temperature on the catalytic performance of **1'** for the cycloaddition reaction of CO_2 with epichlorohydrin.

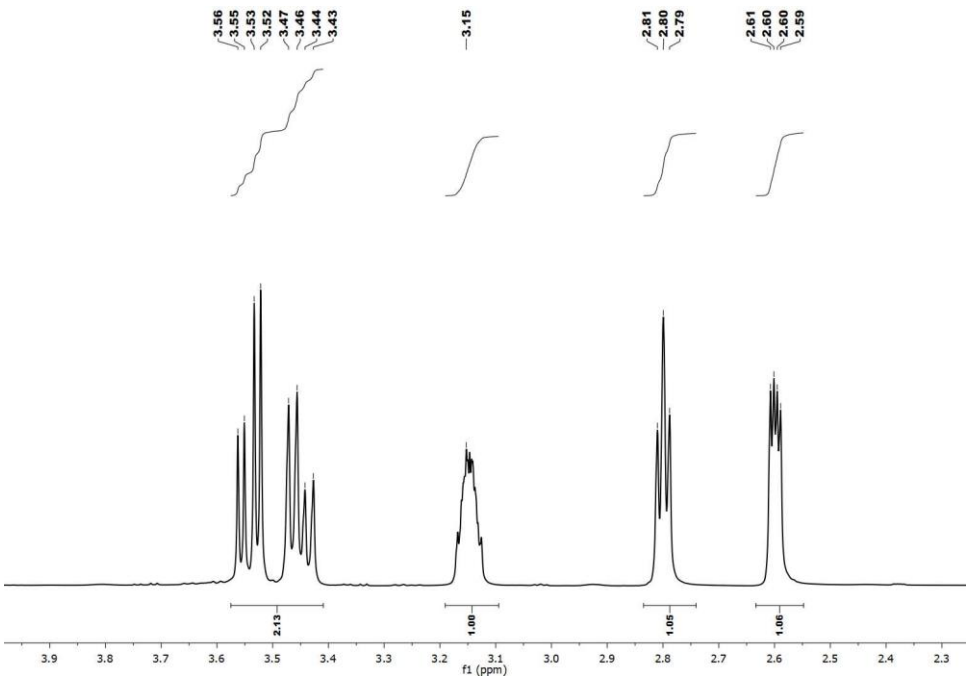

Figure S17. ^{1}H NMR ($CDCl_3$, 400 MHz) spectra for the cycloaddition reaction of epichlorohydrin using **1′** as catalyst in absence of any cocatalyst (Table 1, entry no. 1).

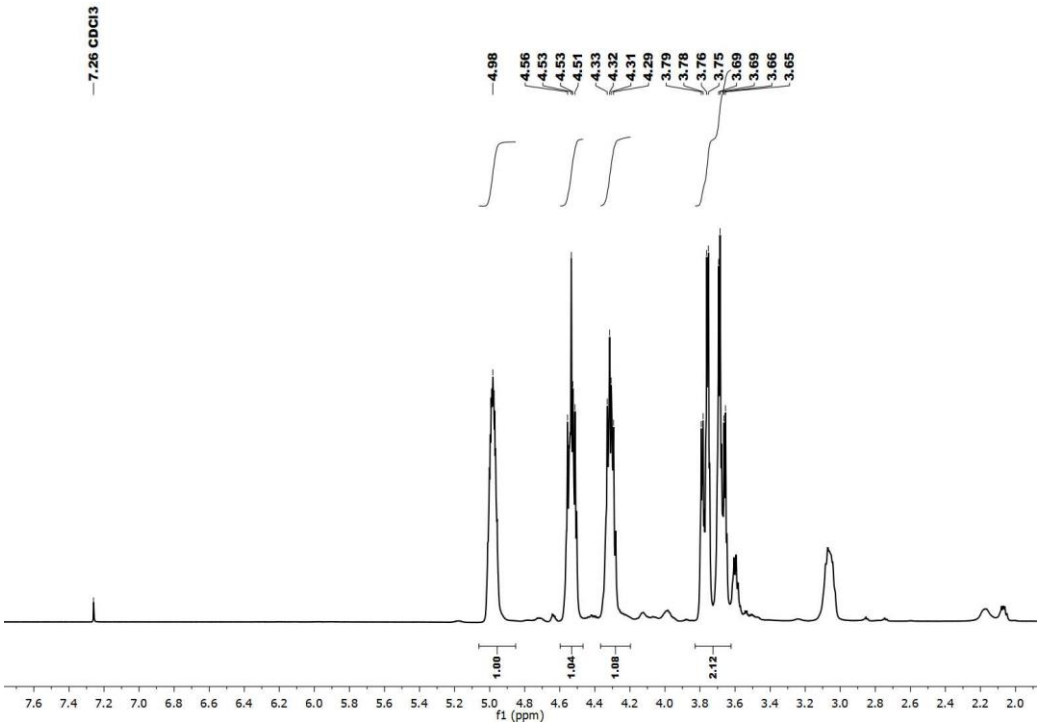

Figure S18. ^{1}H NMR ($CDCl_3$, 400 MHz) spectra for the cycloaddition reaction of epichlorohydrin using **1′** as catalyst (Table 1, entry no. 2).

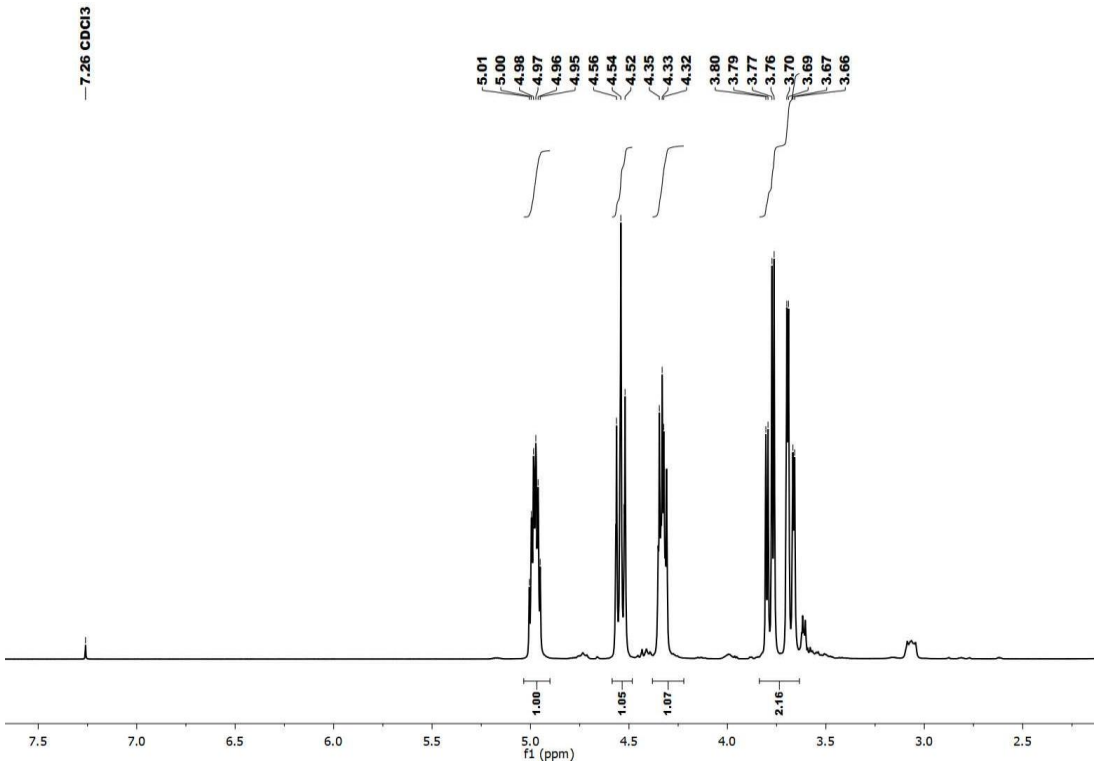

Figure S19. ^{1}H NMR ($CDCl_3$, 400 MHz) spectra for the cycloaddition reaction of epichlorohydrin using **1′** as catalyst (Table 1, entry no. 3).

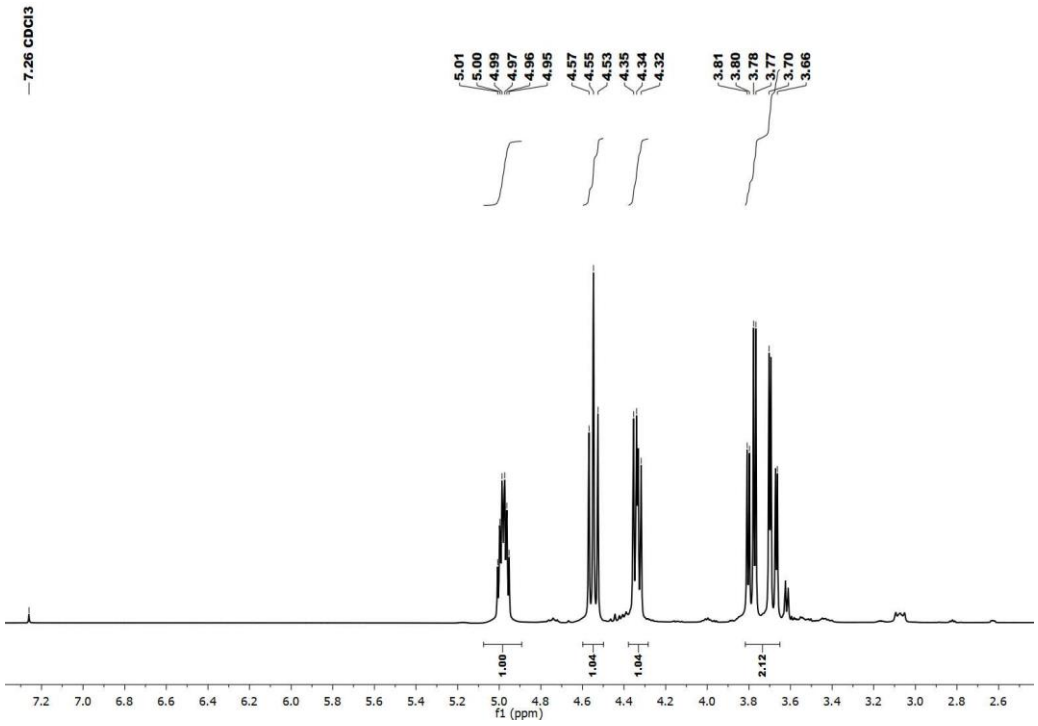

Figure S20. ^{1}H NMR ($CDCl_3$, 400 MHz) spectra for the cycloaddition reaction of epichlorohydrin using **1′** as catalyst (Table 1, entry no. 4).

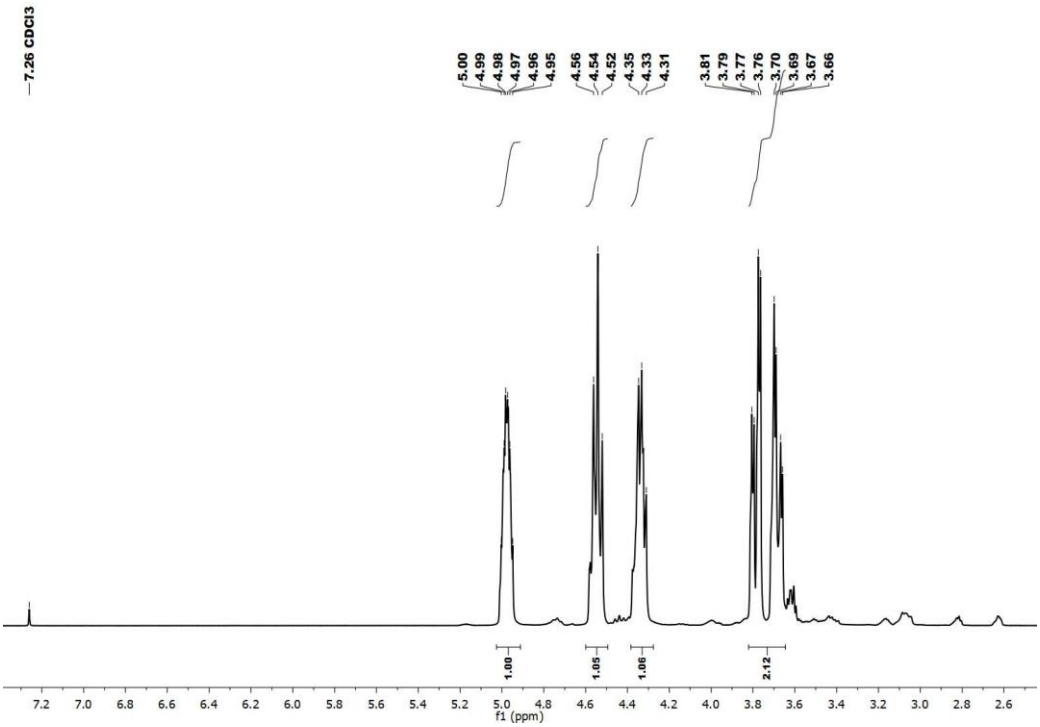

Figure S21. ^{1}H NMR ($CDCl_3$, 400 MHz) spectra for the cycloaddition reaction of epichlorohydrin using **1′** as catalyst (Table 1, entry no. 5).

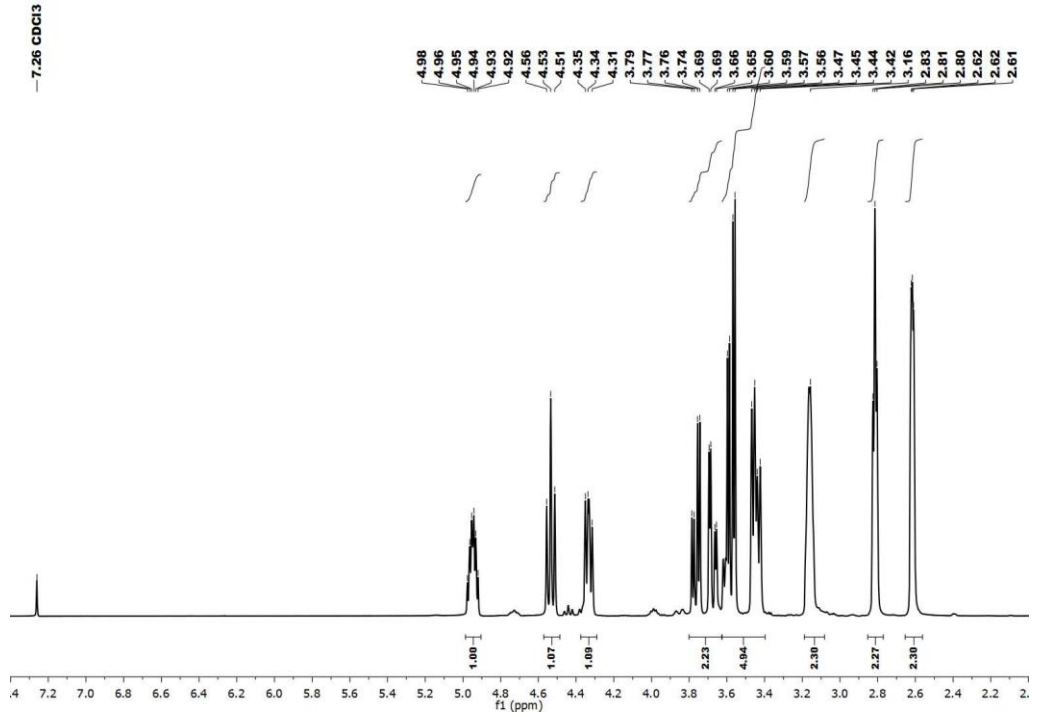

Figure S22. ^{1}H NMR ($CDCl_3$, 400 MHz) spectra for the cycloaddition reaction of epichlorohydrin using **1′** as catalyst (Table 1, entry no. 6).

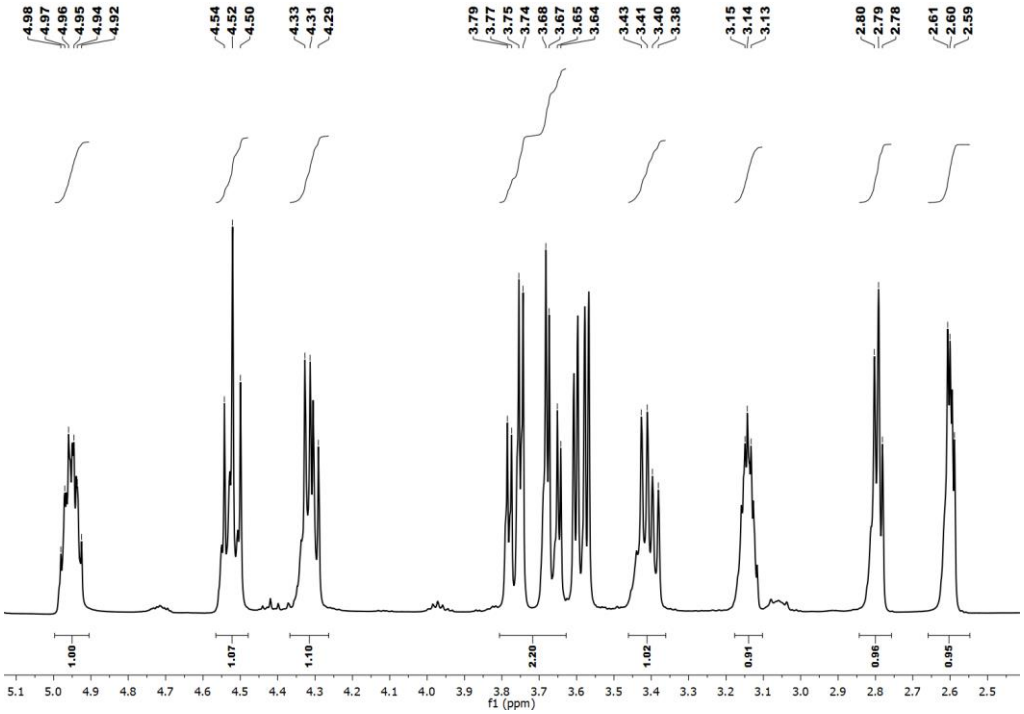

Figure S23. ^{1}H NMR ($CDCl_3$, 400 MHz) spectra for the cycloaddition reaction of epichlorohydrin in presence of only co-catalyst TBAB (0.4 mol%) (Table 1, entry no. 7).

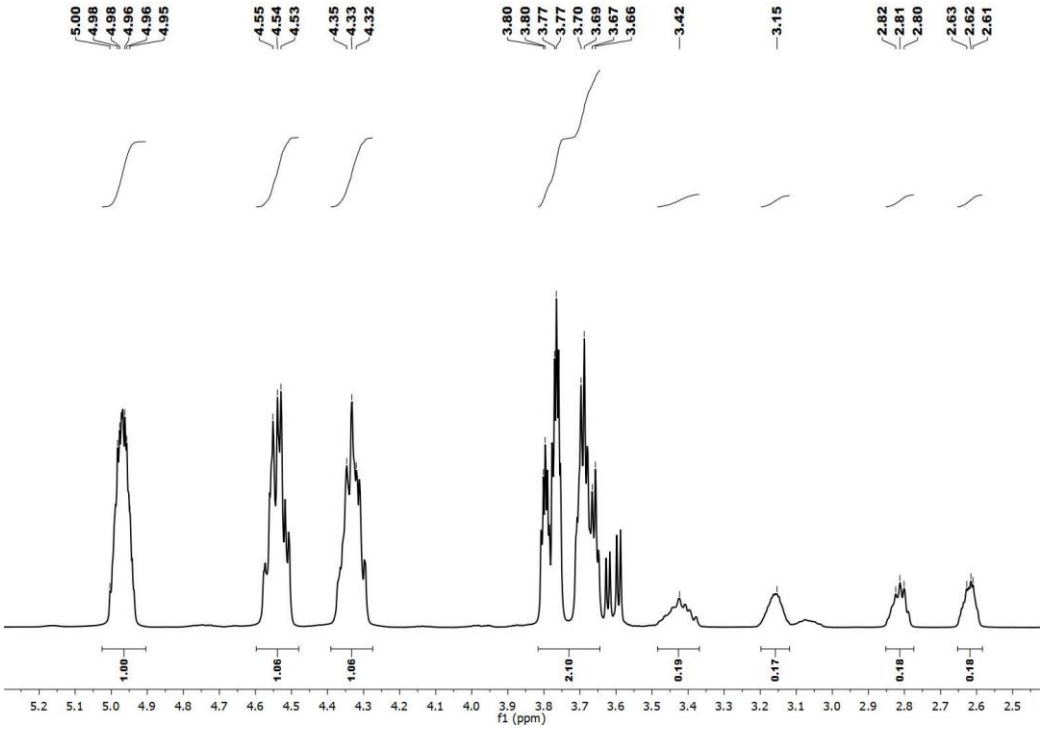

Figure S24. ^{1}H NMR ($CDCl_3$, 400 MHz) spectra for the cycloaddition reaction of epichlorohydrin using **1′** as catalyst (Table 1, entry no. 8).

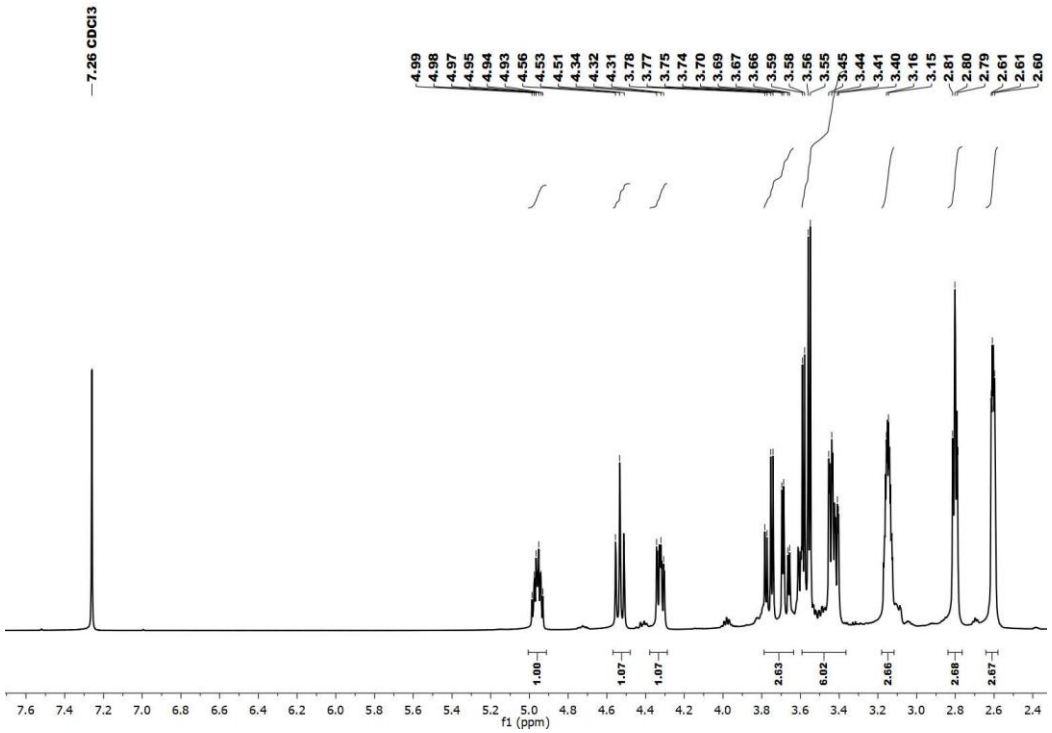

Figure S25. ^{1}H NMR ($CDCl_3$, 400 MHz) spectra for the cycloaddition reaction of epichlorohydrin using **1′** as catalyst (Table 1, entry no. 9).

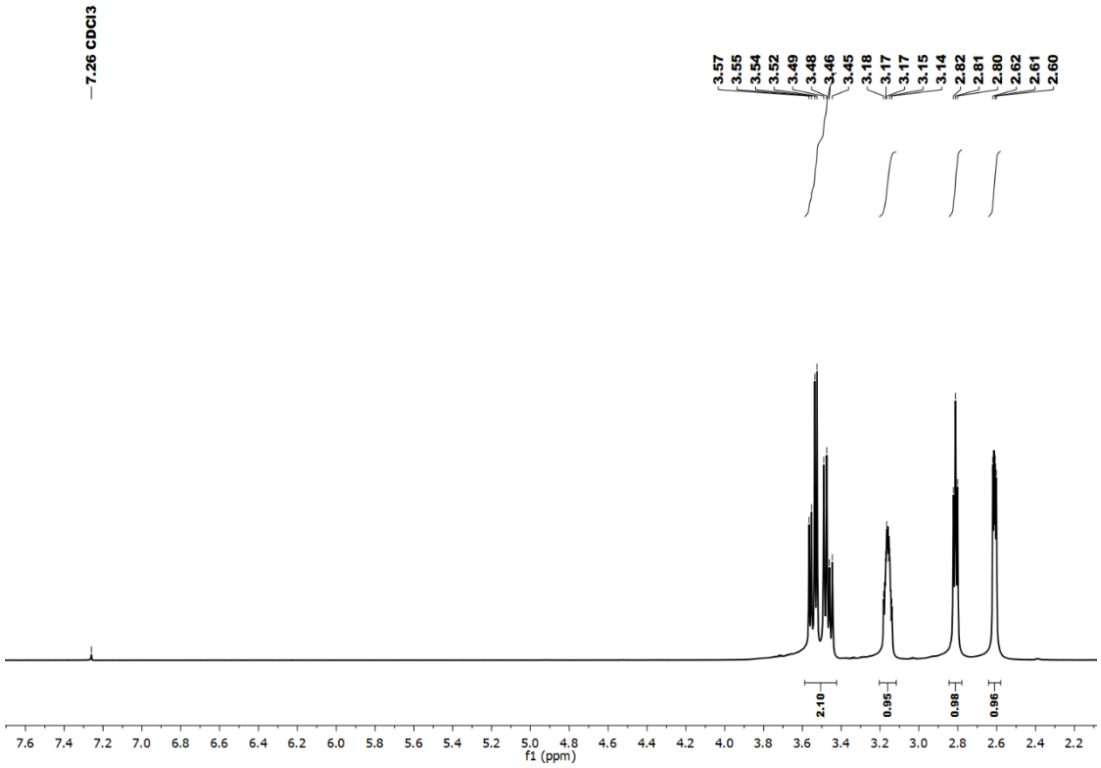

Figure S26. ^{1}H NMR ($CDCl_3$, 400 MHz) spectra for the cycloaddition reaction of epichlorohydrin using $ZrCl_4$ as catalyst (Table 1, entry no. 10).

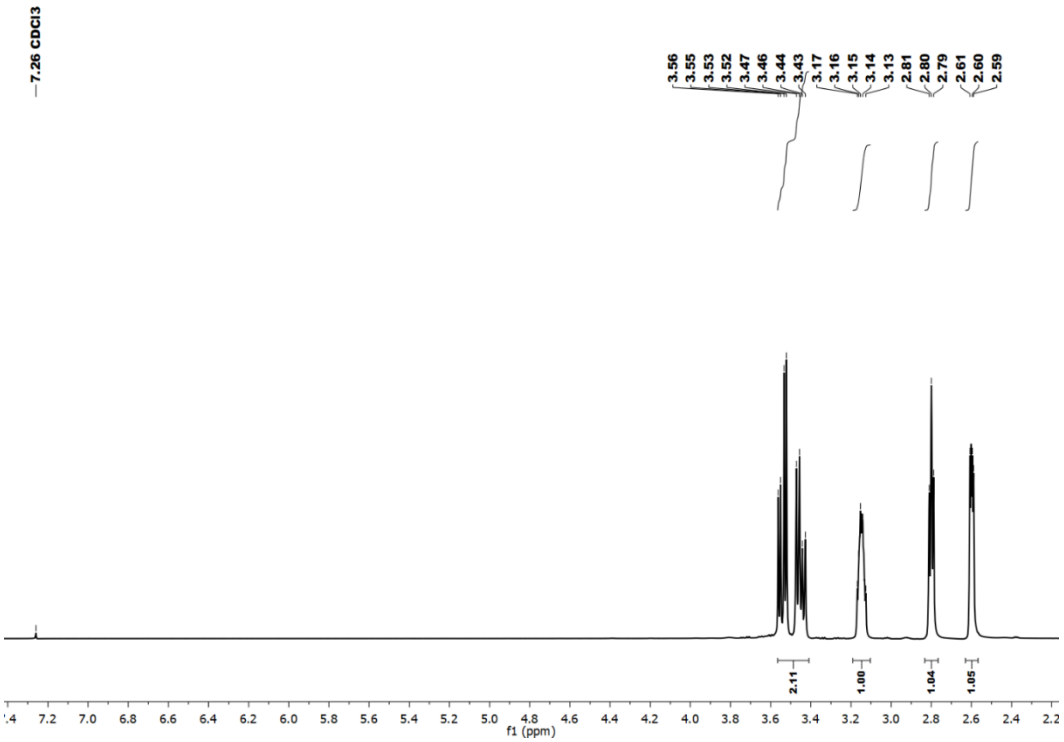

Figure S27. ^{1}H NMR ($CDCl_3$, 400 MHz) spectra for the cycloaddition reaction of epichlorohydrin using H_2L as catalyst (Table 1, entry no.11).

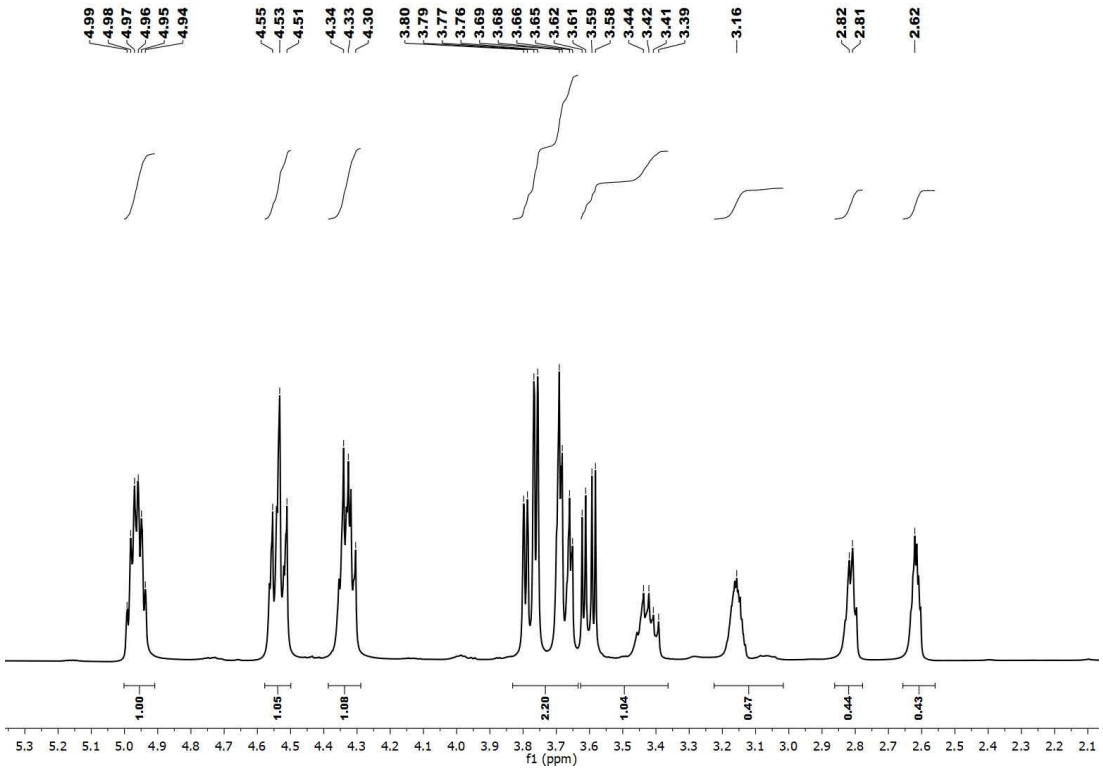

Figure S28. ^{1}H NMR ($CDCl_3$, 400 MHz) spectra for the cycloaddition reaction of epichlorohydrin using $ZrCl_4$ as a catalyst in presence of TBAB (Table 1, entry no.12).

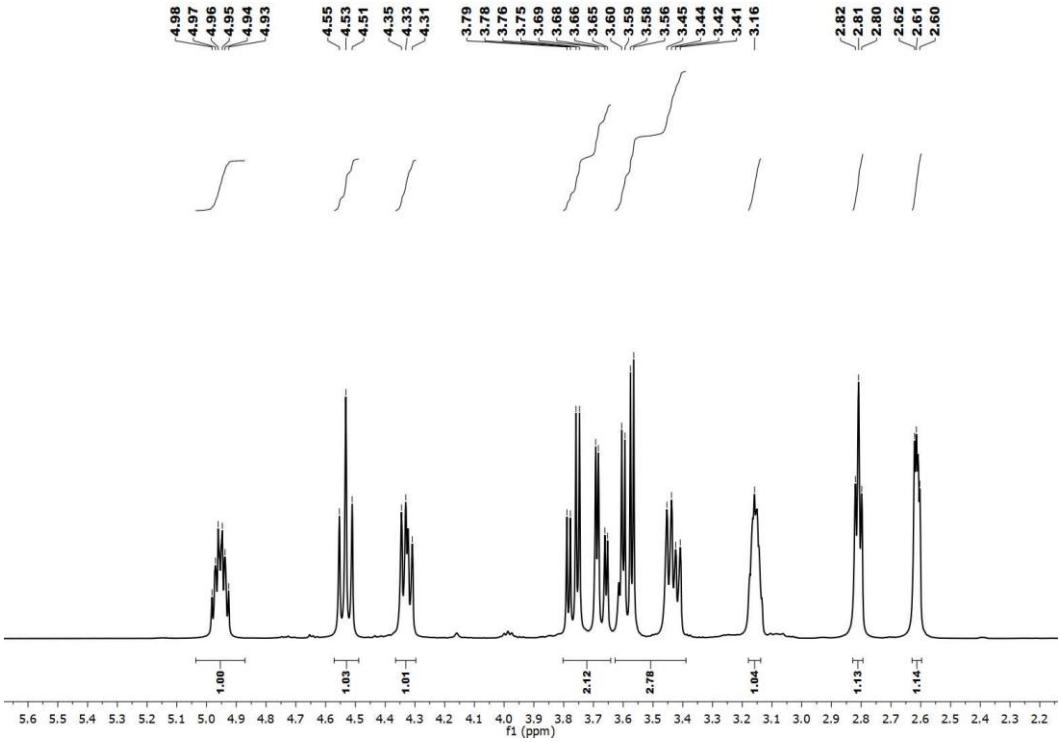

Figure S29. ^{1}H NMR ($CDCl_3$, 400 MHz) spectra for the cycloaddition reaction of epichlorohydrin using H_2L as catalyst in presence of TBAB (Table 1, entry no.13).

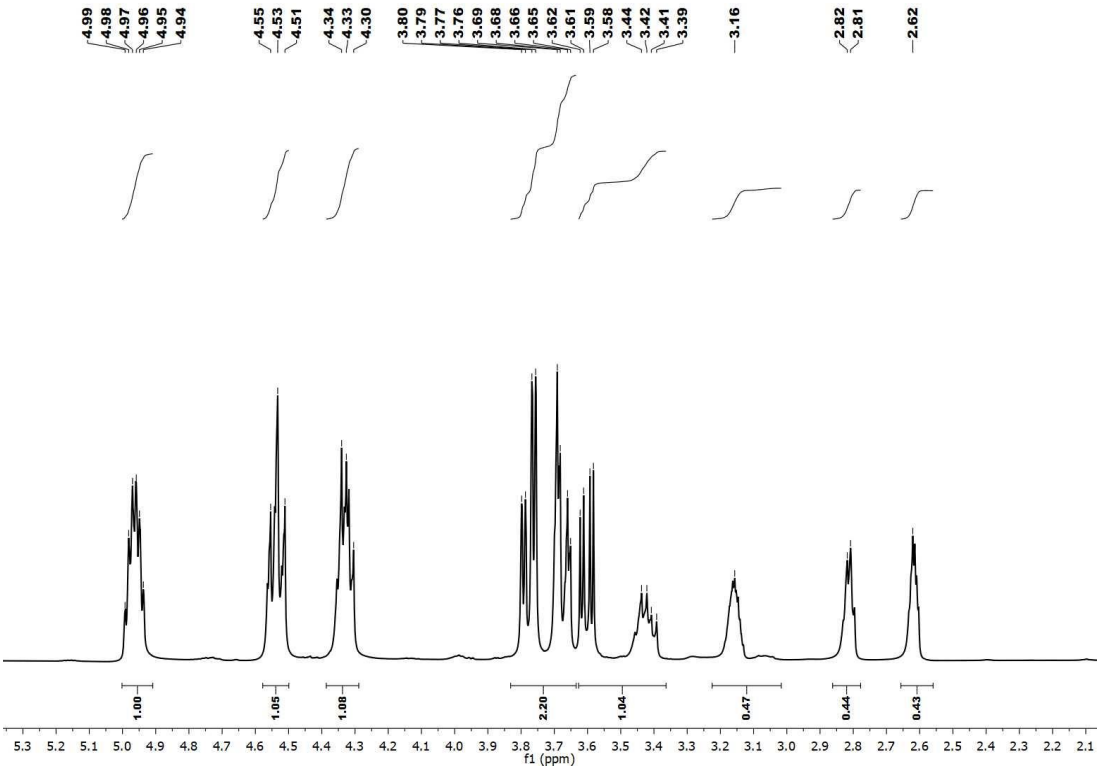

Figure S30. ^{1}H NMR ($CDCl_3$, 400 MHz) spectra for the cycloaddition reaction of epichlorohydrin using H_2L and $ZrCl_4$ as catalyst in presence of TBAB (Table 1, entry no.14).

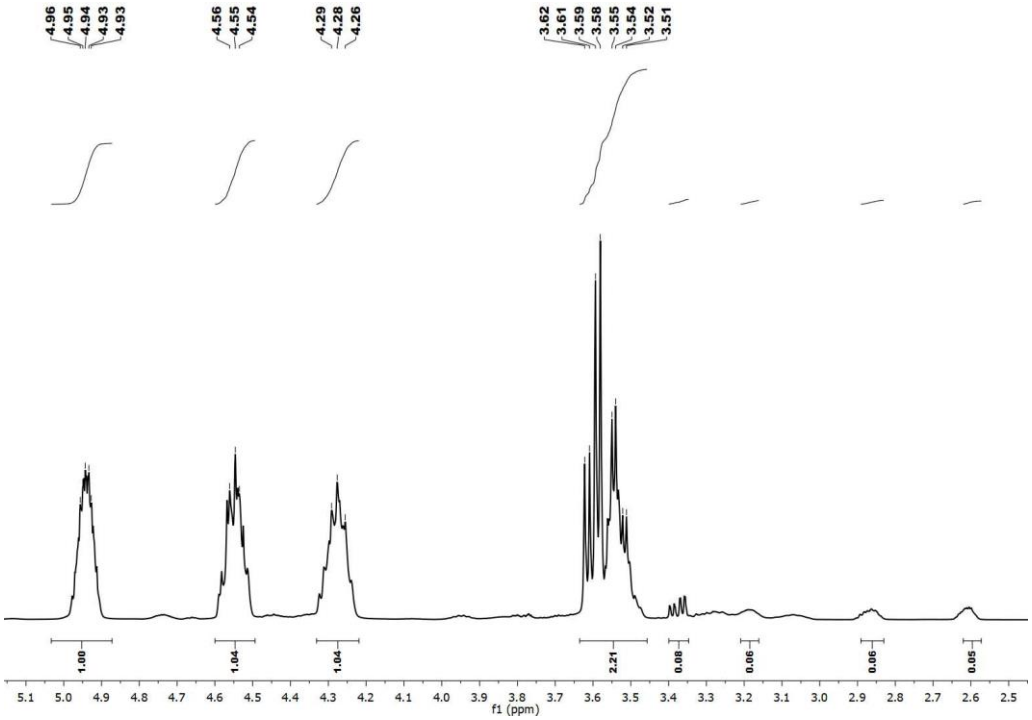

Figure S31. ^{1}H NMR ($CDCl_3$, 400 MHz) spectra for the cycloaddition reaction of epibromohydrin using **1′** as catalyst (Table 2, entry no. 2).

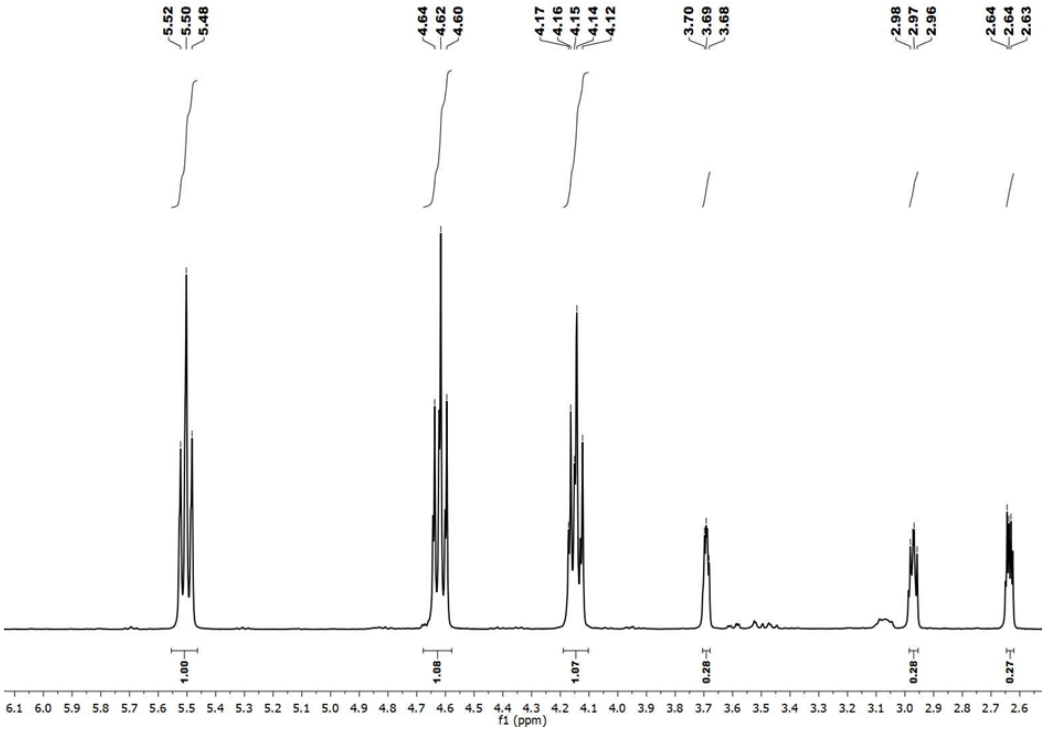

Figure S32. ^{1}H NMR ($CDCl_3$, 400 MHz) spectra for the cycloaddition reaction of styrene oxide using **1′** as catalyst (Table 2, entry no. 3).

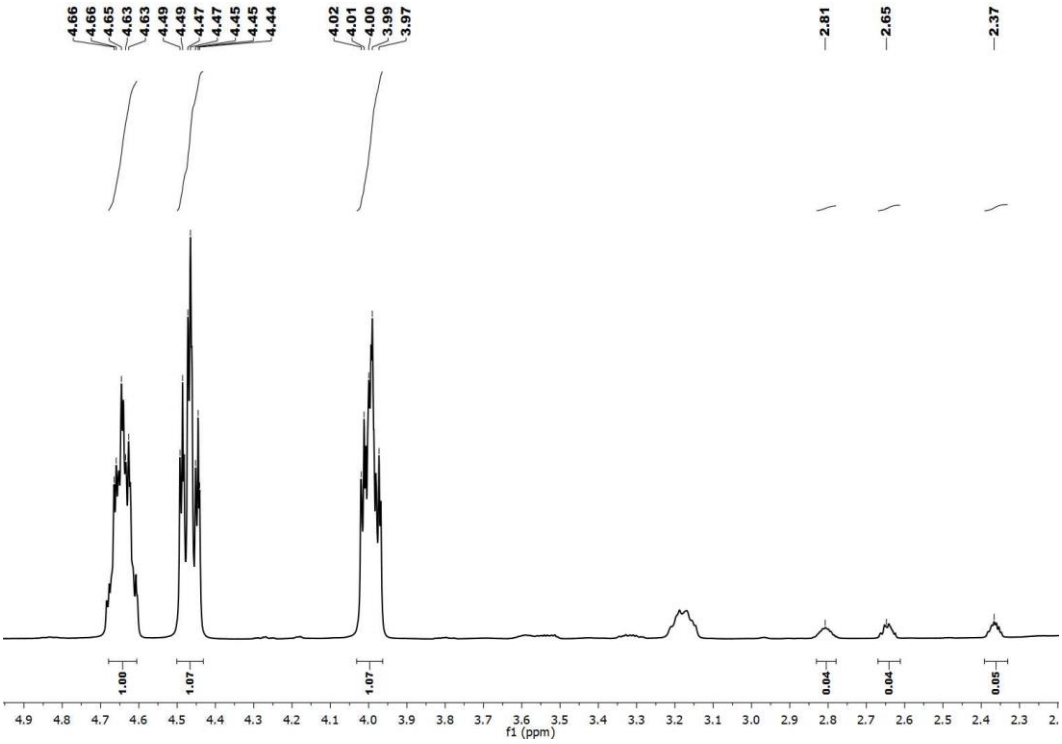

Figure S33. ^{1}H NMR ($CDCl_3$, 400 MHz) spectra for the cycloaddition reaction of 1,2-epoxyhexane using **1′** as catalyst (Table 1, entry no. 4).

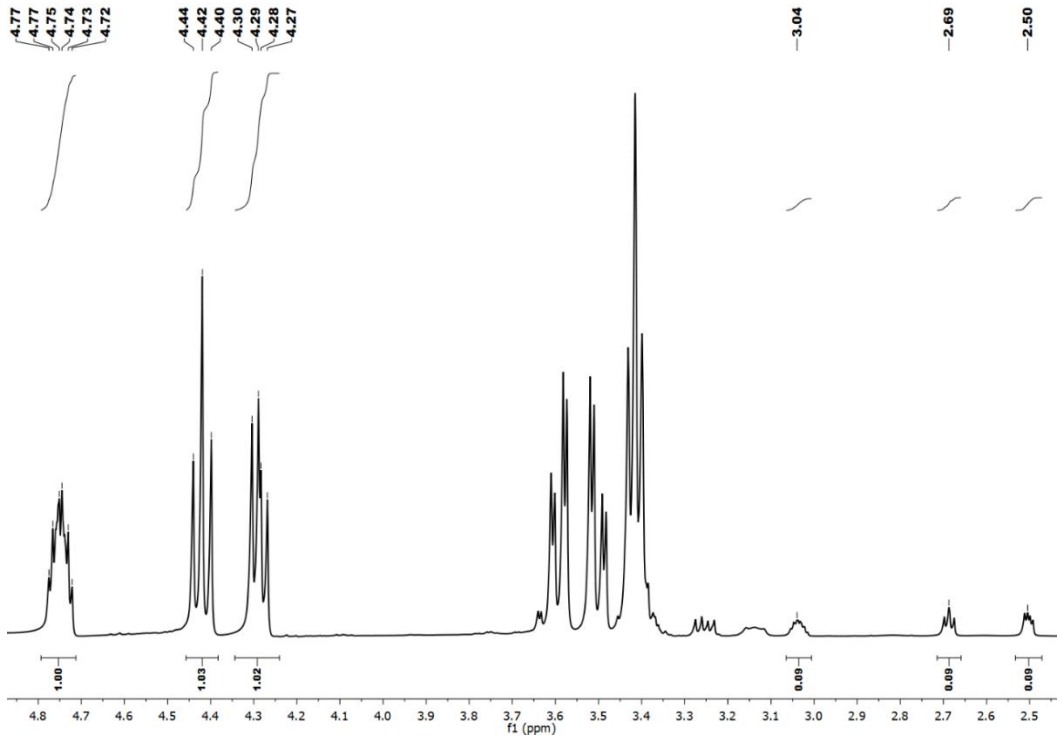

Figure S34. ^{1}H NMR ($CDCl_3$, 400 MHz) spectra for the cycloaddition reaction of butyl glycidyl ether using **1′** as catalyst (Table 2, entry no. 5).

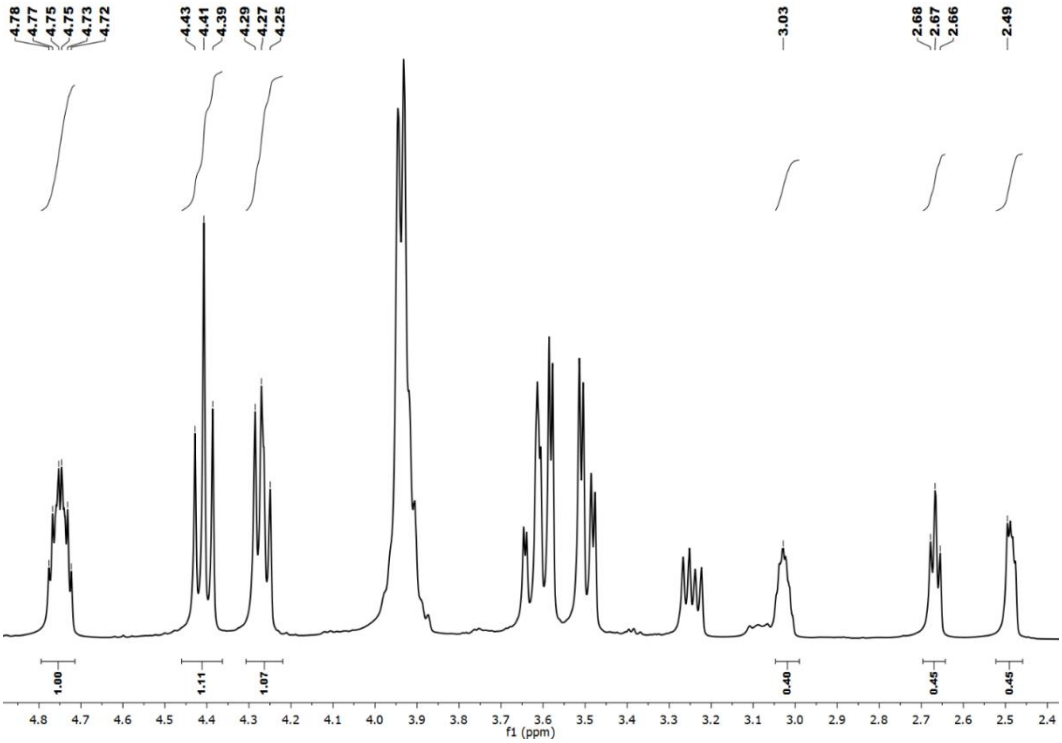

Figure S35. ^{1}H NMR ($CDCl_3$, 400 MHz) spectra for the cycloaddition reaction of allyl glycidyl ether using **1′** as catalyst (Table 2, entry no. 6).

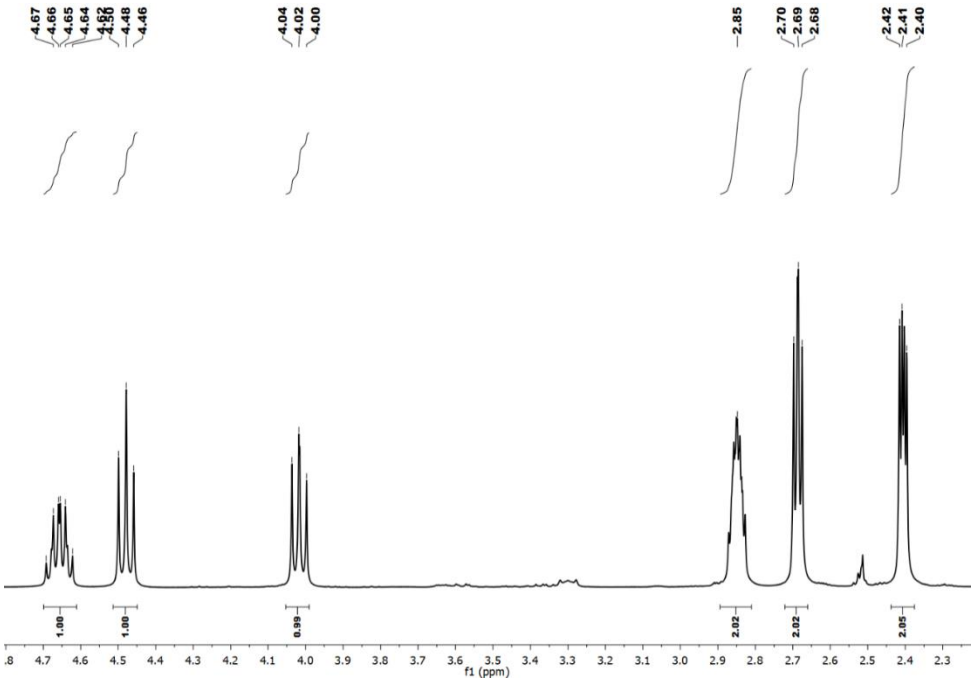

Figure S36. ^{1}H NMR ($CDCl_3$, 400 MHz) spectra for the cycloaddition reaction of 1,2-epoxy dodecane using **1′** as catalyst (Table 2, entry no. 7).

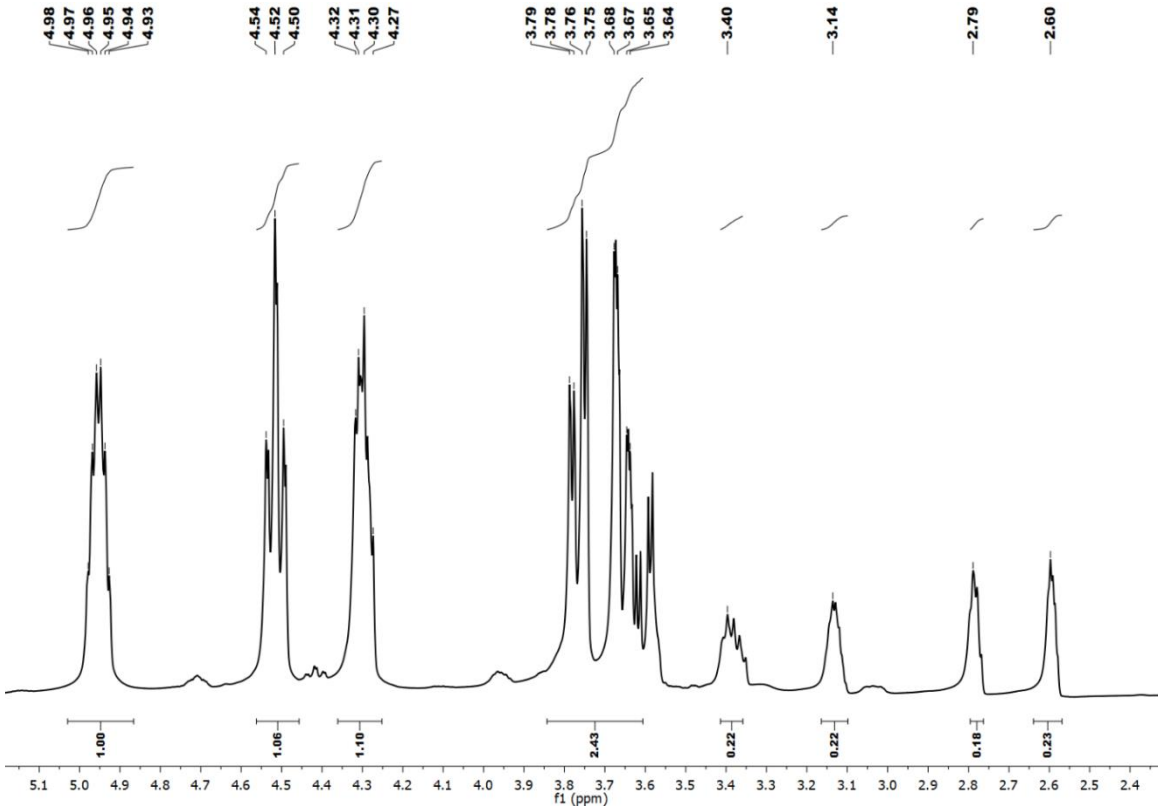

Figure S37. ^{1}H NMR ($CDCl_3$, 400 MHz) spectra for the cycloaddition reaction of epichlorohydrin using **1′** as catalyst after 4th cycle of recyclability.

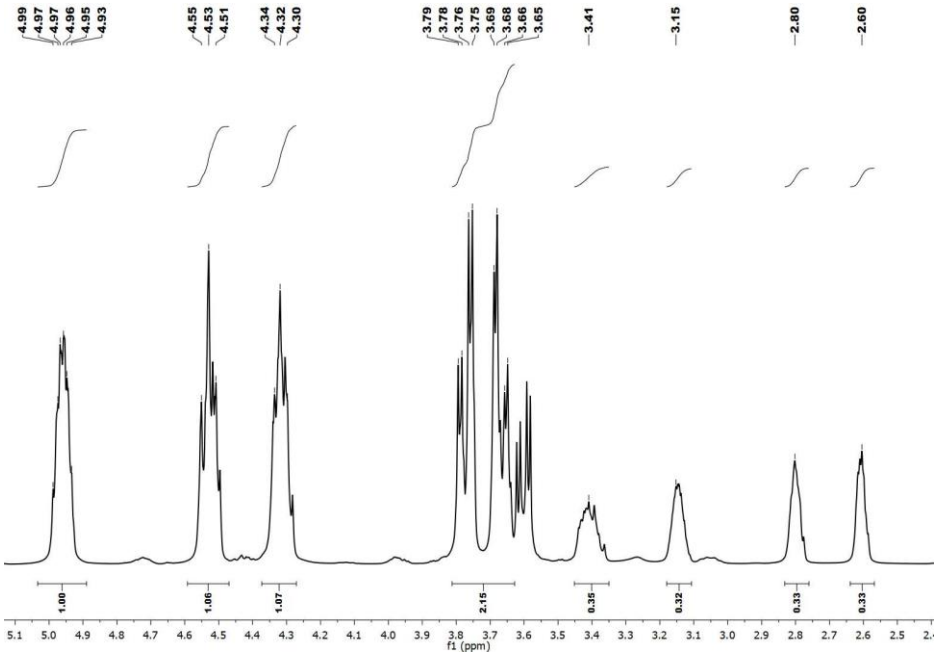

Figure S38. ^{1}H NMR ($CDCl_3$, 400 MHz) spectra for the cycloaddition reaction of epichlorohydrin using UiO-66 MOF as catalyst.

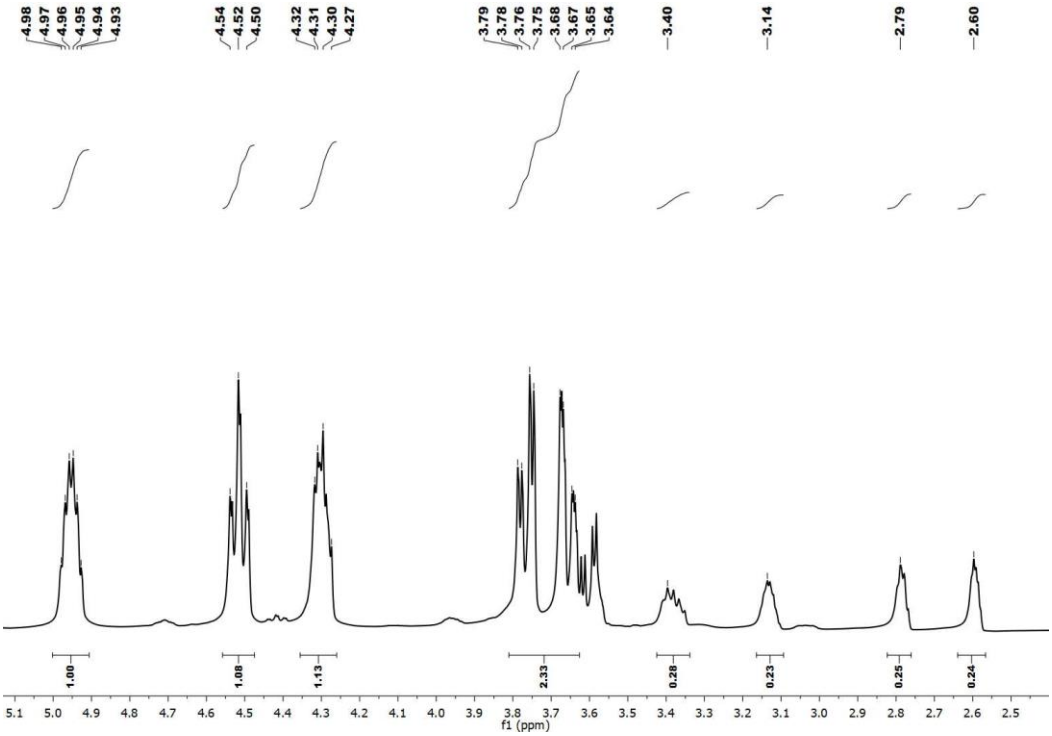

Figure S39. ^{1}H NMR ($CDCl_3$, 400 MHz) spectra for the cycloaddition reaction of epichlorohydrin using UiO-66-NH_2 MOF as catalyst.

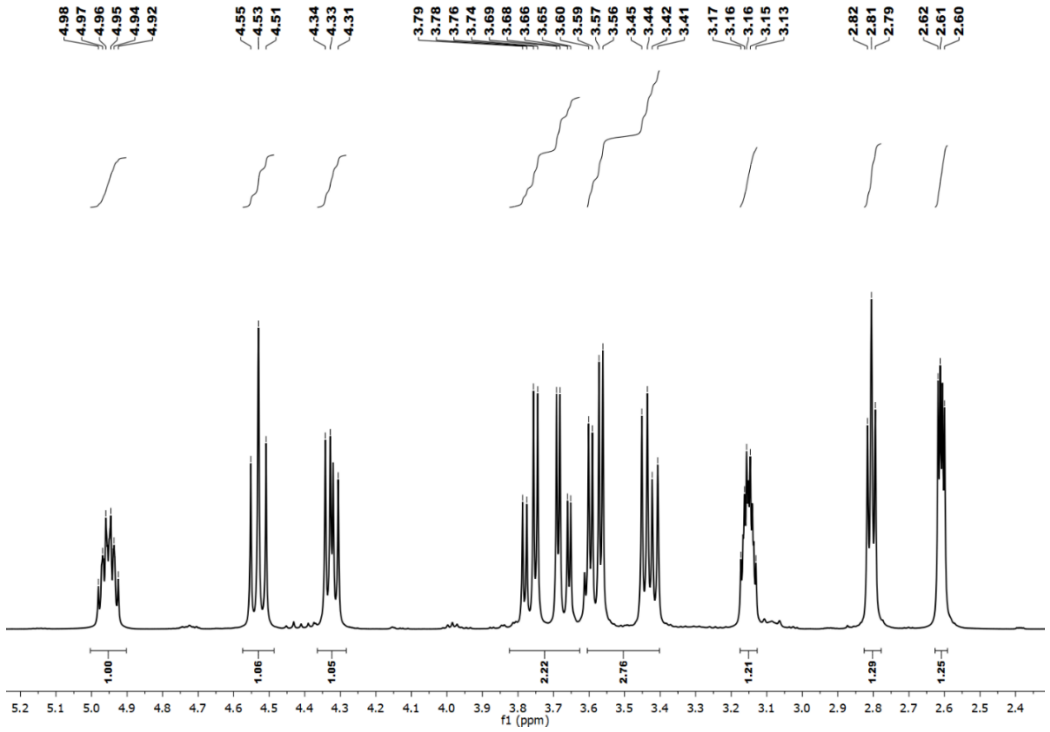

Figure S40. ^{1}H NMR ($CDCl_3$, 400 MHz) spectra for the cycloaddition reaction of epichlorohydrin using **1′** as catalyst after 3 h (before hot filtration experiment).

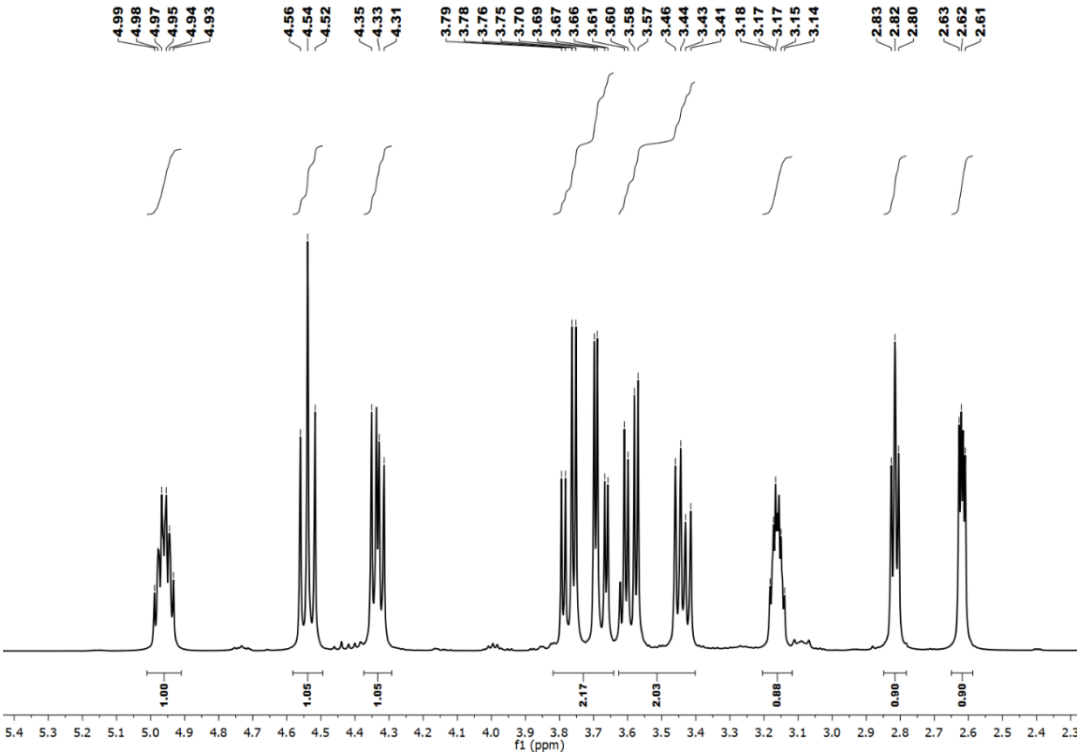

Figure S41. ^{1}H NMR ($CDCl_3$, 400 MHz) spectra for the cycloaddition reaction of epichlorohydrin using **1′** as catalyst 9 h (after hot filtration experiment).

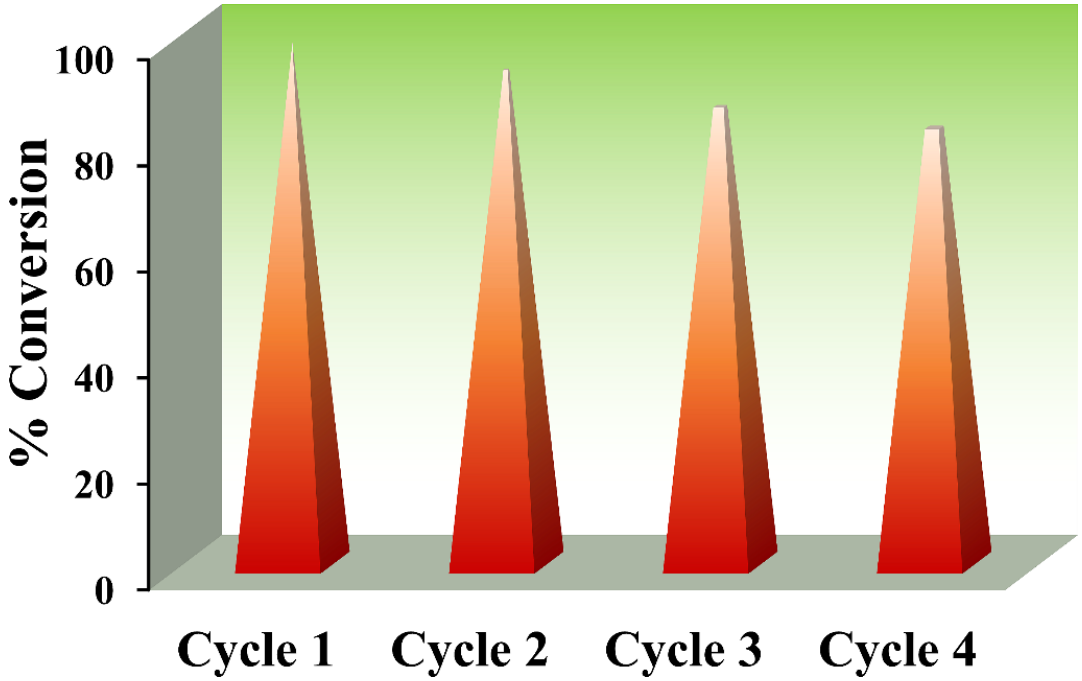

Figure S42. Recyclability test of **1'** up to four consecutive cycles.

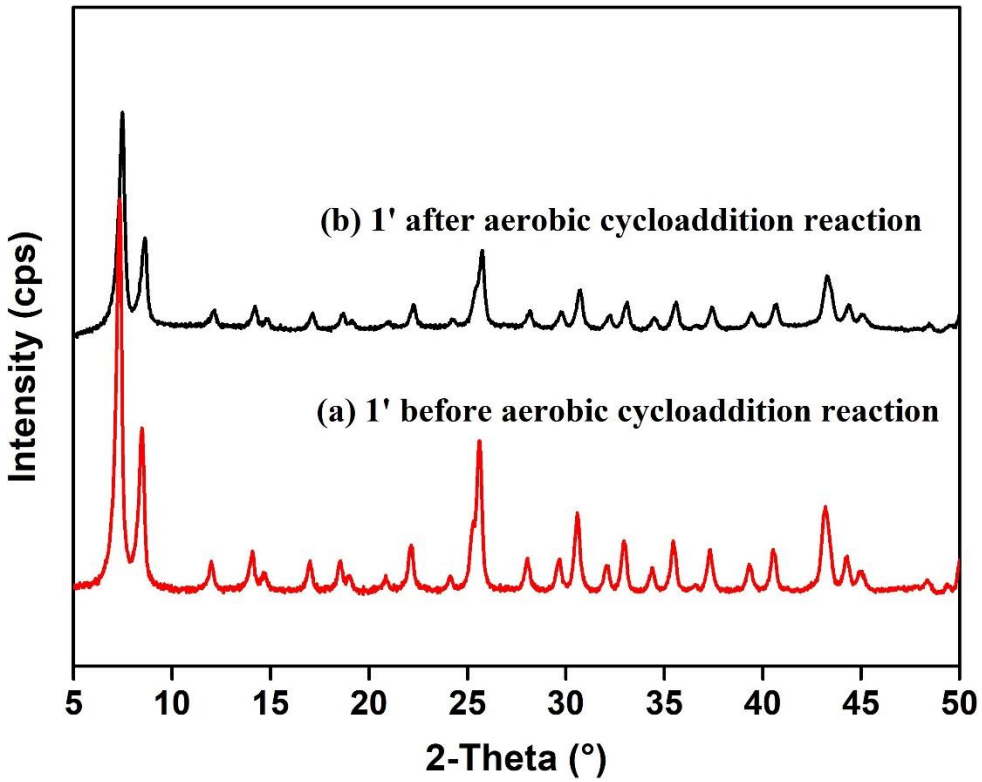

Figure S43. PXRD patterns of fresh **1′** (a) and **1′** after cycloaddition reaction (b).

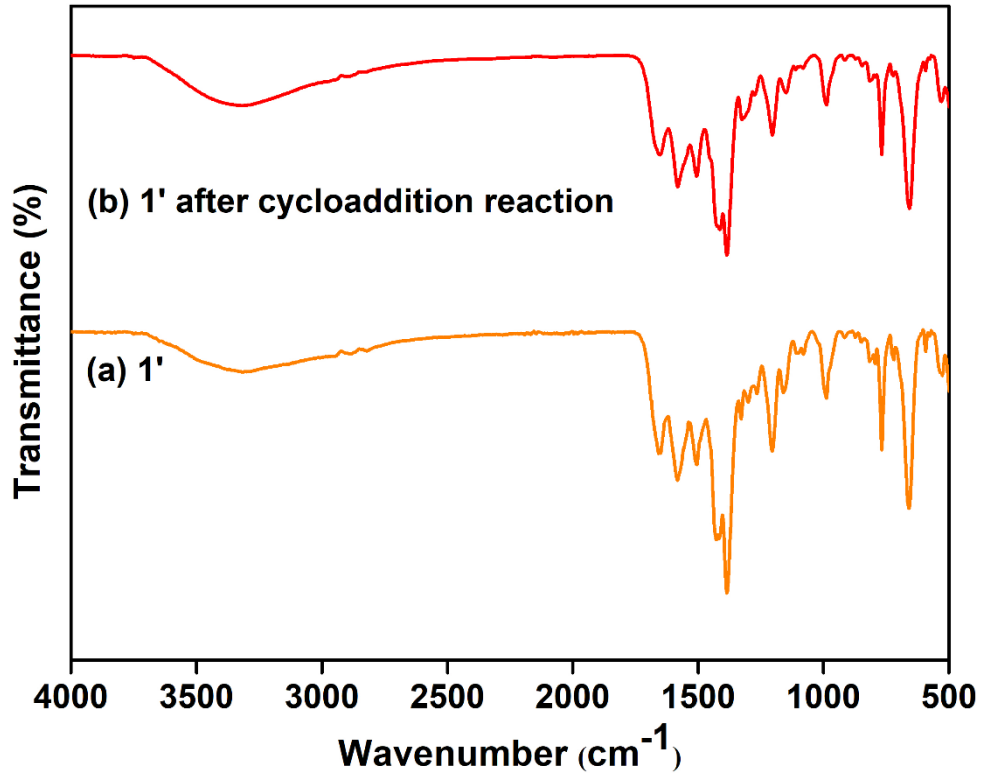

Figure S44. ATR-IR spectra of fresh **1′** (a) and **1′** after cycloaddition reaction (b).

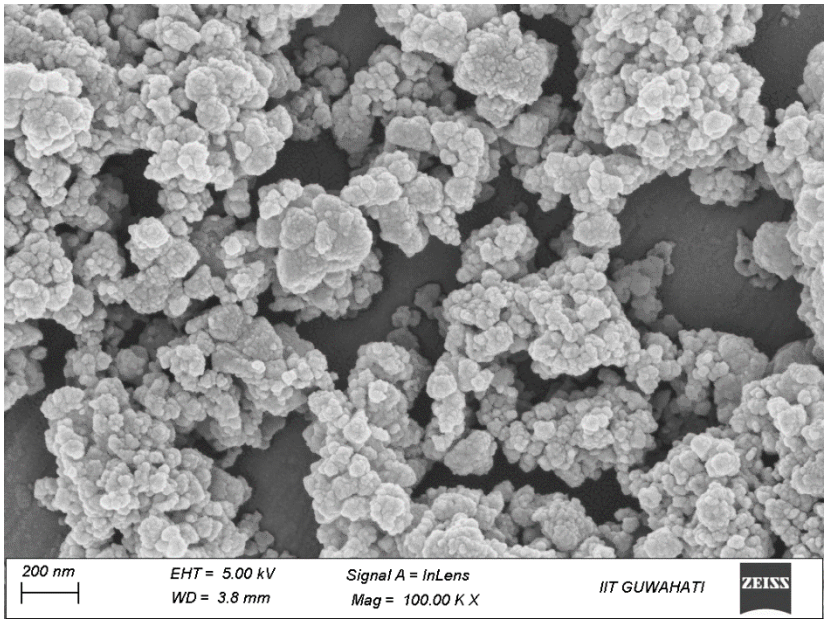

Figure S45. FE-SEM image of **1′** after cycloaddition reaction.

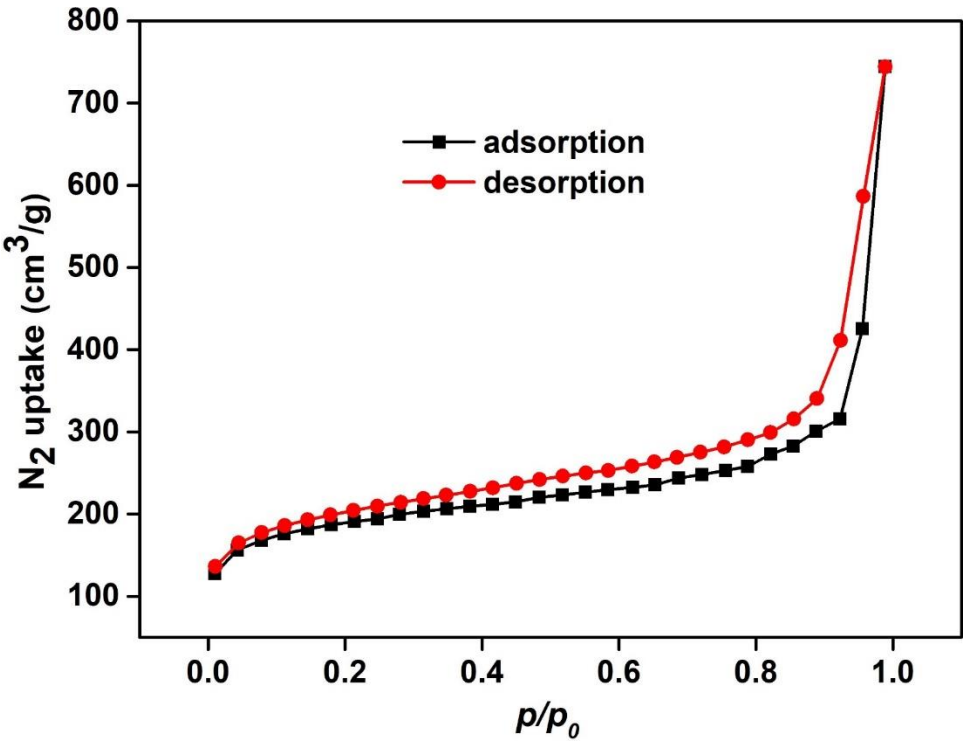

Figure S46. N_2 adsorption (black squares) and desorption (red circles) isotherms of thermally activated reused **1′** after cycloaddition reaction recorded at –196 °C.

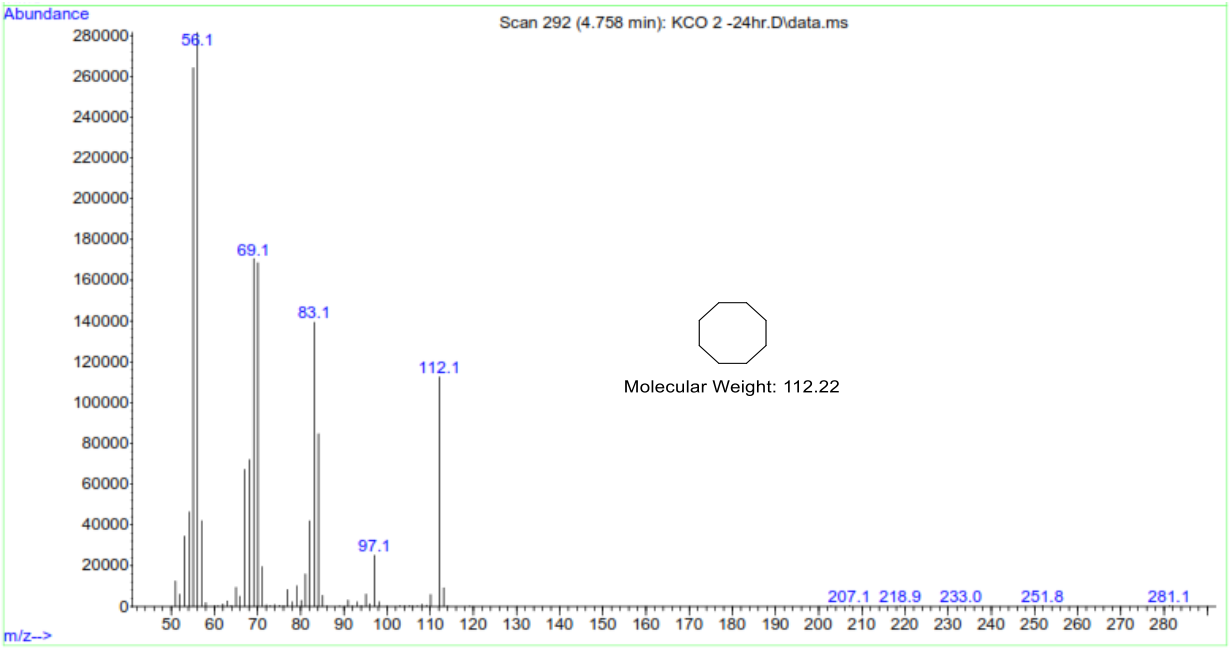

Figure S47. GC-MS trace of cyclooctane,

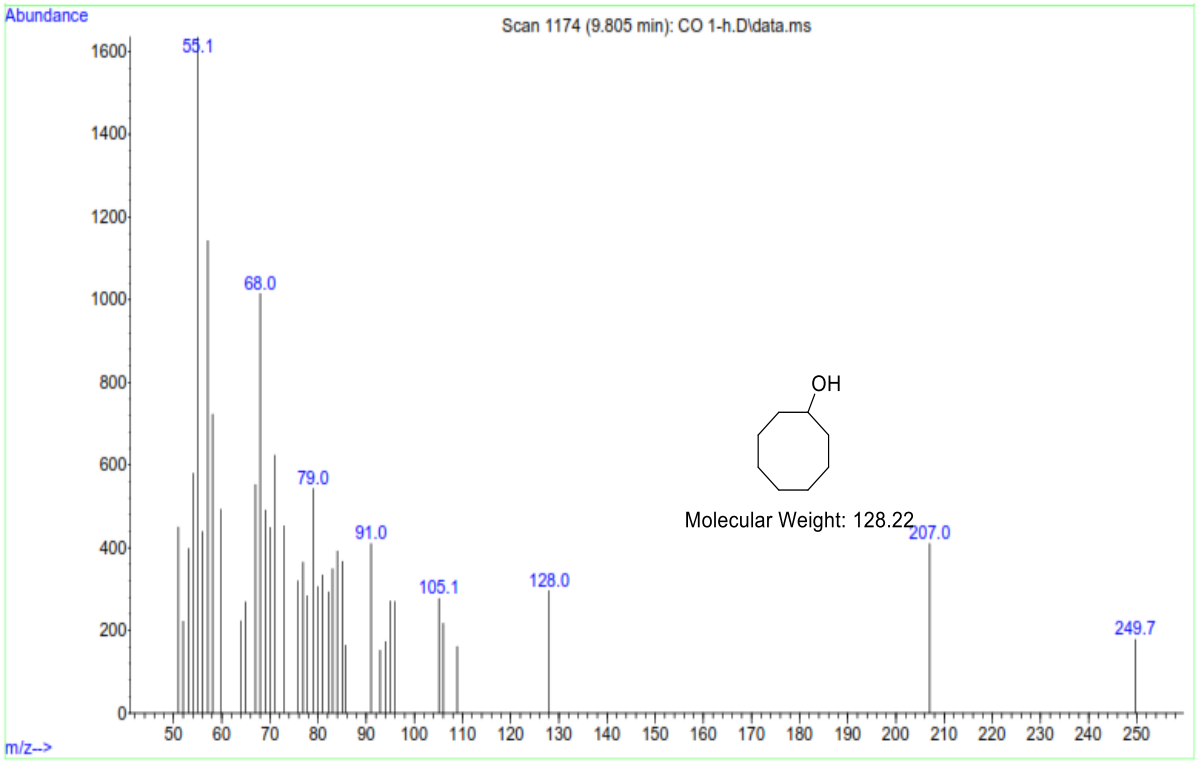

Figure S48. GC-MS trace of cyclooctanol.

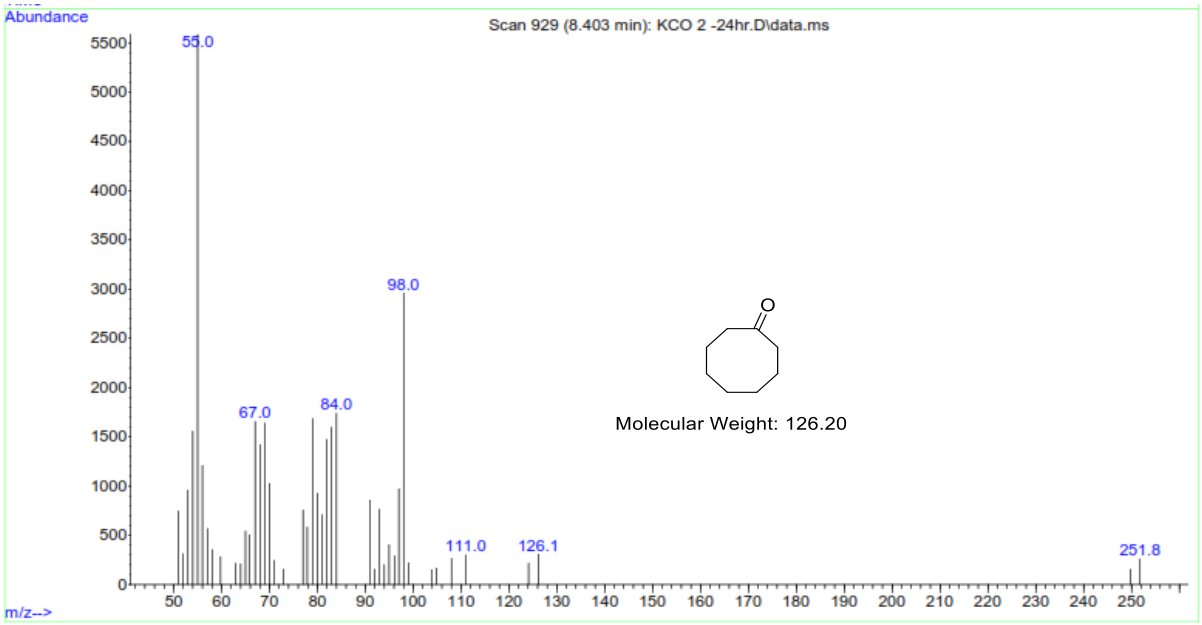

Figure S49. GC-MS trace of cyclooctanone.

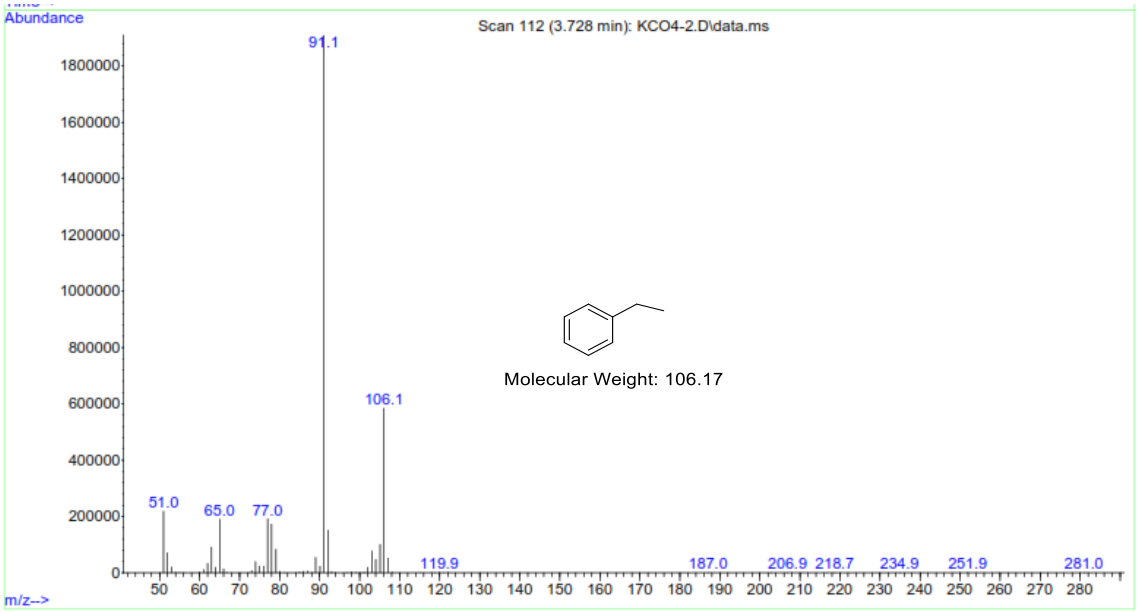

Figure S50. GC-MS trace of ethylbenzene.

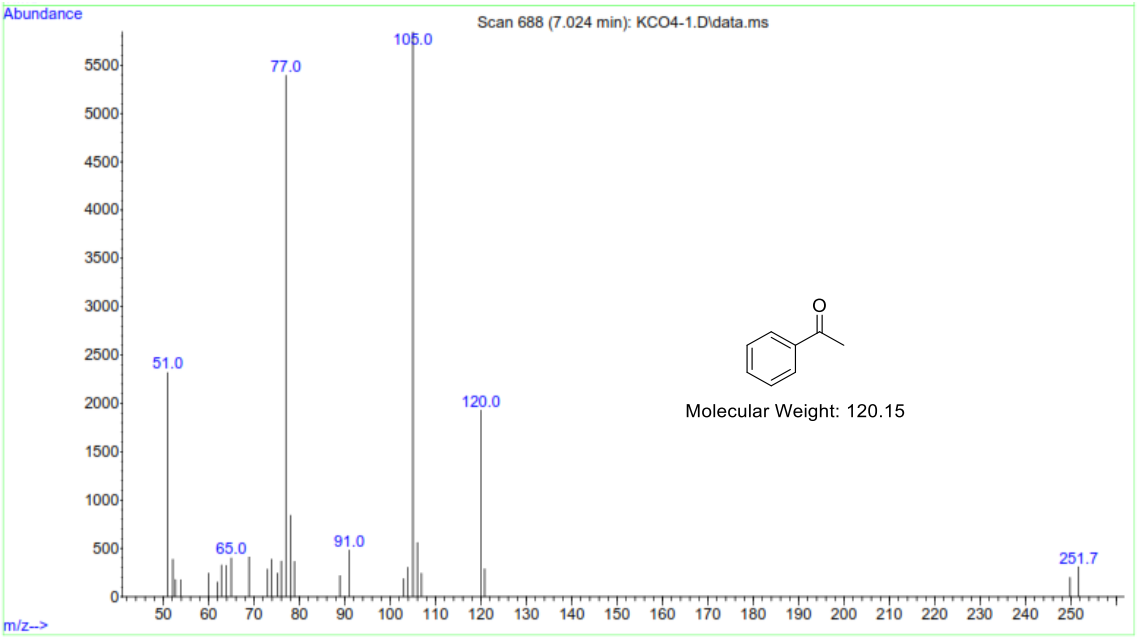

Figure S51. GC-MS trace of acetophenone.

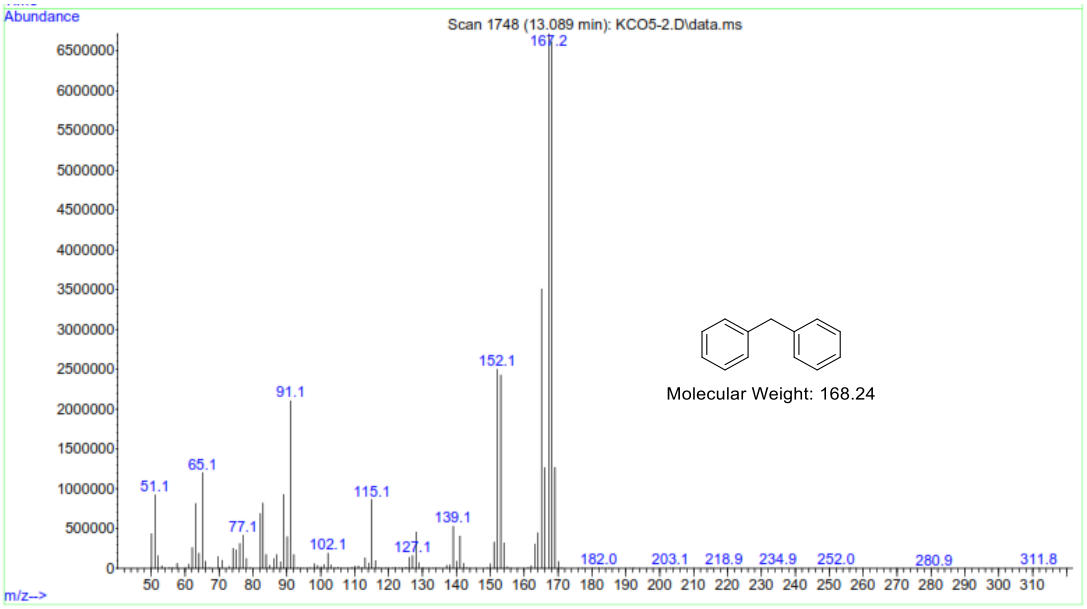

Figure S52. GC-MS trace of diphenylmethane.

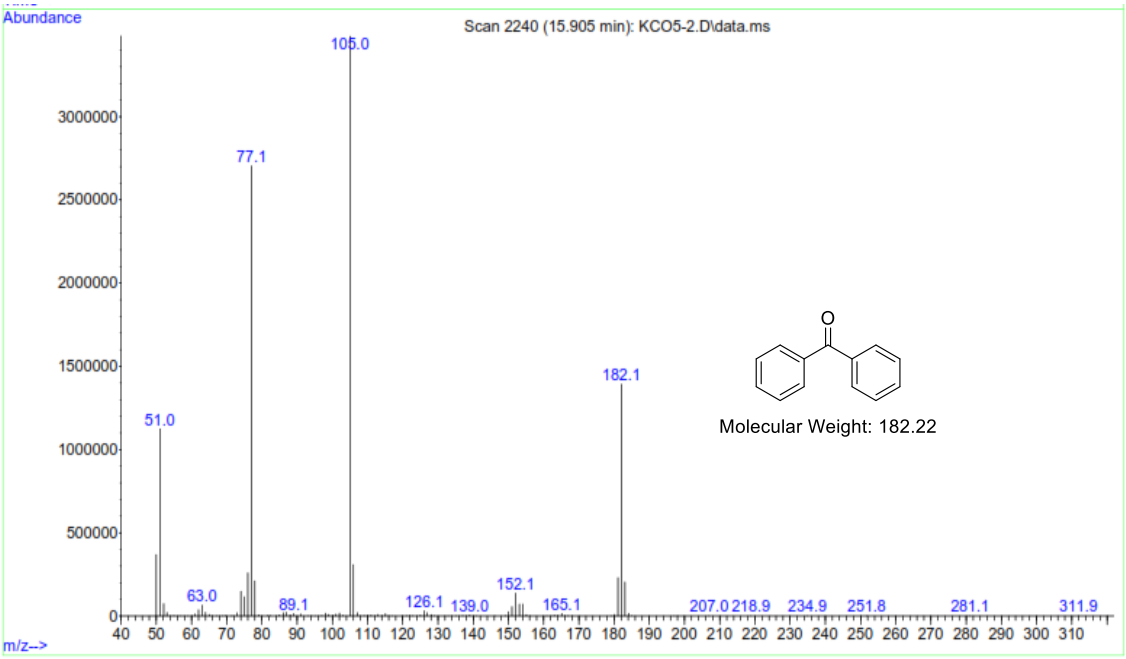

Figure S53. GC-MS trace of benzophenone.

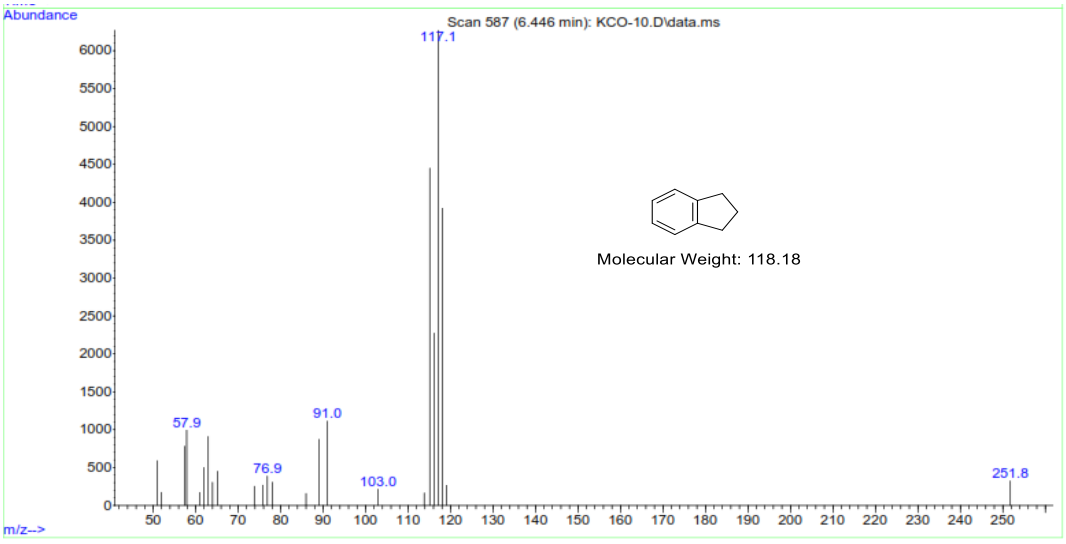

Figure S54. GC-MS trace of indane.

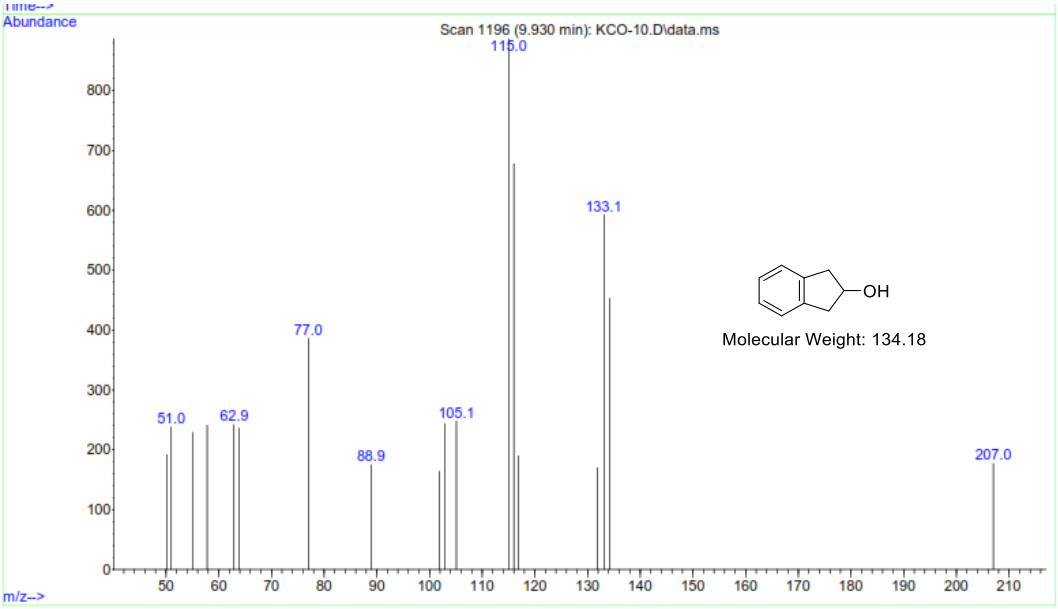

Figure S55. GC-MS trace of indanol.

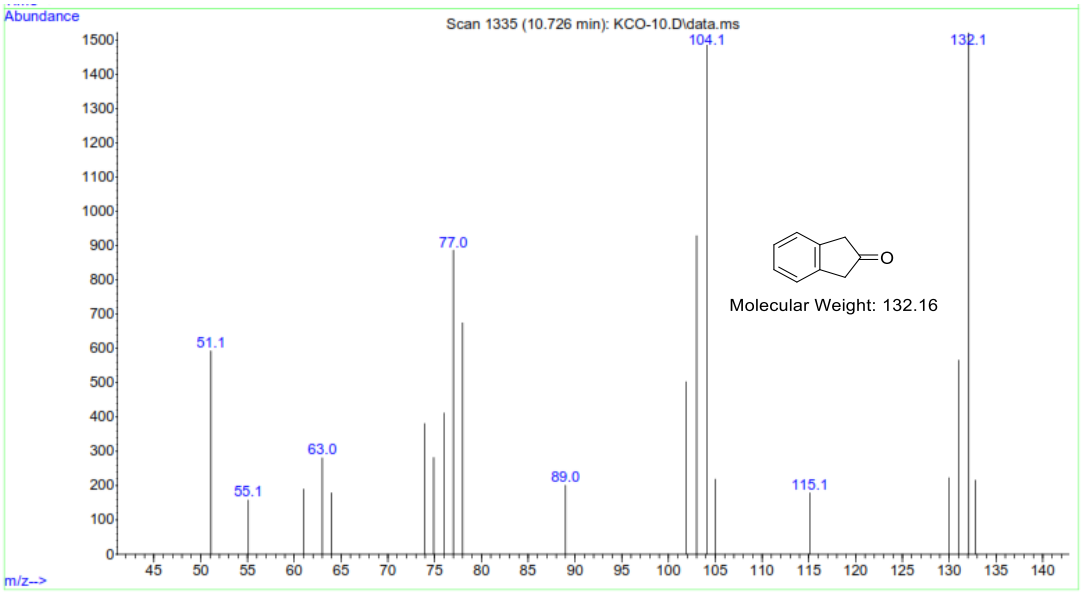

Figure S56. GC-MS trace of indanone.

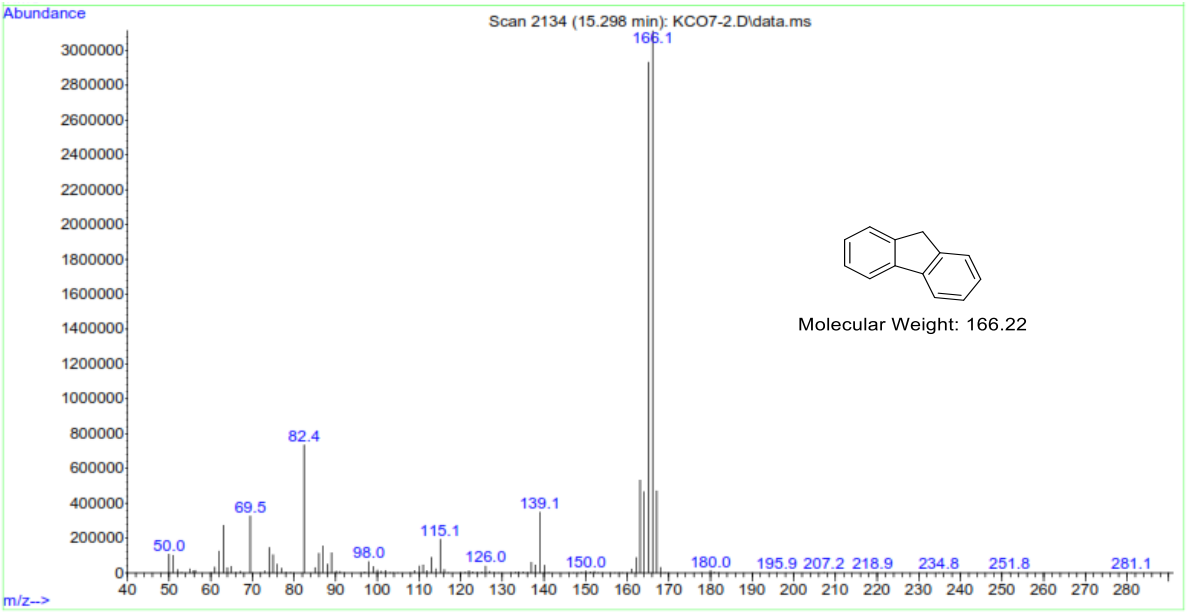

Figure S57. GC-MS trace of 9H-fluorene.

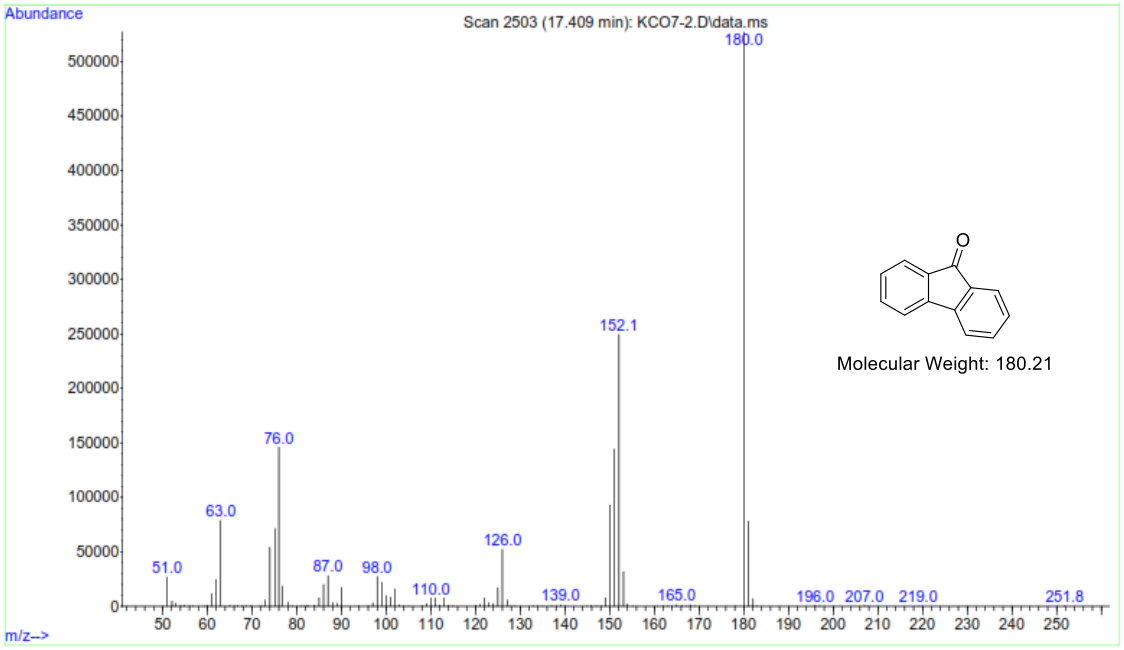

Figure S58. GC-MS trace of 9H-fluoren-9-one.

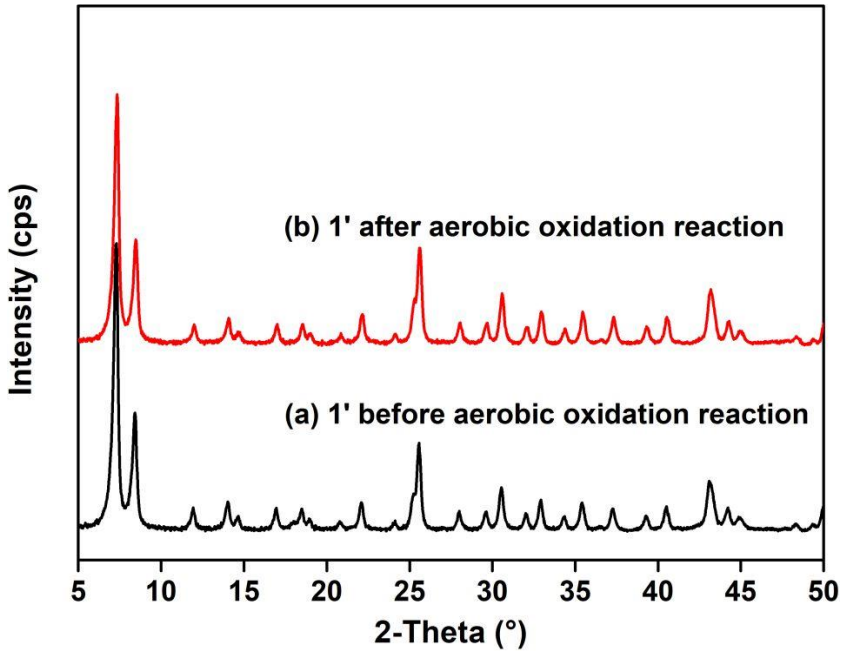

Figure S59. PXRD patterns of fresh **1′** (a) and two times reused **1′** for the aerobic oxidation of cyclooctane (b).

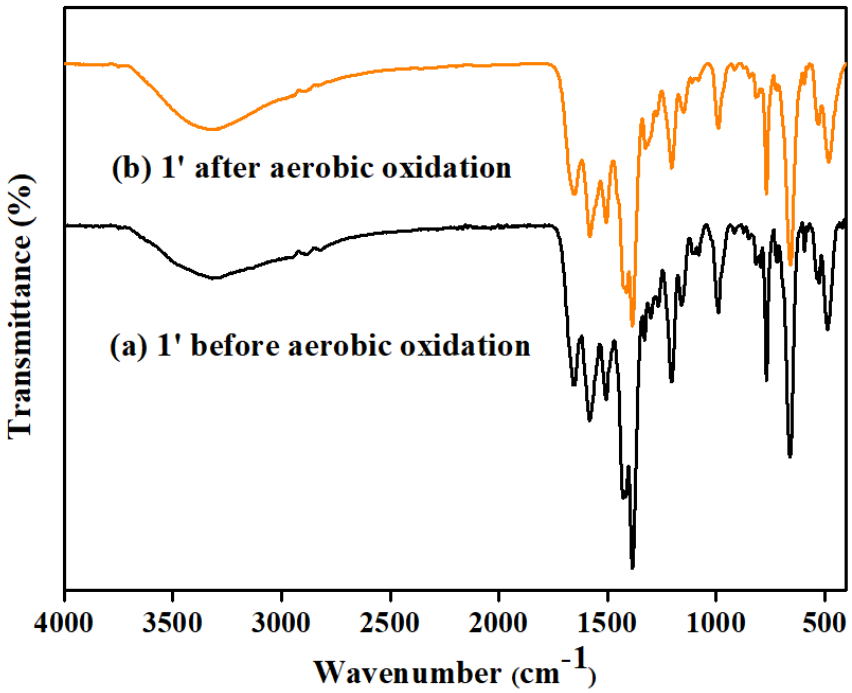

Figure S60. ATR-IR spectra of fresh **1′** (a) and two times reused **1′** for the aerobic oxidation of cyclooctane (b).

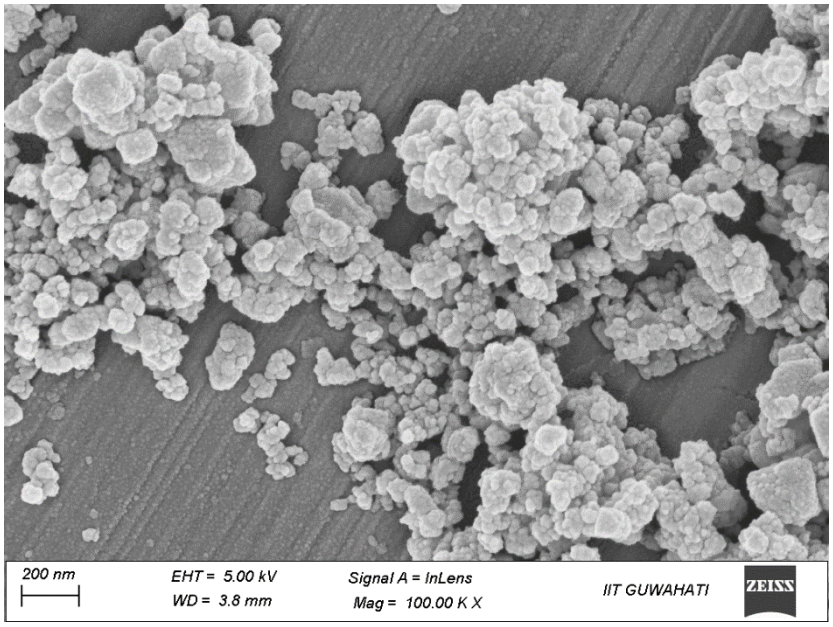

Figure S61. FE-SEM image of **1′** after two times reused **1′** for the aerobic oxidation of cyclooctane.

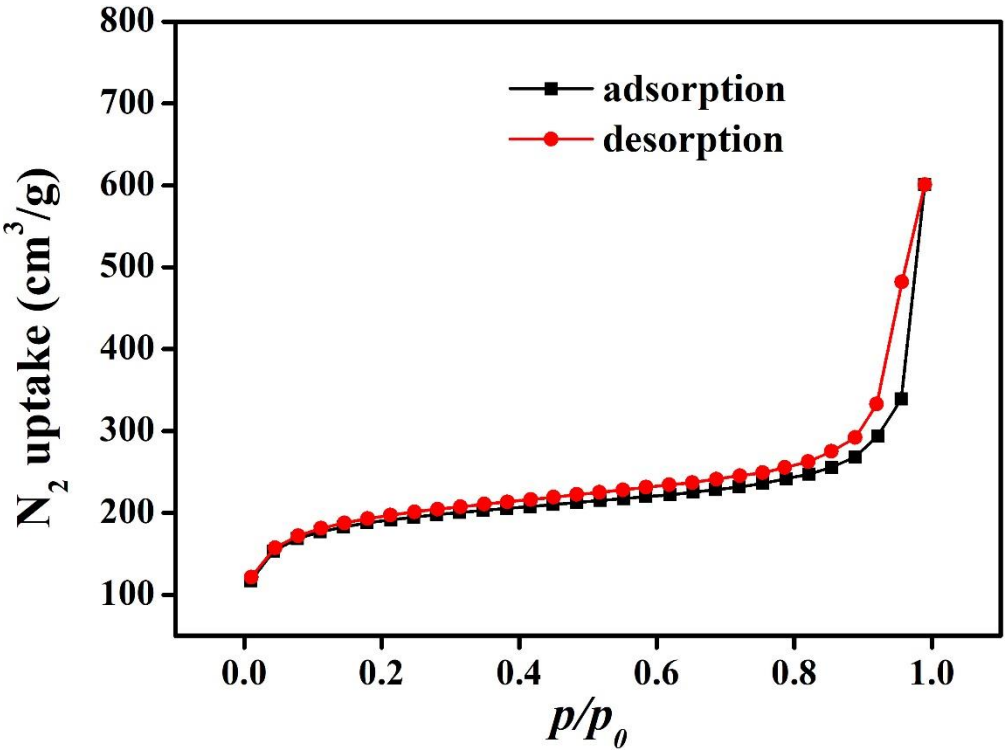

Figure S62. N_2 adsorption (black squares) and desorption (red circles) isotherms of thermally activated reused **1′** after aerobic oxidation of cyclooctane recorded at –196 °C.

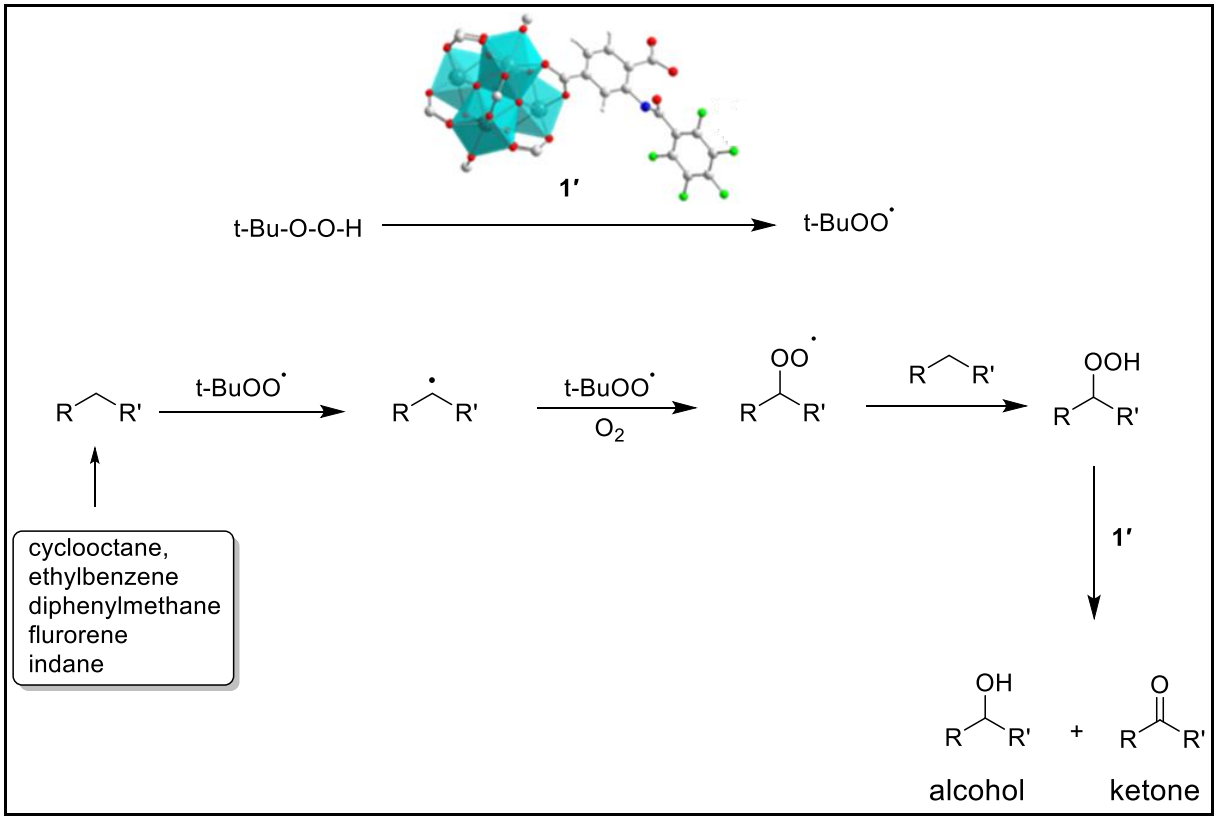

Scheme S2. A proposed reaction mechanism for the aerobic oxidation of hydrocarbons using **1′**.

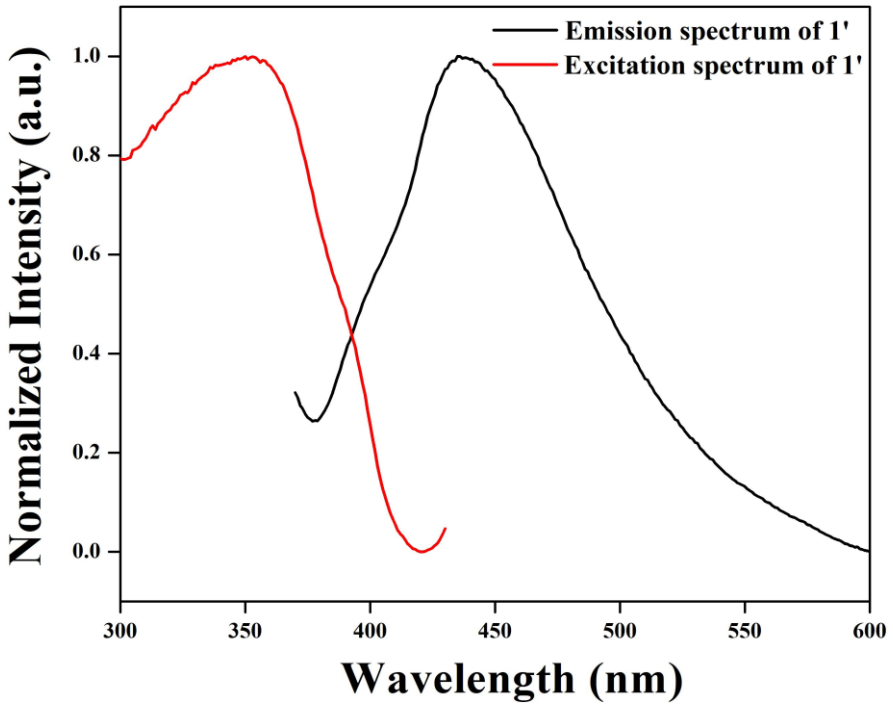

Figure S63. Excitation (red) and emission (black) spectra of **1′**.

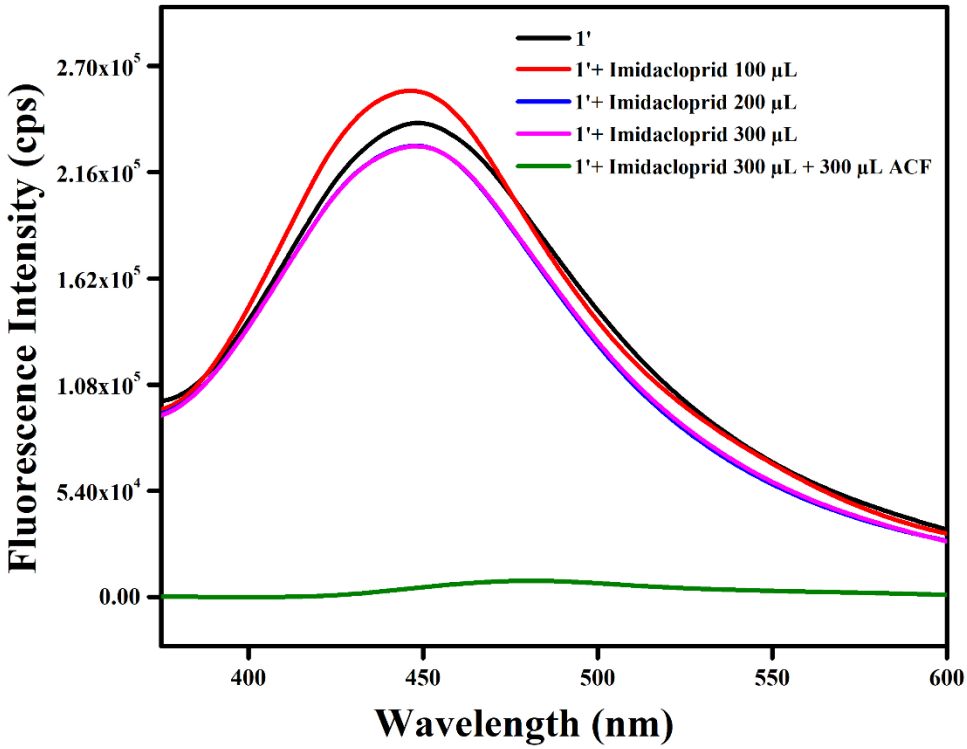

Figure S64. Change in fluorescence emission intensity of activated **1′** upon addition of 300 µL of 10 mM aclonifen (ACF) in presence of 300 µL of 10 mM imidacloprid solution.

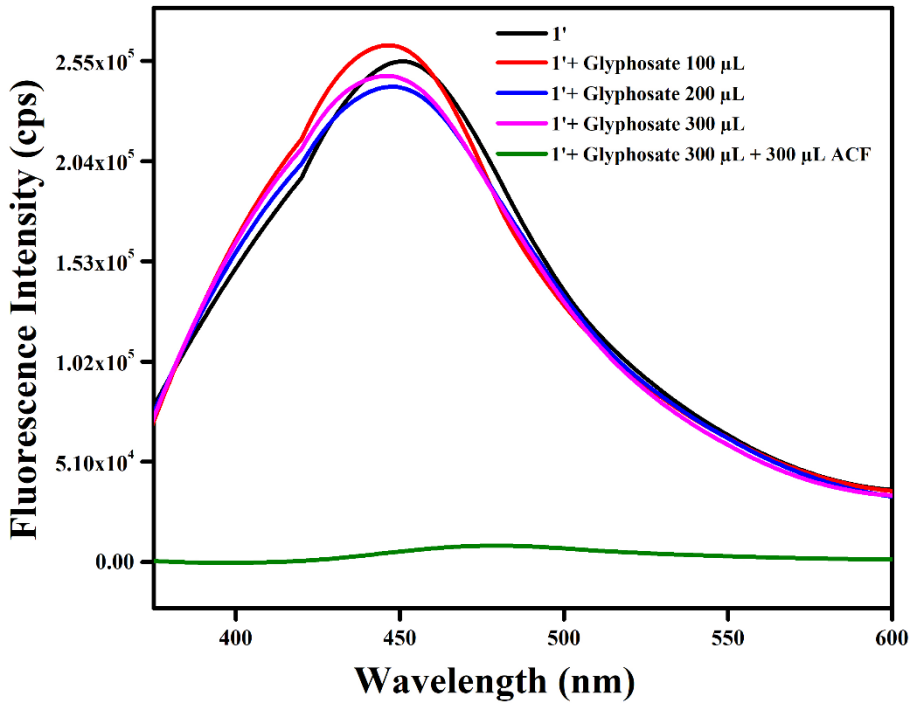

Figure S65. Change in fluorescence emission intensity of activated **1′** upon addition of 300 µL of 10 mM aclonifen (ACF) in presence of 300 µL of 10 mM glyphosate solution.

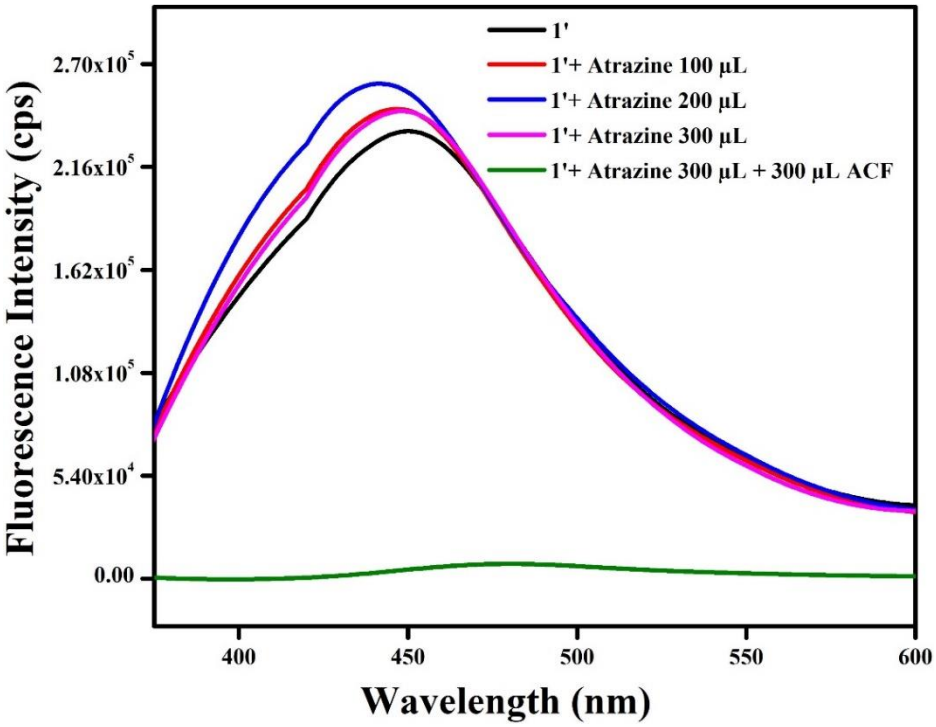

Figure S66. Change in fluorescence emission intensity of activated **1′** upon addition of 300 µL of 10 mM aclonifen (ACF) in presence of 300 µL of 10 mM atrazine solution (λ_{ex} = 350 nm and λ_{em} = 450 nm).

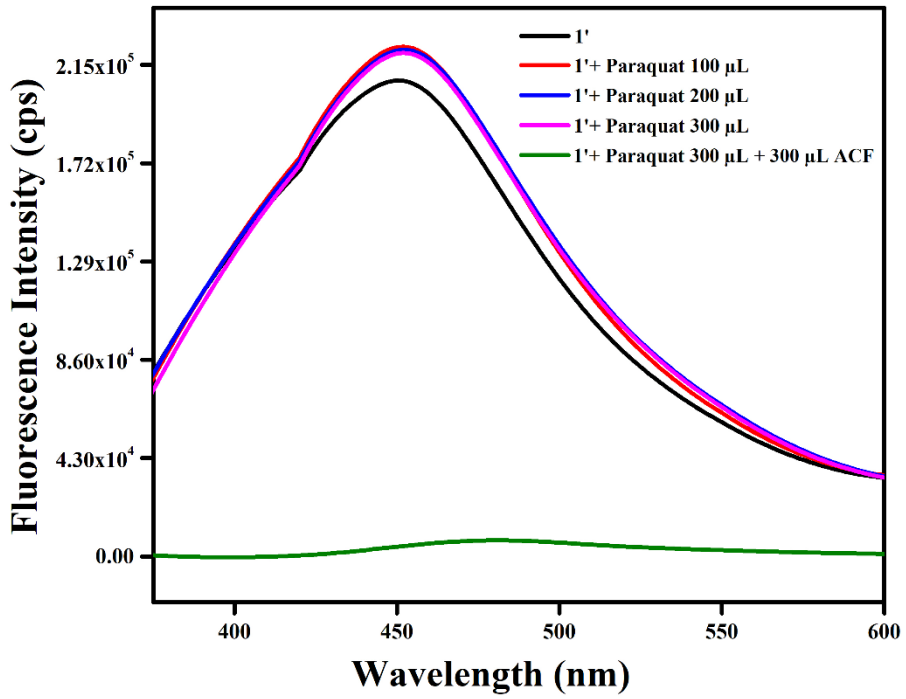

Figure S67. Change in fluorescence emission intensity of activated **1′** upon addition of 300 µL of 10 mM aclonifen (ACF) in presence of 300 µL of 10 mM paraquat solution (λ_{ex} = 350 nm and λ_{em} = 450 nm).

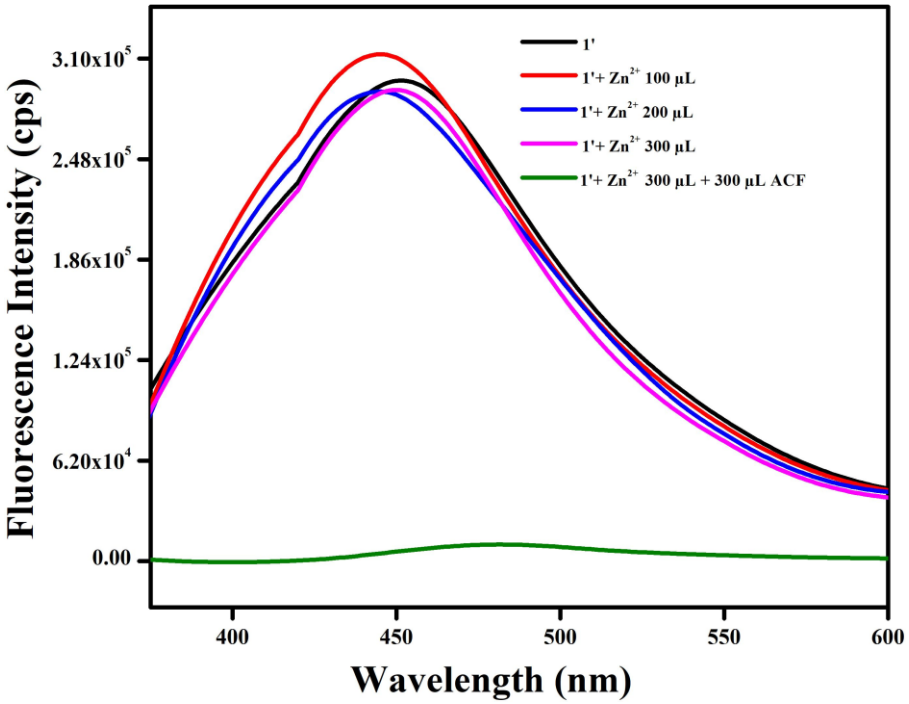

Figure S68. Change in fluorescence emission intensity of activated **1′** upon addition of 300 µL of 10 mM aclonifen (ACF) in presence of 300 µL of 10 mM Zn^{2+} solution (λ_{ex} = 350 nm and λ_{em} = 450 nm).

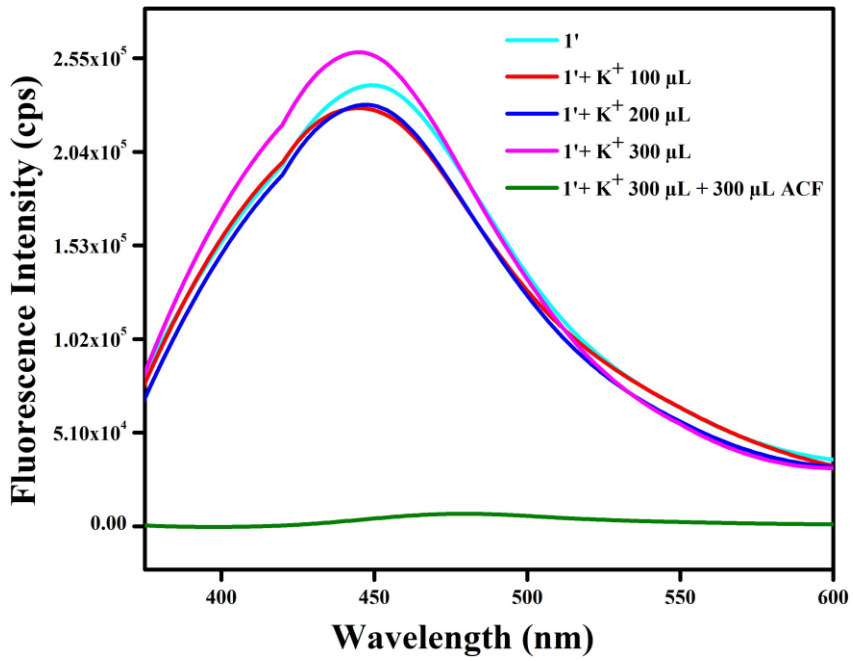

Figure S69. Change in fluorescence emission intensity of activated **1′** upon addition of 300 µL of 10 mM aclonifen (ACF) in presence of 300 µL of 10 mM K^{+} solution (λ_{ex} = 350 nm and λ_{em} = 450 nm).

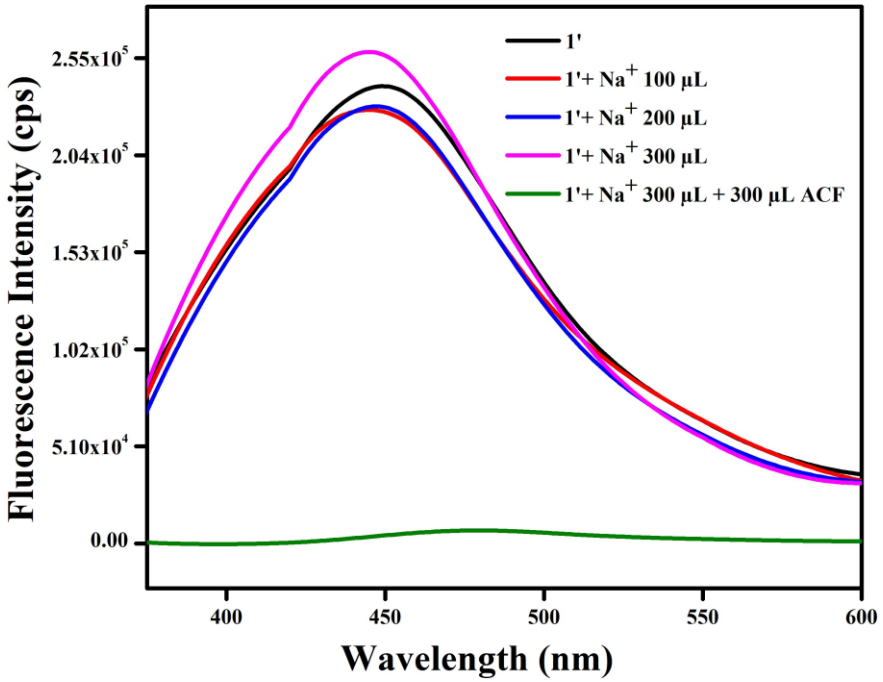

Figure S70. Change in fluorescence emission intensity of activated **1′** upon addition of 300 µL of 10 mM aclonifen (ACF) in presence of 300 µL of 10 mM Na^+ solution (λ_{ex} = 350 nm and λ_{em} = 450 nm).

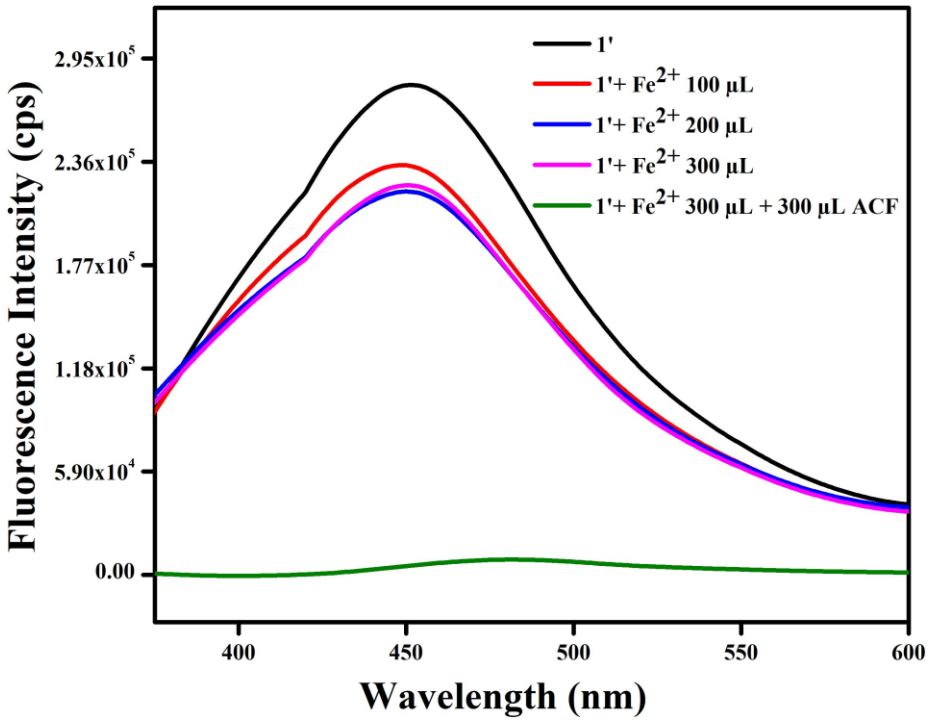

Figure S71. Change in fluorescence emission intensity of activated **1′** upon addition of 300 µL of 10 mM aclonifen (ACF) in presence of 300 µL of 10 mM Fe^{2+} solution (λ_{ex} = 350 nm and λ_{em} = 450 nm).

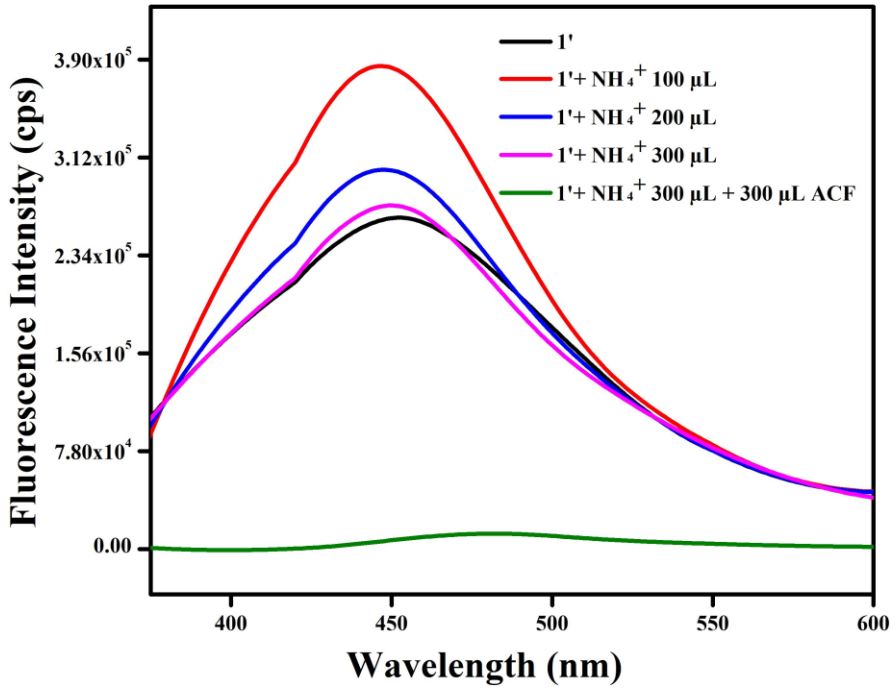

Figure S72. Change in fluorescence emission intensity of activated **1′** upon addition of 300 µL of 10 mM aclonifen (ACF) in presence of 300 µL of 10 mM NH_4^+ solution (λ_{ex} = 350 nm and λ_{em} = 450 nm).

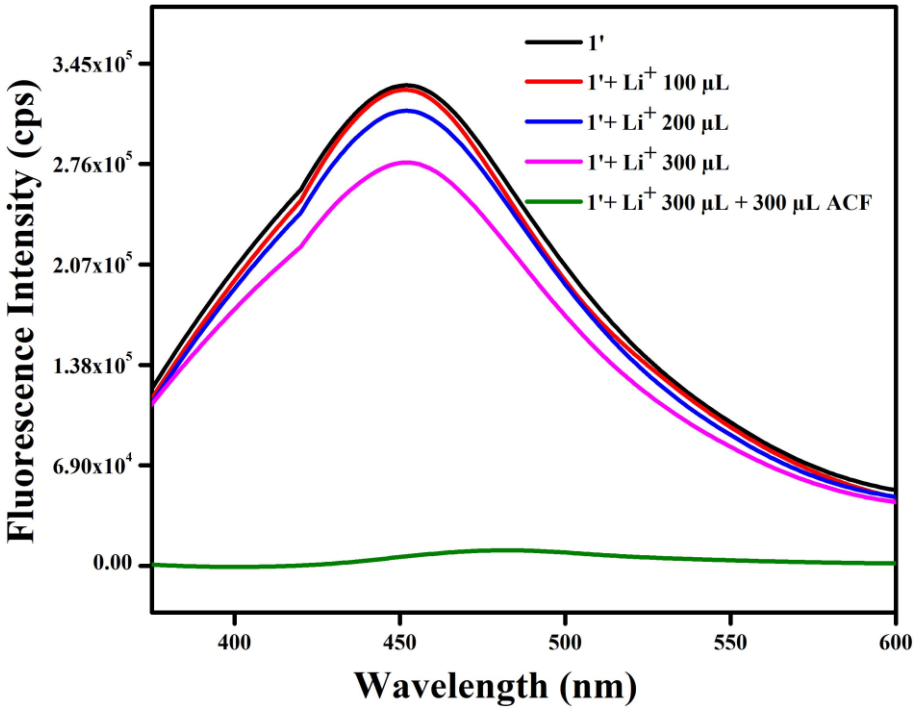

Figure S73. Change in fluorescence emission intensity of activated **1′** upon addition of 300 µL of 10 mM aclonifen (ACF) in presence of 300 µL of 10 mM Li^+ solution (λ_{ex} = 350 nm and λ_{em} = 450 nm).

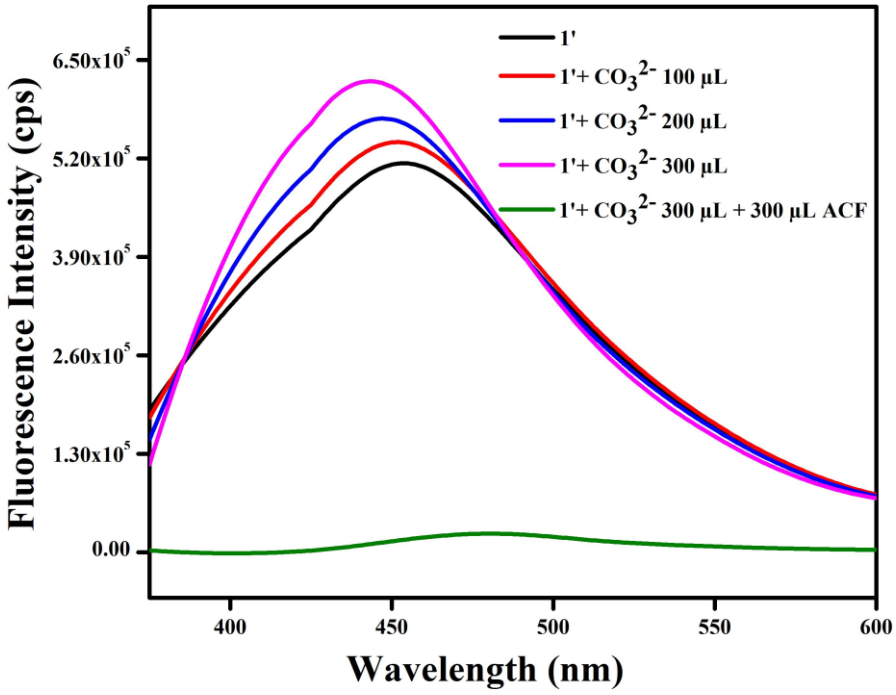

Figure S74. Change in fluorescence emission intensity of activated **1′** upon addition of 300 µL of 10 mM aclonifen (ACF) in presence of 300 µL of 10 mM CO_3^{2-} solution (λ_{ex} = 350 nm and λ_{em} = 450 nm).

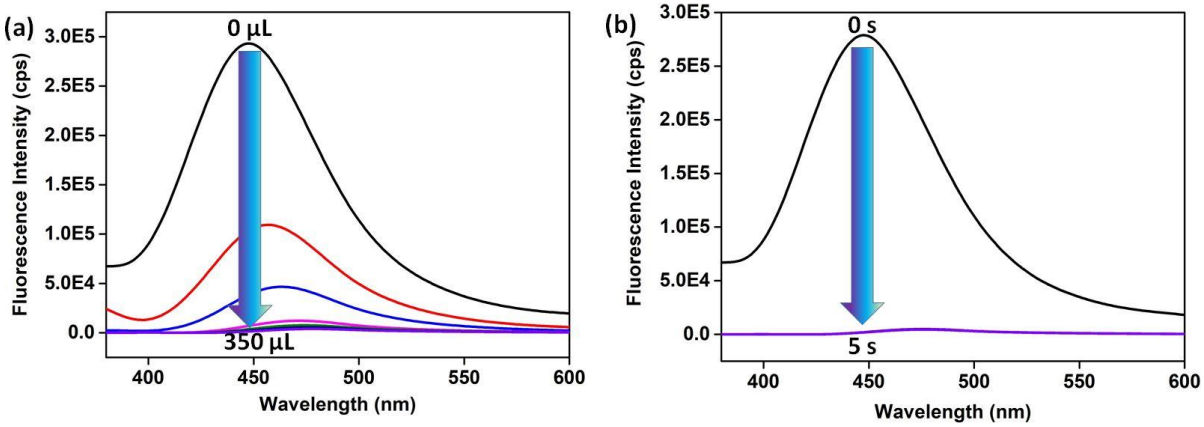

Fig. S75. (a) Change in fluorescence of **1** after gradual addition of ACF from 0 to 350 µL and (b) as a function of time.

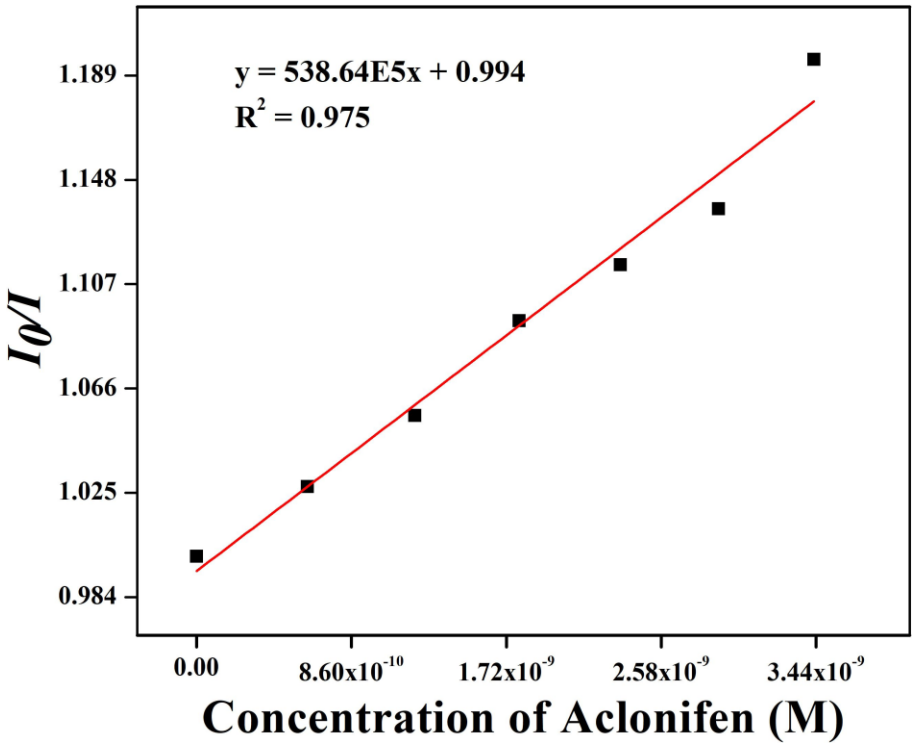

Figure S76. Stern-Volmer plot for fluorescence quenching of activated **1′** against increasing concentration of aclonifen (ACF).

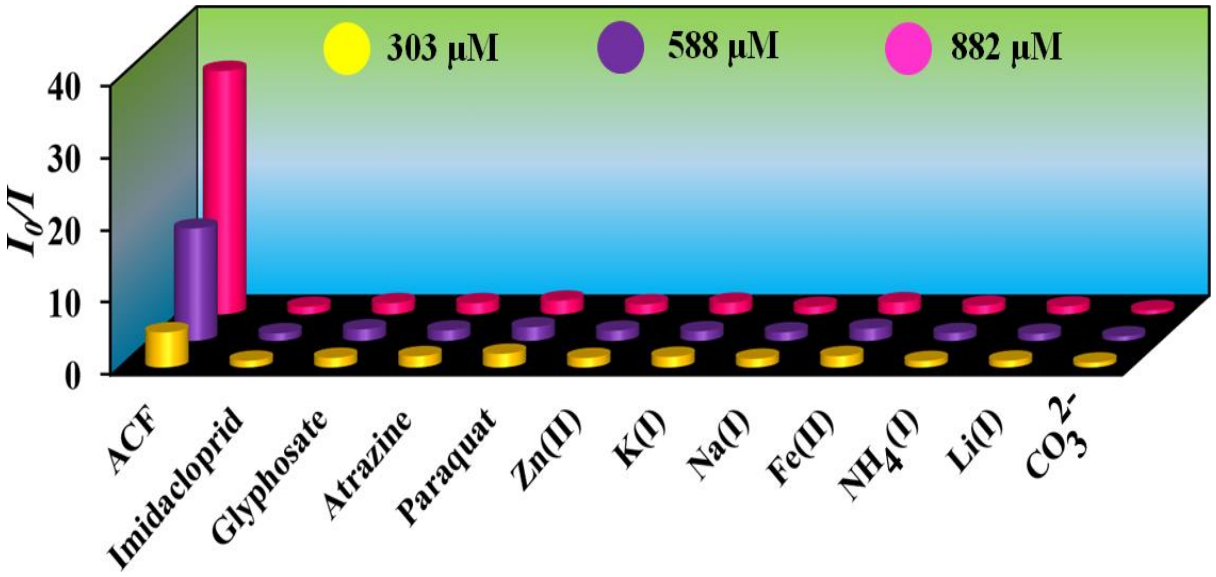

Figure S77. Stern-Volmer plot for the decrease in luminescence intensities of **1′** with gradual addition of various analytes in case of aclonifen (ACF) sensing.

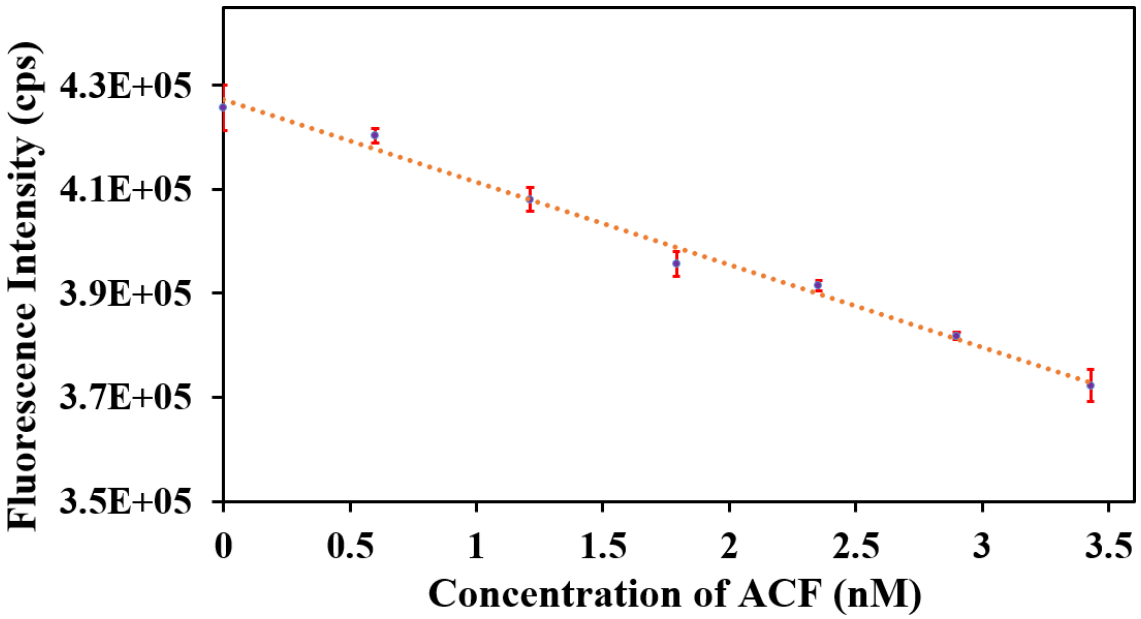

Figure S78. Change in fluorescence emission intensity of activated **1′** in as a function of aclonifen (ACF) concentration.

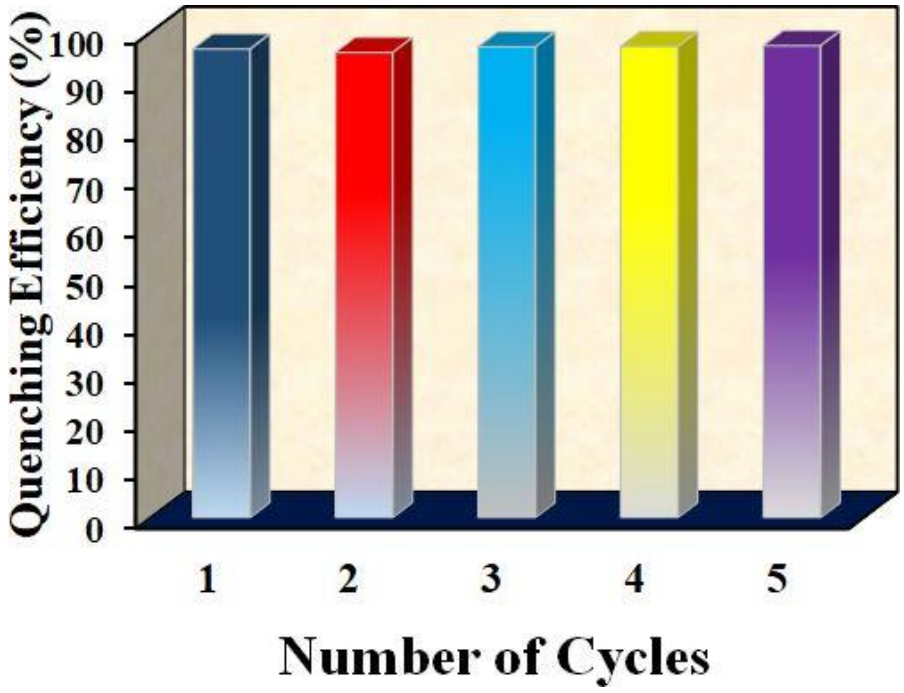

Figure S79. Recyclability test of probe **1'** for the sensing aclonifen (ACF) in methanol.

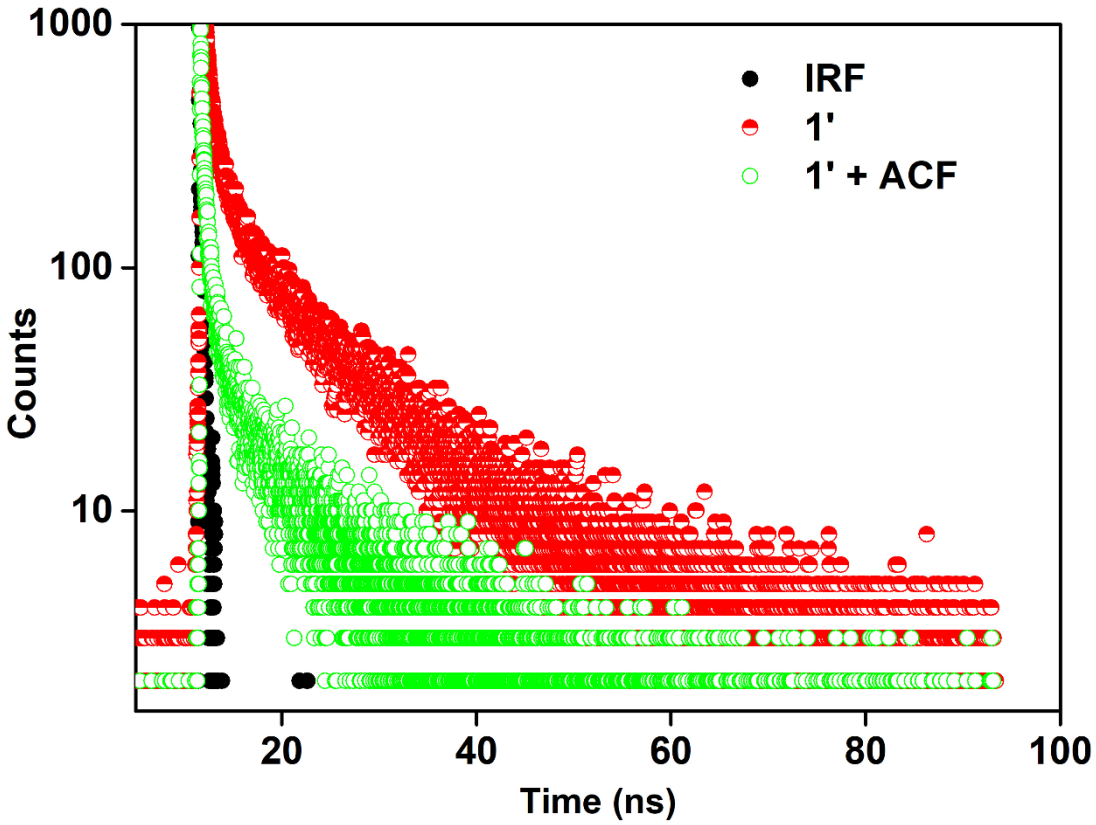

Figure S80. Lifetime decay profile of **1′** in absence and presence of ACF solution (λ_{ex} = 350 nm, monitored at 374 nm). Here, IRF = instrument response function.

Table S2. Fluorescence lifetimes of **1′** before and after the addition of ACF solution (λ_{ex} = 374 nm, pulsed diode laser).

Volume of ACF Solution Added (μL)	a_1	a_2	a_3	τ_1 (ns)	τ_2 (ns)	τ_3 (ns)	$<\tau>$* (ns)	χ^2
0	0.28	0.46	0.26	0.88	9.54	0.09	4.65	1.16
300	0.31	0.47	0.19	0.63	4.68	0.08	2.41	1.09

* $<\tau> = a_1\tau_1 + a_2\tau_{2+} a_3\tau_3$

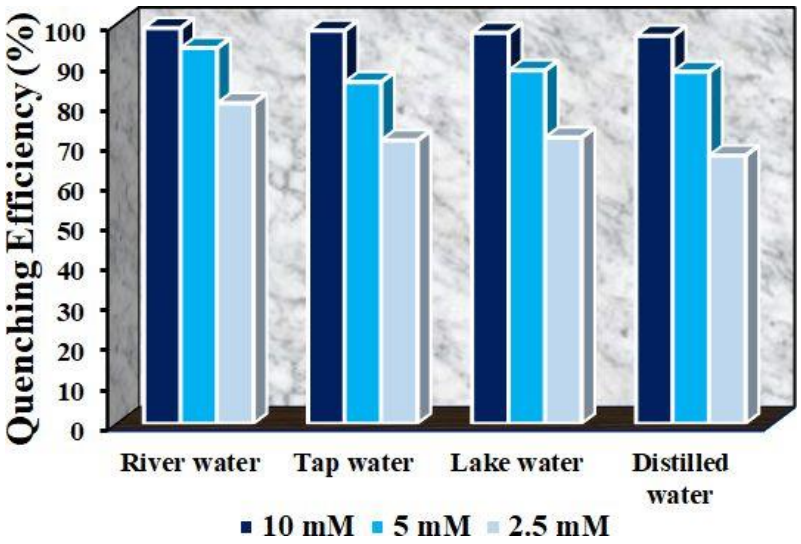

Figure S81. Quenching efficiency of activated **1′** with introduction of aclonifen (ACF) (10 mM, 300 µL) in different aqueous media.

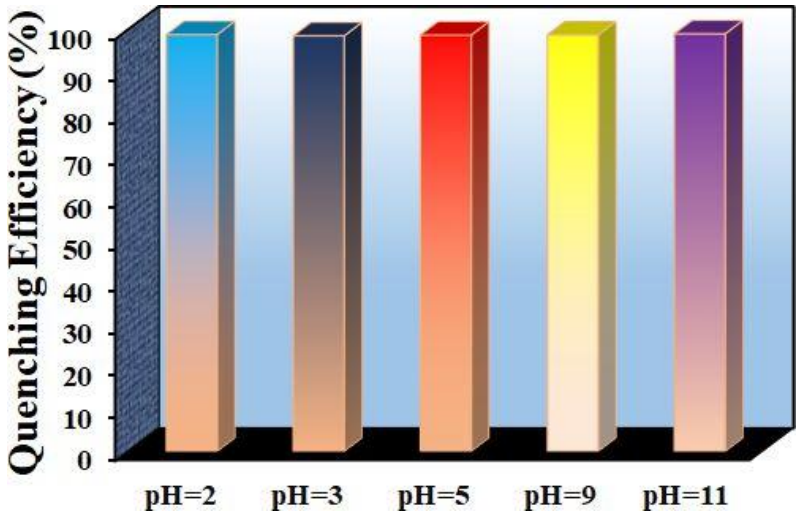

Figure S82. Quenching efficiency of activated **1′** with introduction of aclonifen (ACF) (10 mM, 300 µL) in different pH media.

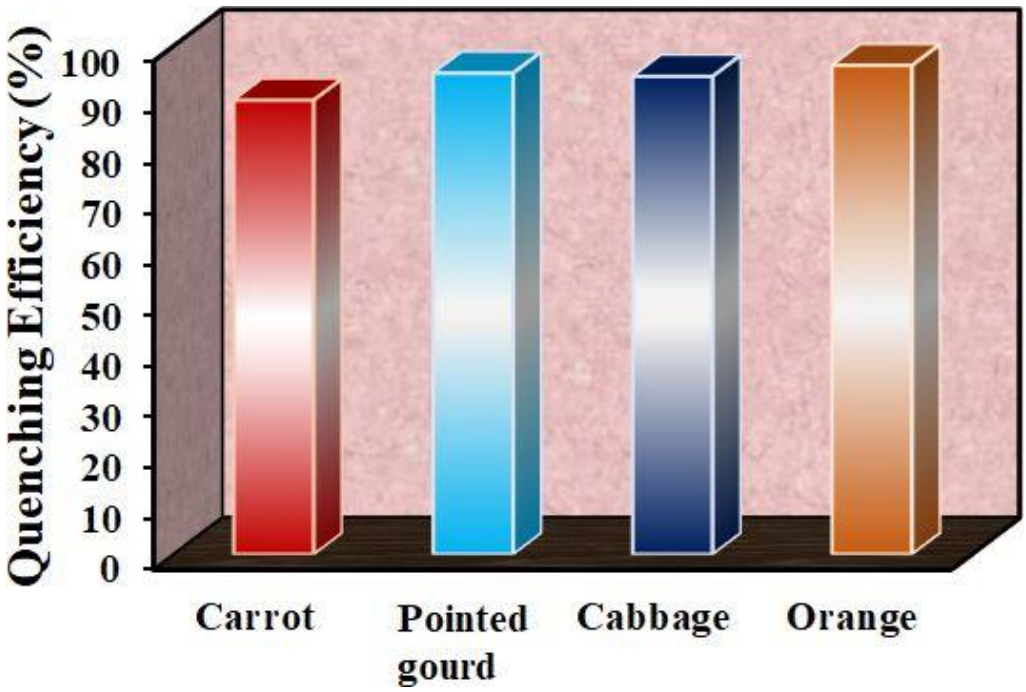

Figure S83. Quenching efficiency of activated **1′** with introduction of aclonifen (ACF) (10 mM, 300 µL) in different vegetable samples.

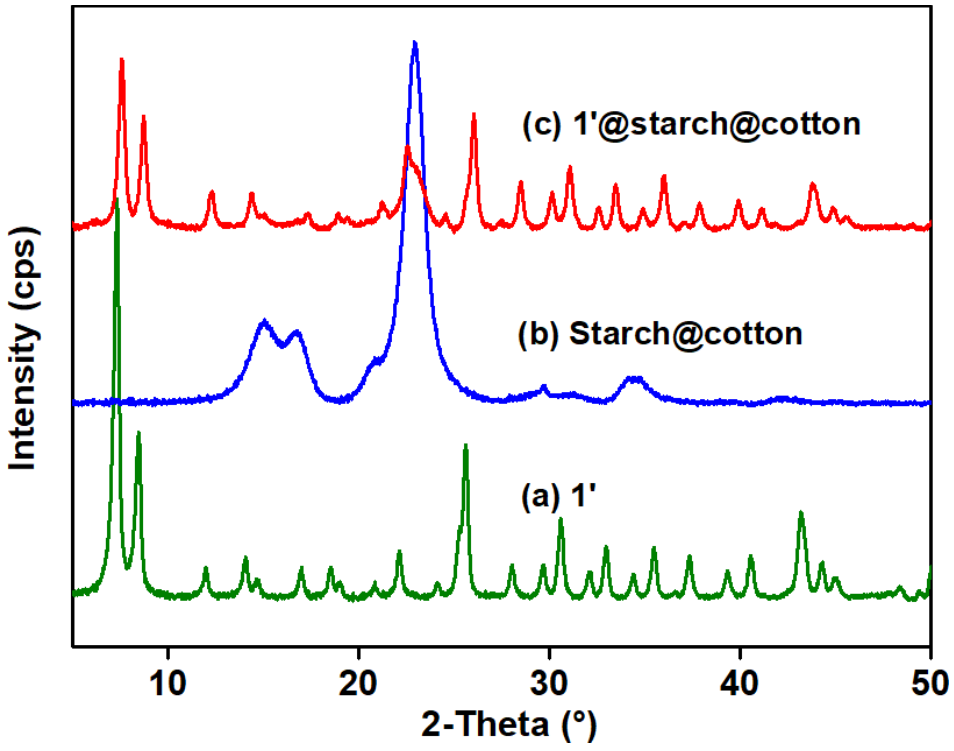

Figure S84. PXRD patterns of (a) compound **1′**, (b) starch@cotton and (c) **1′@ starch@cotton** composite.

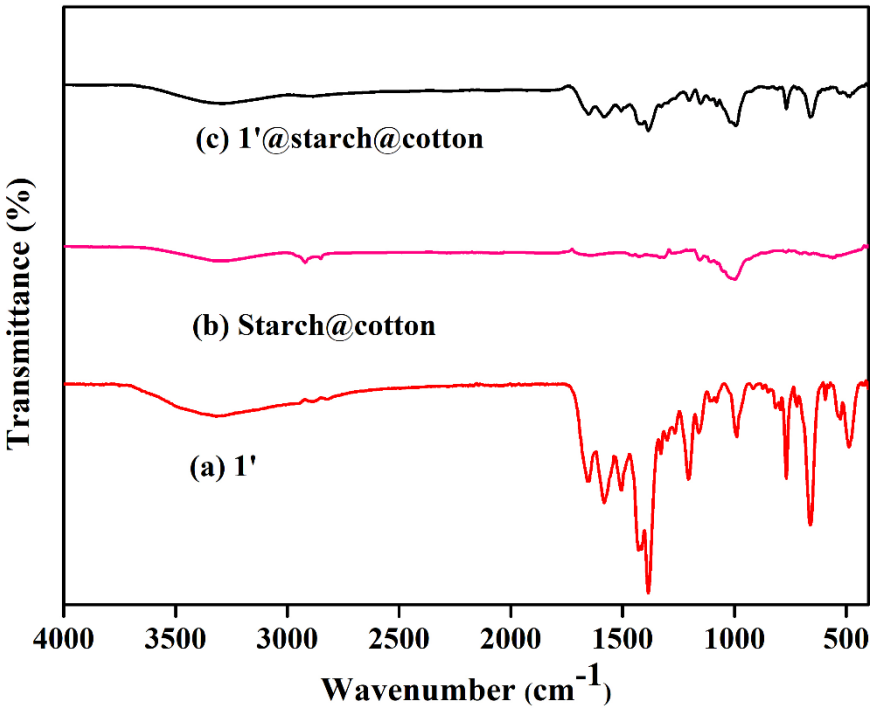

Figure S85. ATR-IR spectra of compound (a) **1′**, (b) starch@cotton, and (c) **1′@ starch@cotton** composite.

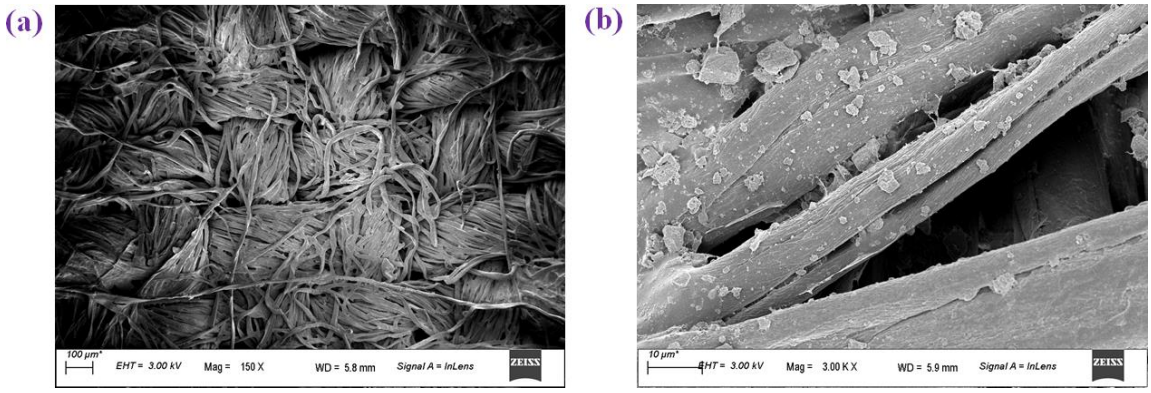

Figure S86. FE-SEM images of (a) starch@cotton and (b) **1′@ starch@cotton** composite.

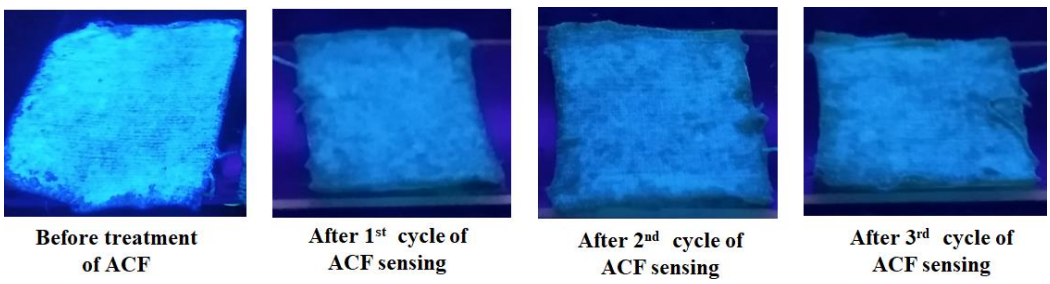

Figure S87. Digital images of **1′@starch@cotton** composite after each cycle of sensing of ACF.

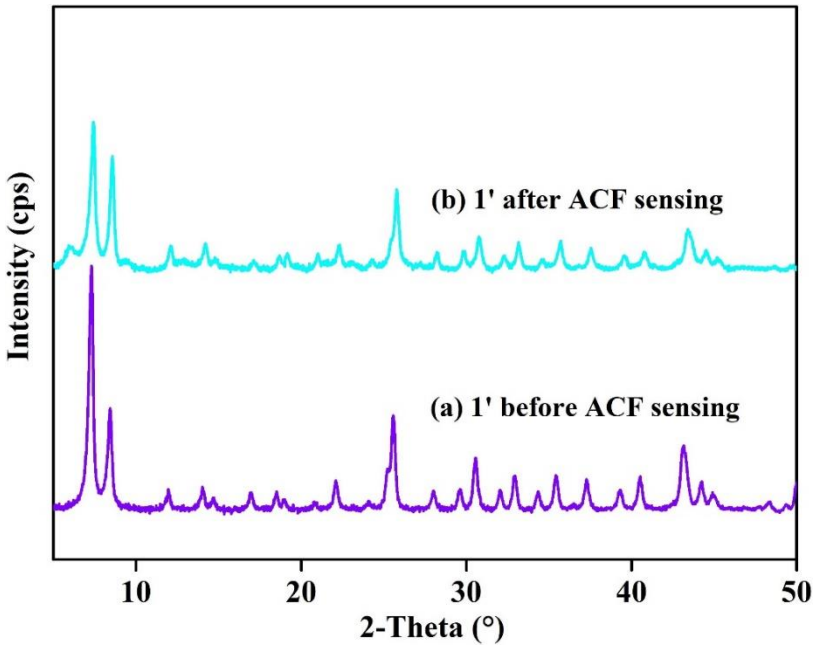

Figure S88. PXRD patterns of fresh **1′** (a) and **1′** after ACF sensing (b).

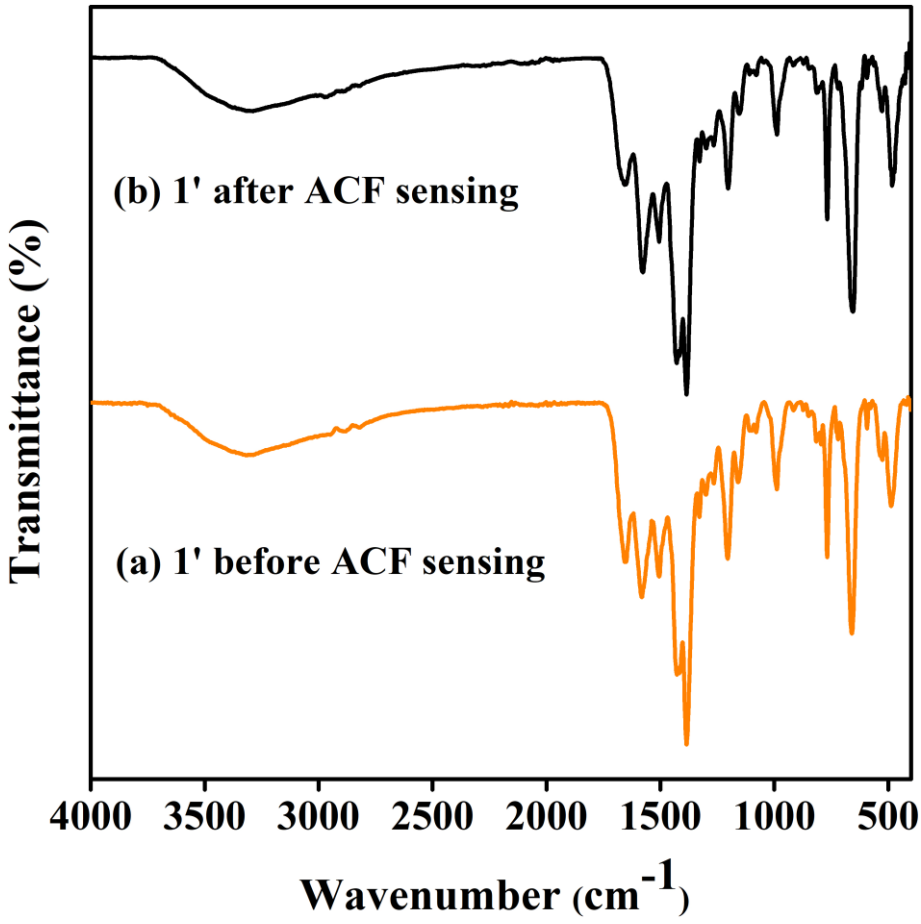

Figure S89. ATR-IR spectra of fresh **1′** (a) and **1′** after ACF sensing.

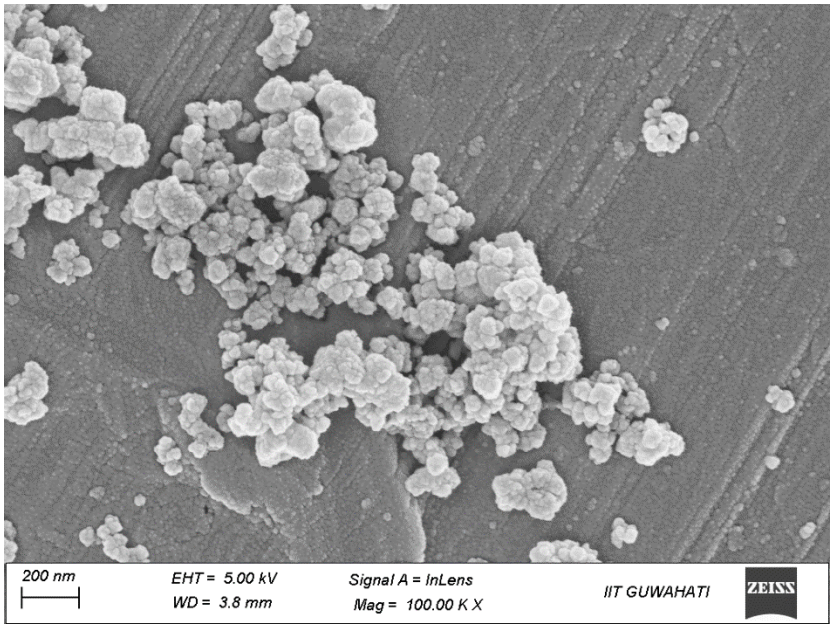

Figure S90. FE-SEM image of **1′** after ACF sensing.

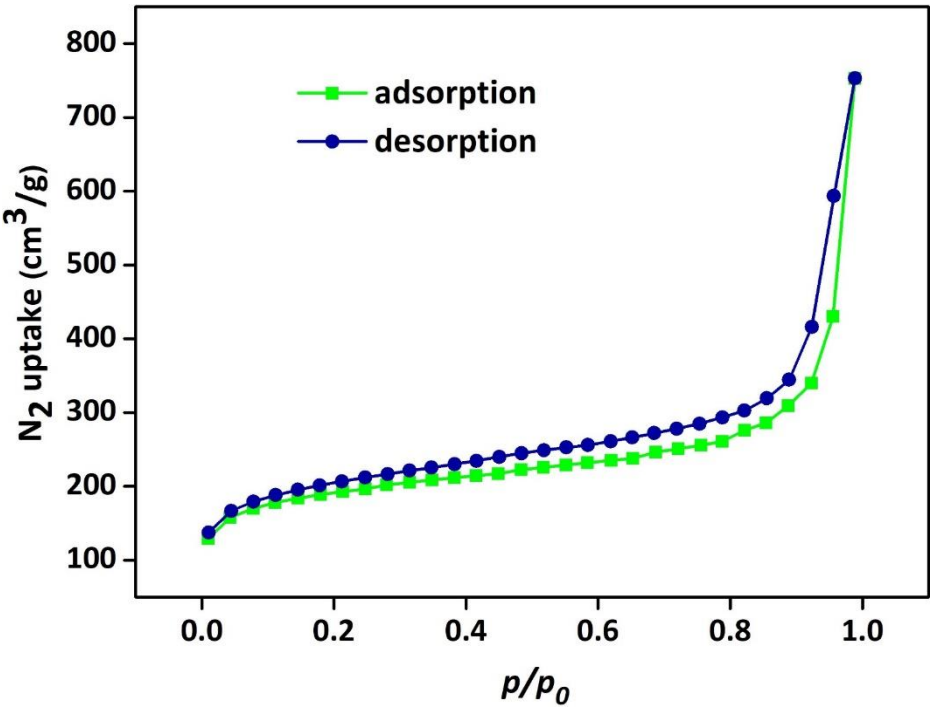

Figure S91. N_2 adsorption (green squares) and desorption (violet circles) isotherms of thermally activated reused **1′** after ACF sensing recorded at –196 °C.

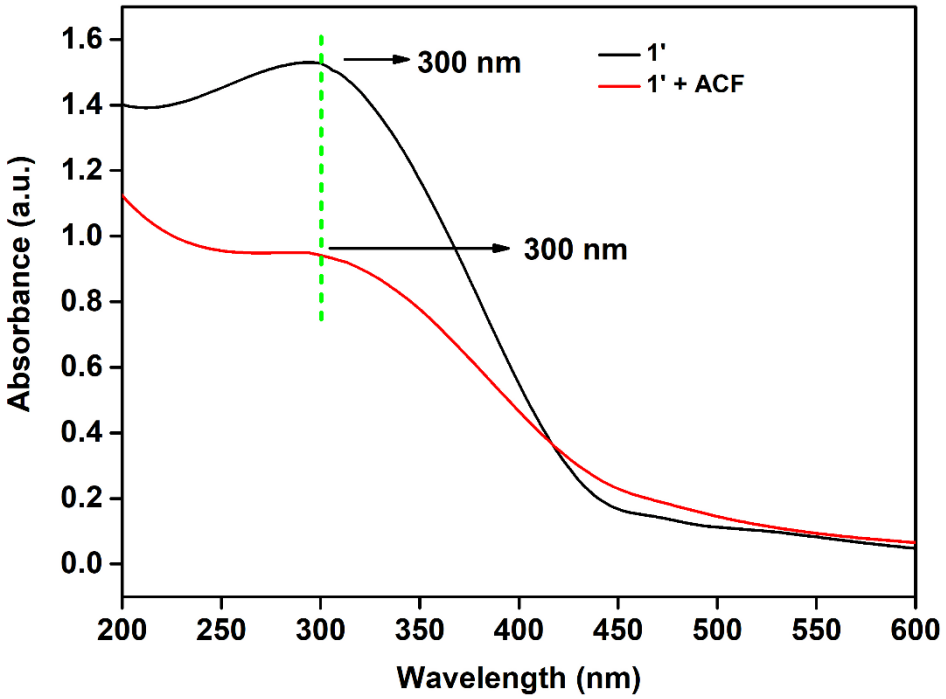

Figure S92. Solid-state UV-Vis spectra of **1′** before and after the treatment of ACF.

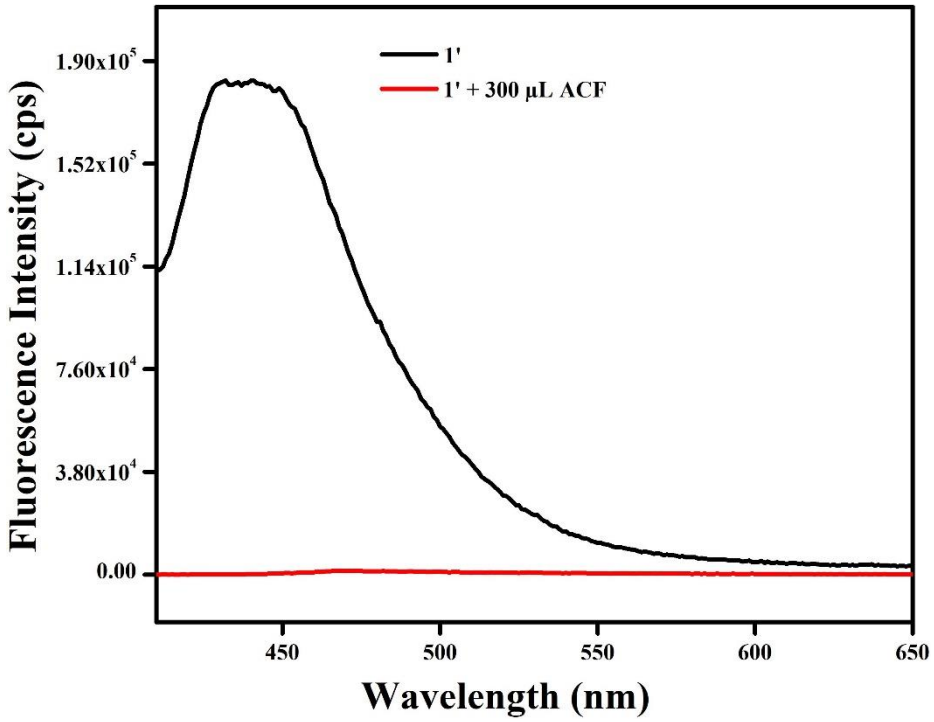

Figure S93. Change in fluorescence intensity of **1′** after addition of 300 µL mM solution of ACF (λ_{ex} = 390 nm).

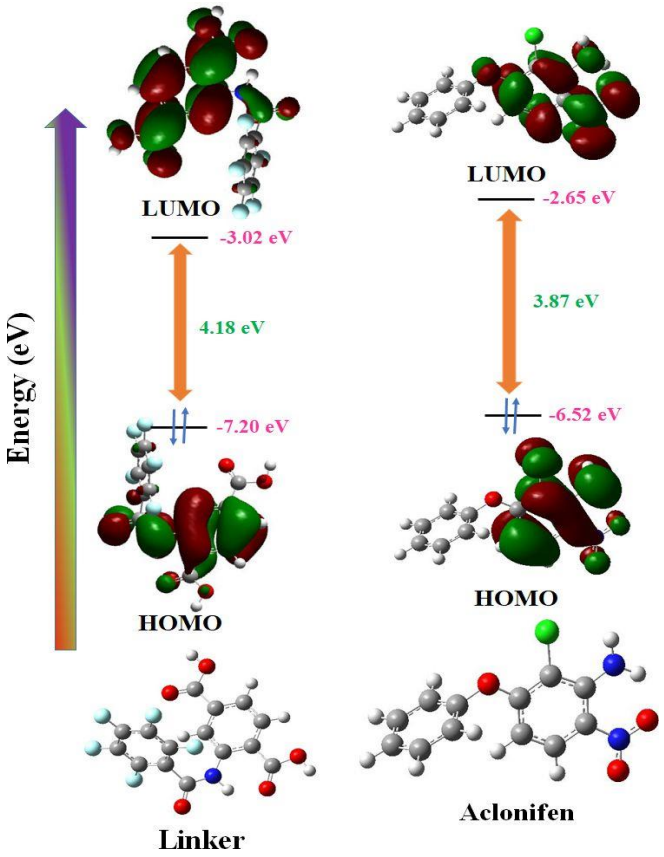

Figure S94. HOMO and LUMO energy levels of free linker and ACF.

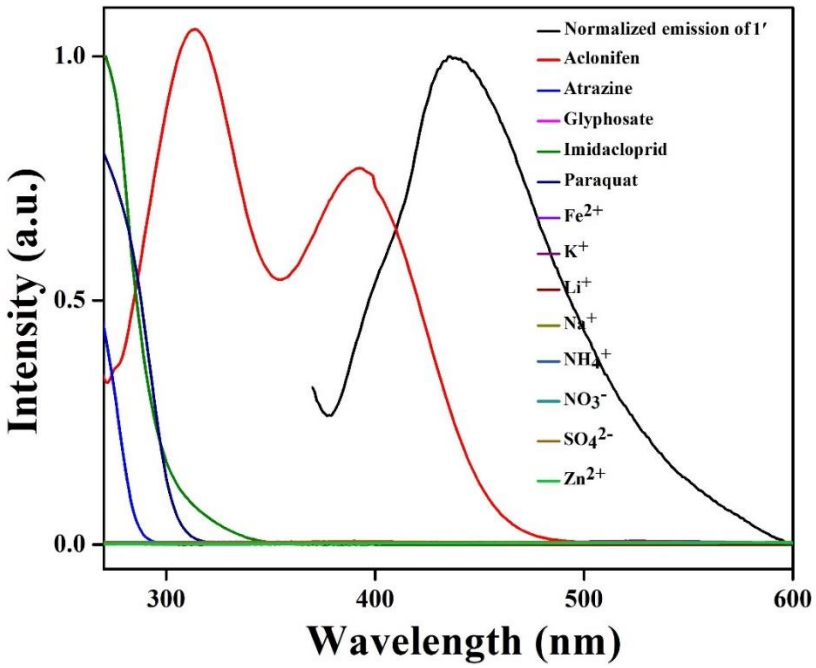

Figure S95. UV-Vis absorption spectra of all analytes and emission spectrum of **1′** MOF.

Table S4. Statistical details of different analytical parameters for the sensing of ACF by **1′**.

Concentration Range (nM)	Slopes	Intercepts	Correlation Coefficient (R^2)	$S_{y/x}$ [a]	LOD[b] (nM)	LOQ[c] (nM)	Regression Equation
0-44.8	17080.9	429195.6	0.998	5590.6	0.982	3.27	17080.9x + 429195.6
	14886.2	424935.9	0.995	6621.0	1.33	4.44	14886.2x + 424935.9
	15647.6	427488.4	0.997	5457.5	1.04	3.48	15647.6x + 427488.4
Average	15871.6	427206.7	0.996	5889.7	1.12	3.74	15871.6x+ 427206.7
SD	1114.4	2143.7	0.002	636.8	0.18	0.63	(15871.6 ± 1114.4)x + (427206.7 ± 2143.7)

[a] Standard deviation of the residuals, [b] Limit of detection, [c] Limit of quantification

Table S5. Comparison between the spiked and observed concentrations and recovery of ACF in different real water specimens.

Type of Water	Spiked Conc. of ACF (μM)	Observed Conc. of ACF (μM)	Recovery (%)
Milli-Q Water	(i) 1111.1 (ii) 555.5 (iii) 277.7	(i) 1105.0 (ii) 552.4 (iii) 274.6	(i) 99.4 (ii) 99.4 (iii) 98.8
Lake Water	(i) 1111.1 (ii) 555.5 (iii) 277.7	(i) 1100.9 (ii) 542.5 (iii) 266.6	(i) 99.1 (ii) 97.6 (iii) 96.0
Tap Water	(i) 1111.1 (ii) 555.5 (iii) 277.7	(i) 1104.2 (ii) 540.9 (iii) 265.2	(i) 99.7 (ii) 97.3 (iii) 95.5
River Water	(i) 1111.1 (ii) 555.5 (iii) 277.7	(i) 1107.1 (ii) 548.2 (iii) 266.9	(i) 99.3 (ii) 98.7 (iii) 96.1

Table S6. Evaluation of intra-day, inter-day accuracy and precision study of change in fluorescence intensity of **1′** after incremental addition of ACF.

Parameter	Amount of ACF Added (μL)	Fluorescence Intensity (cps) at λ_{max} = 450 nm SD			Average PL Intensity (cps)	SD	RE%
Repeatability Intra-day precision	0	264634.7	261905.2	260551.2	262363.7	2079.9	0.008
	100	50436.0	51653.3	51973.3	51354.2	811.1	0.017
	200	12027.0	12472.3	13073.3	12524.2	525.1	0.039
	300	3955.4	4274.2	4167.8	4132.5	162.3	0.043
Reproducibility Inter-day precision	0	3955.4	259007.4	256264.9	259969	4266.9	0.017
	100	50436.0	53058.9	53885.3	52460.1	1800.9	0.038
	200	12027.0	13629.4	14080.8	13245.7	1079.3	0.092
	300	3955.4	4778.6	4858.7	4530.9	500.0	0.127

Table S7. ICP-MS analysis of the extracts obtained after catalysis and sensing experiments.

Sl. No.	Filtrate*	Concentration of Zr(IV) ion (ppm)
1	Filtrate obtained after catalytic CO_2 cycloaddition reaction	0.001
2	Filtrate obtained after aerobic oxidation reaction	0.002
3	Filtrate obtained after sensing of ACF	0.094

* After the utilization of **1′** for specific application, it was separated by filtration with 0.22 μM membrane filter paper and the filtrate was directly utilized for the ICP-MS analysis to examine the leaching of the Zr(IV) ion.

Table S8. Comparison of the detection performance of present probe (**1′**) with some previously reported probes of ACF.

Sl. No.	Sensor Material	Analytical Method	Response Time (s)	LOD	Ref.
1	$[Zr_6O_4(OH)_4(C_{15}H_4F_5NO_5)_6]$ (**1′**)	fluorometric	5 s	1.1 ± 0.2 nM	this work
2	g-C3N4/GCE	voltammetric	-	1.28 nM	1
3	PNIPAM/PANI-Cu	electrochemical	-	0.009 μM	2
4	TCP CPE	electrochemical	-	2 μM	3
5	Hg(Ag)FE	electrochemical	-	0.031 μM	4
6	GCE	electrochemical	-	2.27 μM	5

Table S9. Comparison of the catalytic performance of activated **1′** with some previously reported MOF catalysts for CO_2 cycloaddition reaction.

Sl. No.	MOF	Reaction Condition	Yield	Ref.
1	**$[Zr_6O_4(OH)_4(C_{15}H_4F_5NO_5)_6]$ (1′)**	**80 °C, 1 bar, 24 h**	**>99%**	**this work**
2	Zn/Mg-MOF-74	60 °C, 8 bar, 5 h	99%	6
3	$(CH_3)_2NH_2{\cdot}[Co_3(L)_2$ (μ_2-OH)-(bpy)1.5($H_2O)_3$]·1.5DMF·1.5H_2O	60 °C, 5 bar, 8 h	98%	7
4	$[Cd_{1.5(}$TCA)$(bpg)_{0.5}$(H_2O)]·3DMA·2H_2O	65 °C, 10 bar, 6 h	>99%	8
5	66Pym-MeI	100 °C, 5 bar, 24 h	>99%	9
6	JLU-Liu21	60 °C, 20 bar, 6 h	99%	10
7	Zn(Bmic)(AT)	60 °C, 10 bar, 24 h	85%	11
8	SNNU-5-Al	80 °C, 8 bar, 5 h	72.8%	12
9	Cu-NTTA	100 °C, 10 bar, 8 h	95.9%	13
10	Zn-DAT	RT, 8 bar, 24 h	>99%	14
11	Cu(tactmb)	RT, 1 bar, 48 h	47.5%	15
12	UMCM-1NH_2	RT, 12 bar, 24 h	90%	16
13	MOF-Zn-1	RT, 10 bar, 24 h	98%	17
14	CSMCRI-15	50 °C, 5 bar, 6 h	>99%	18
15	Zn–TDA	100 °C, 10 bar, 1.5 h	>99%	19
16	$[Cu_{1.5}$(L)- (bpy)]·DMF·$_{1.5}H_2O$	70 °C, 8 bar, 6 h	>99%	20
17	MOF-5-(NH_2OH)	50 °C, 12 bar, 6 h	99%	21
18	$Zn_3(L)_3(H_2L)$	80 °C, 10 bar, 5 h	99%	22
19	DUT-52(Zr)	80 °C, 12 bar, 6 h	88%	23
20	PNU-21	80 °C, 4 bar, 8 h	91%	24

Table S10. Comparison of the activity of **1′** with other hydrophobic MOFs for the oxidation reactions.

Catalyst	Substrate	Oxidant	Temp. (^oC)	Con. (%)	Sel. (%)	Ref.
PCN-222(Fe)-F7	cyclohexane	TBHP	80	50	90	25
PCN-224(Mn)-L	cyclohexane	TBHP	80	51	90	26
DUT-52-L	cyclohexane	TBHP/O_2	60	21	84	27
$[Zr_6O_4(OH)_4(C_{15}H_4F_5NO_5)_6]$ (1′)	**cyclooctane**	**TBHP/O_2**	**60**	**28**	**85**	**present work**

References:

1. N. P. Shetti, S. J. Malode, P. R. Vernekar, D. S. Nayak, N. S. Shetty, K. R. Reddy, S. S. Shukla and T. M. Aminabhavi, *Microchem. J.*, 2019, **149**, 103976.
2. B. Mutharani, P. Ranganathan and S.-M. Chen, *Sens. Actuators B: Chem.*, 2020, **304**, 127232.
3. V. Novotný and J. Barek, *Ecol. Chem. Eng. S*, 2015, **22**, 451-458.
4. D. Guziejewski, S. Smarzewska, M. Skowron, W. Ciesielski, A. Nosal-Wiercińska and S. Skrzypek, *Acta Chim. Slov.*, 2016, **63**.
5. A. Zaouak, F. Matoussi and M. Dachraoui, *Int. j. electrochem.*, 2011, **2011**.
6. Z. Gao, L. Liang, X. Zhang, P. Xu and J. Sun, *ACS Appl. Mater. Interfaces*, 2021, **13**, 61334-61345.
7. N. Seal, K. Karthick, M. Singh, S. Kundu and S. Neogi, *Chem. Eng. J.*, 2022, **429**, 132301.
8. N. Seal, M. Singh, S. Das, R. Goswami, B. Pathak and S. Neogi, *Mater. Chem. Front.*, 2021, **5**, 979-994.
9. H. Ji, K. Naveen, W. Lee, T. S. Kim, D. Kim and D.-H. Cho, *ACS Appl. Mater. Interfaces*, 2020, **12**, 24868-24876.
10. J. Gu, X. Sun, X. Liu, Y. Yuan, H. Shan and Y. Liu, *Inorg. Chem. Front.*, 2020, **7**, 4517-4526.
11. Y. Li, X. Zhang, J. Lan, P. Xu and J. Sun, *Inorg. Chem.*, 2019, **58**, 13917-13926.
12. J.-W. Zhang, W.-J. Ji, M.-C. Hu, S.-N. Li, Y.-C. Jiang, X.-M. Zhang, P. Qu and Q.-G. Zhai, *Inorg. Chem. Front.*, 2019, **6**, 813-819.
13. X. Guo, Z. Zhou, C. Chen, J. Bai, C. He and C. Duan, *ACS Appl. Mater. Interfaces*, 2016, **8**, 31746-31756.
14. R. Das, S. S. Dhankhar and C. Nagaraja, *Inorg. Chem. Front.*, 2020, **7**, 72-81.
15. W. Y. Gao, Y. Chen, Y. Niu, K. Williams, L. Cash, P. J. Perez, L. Wojtas, J. Cai, Y. S. Chen and S. Ma, *Angew. Chem., Int. Ed.*, 2014, **53**, 2615-2619.
16. R. Babu, A. C. Kathalikkattil, R. Roshan, J. Tharun, D.-W. Kim and D.-W. Park, *Green Chem.*, 2016, **18**, 232-242.
17. J. Lan, M. Liu, X. Lu, X. Zhang and J. Sun, *ACS Sustain. Chem. Eng.*, 2018, **6**, 8727-8735.
18. N. Seal, A. S. Palakkal, R. S. Pillai and S. Neogi, *Inorg. Chem.*, 2023, **62**, 11528-11540.
19. Y. Li, X. Tian, W. Jiang, P. Wu, H.-S. Li, M. Wang, C. Lin and J. Wang, *Chem. Commun.*, 2021, **57**, 10803-10806.
20. N. Seal and S. Neogi, *ACS Appl. Mater. Interfaces*, 2021, **13**, 55123-55135.
21. J. F. Kurisingal, Y. Rachuri, Y. Gu, Y. Choe and D.-W. Park, *Chem. Eng. J.*, 2020, **386**, 121700.
22. Z. Gao, X. Zhang, P. Xu and J. Sun, *Inorg. Chem. Front.*, 2020, **7**, 1995-2005.
23. J. F. Kurisingal, Y. Rachuri, A. S. Palakkal, R. S. Pillai, Y. Gu, Y. Choe and D.-W. Park, *ACS Appl. Mater. Interfaces*, 2019, **11**, 41458-41471.
24. Y. Rachuri, J. F. Kurisingal, R. K. Chitumalla, S. Vuppala, Y. Gu, J. Jang, Y. Choe, E. Suresh and D.-W. Park, *Inorg. Chem.*, 2019, **58**, 11389-11403.

25. Q. Y. L. Li, S. Chen, X. Hou, B. Liu, J. Lu and H.-L. Jiang, *Chem. Commun.*, 2017, **53**, 10026-10029.
26. J. Ji, F. Liu, W. Yang, M. Tan, W. Luo and S. F. Yin, *ChemCatChem*, 2020, **12**, 4331-4338.
27. C. Gogoi, N. Nagarjun, S. Roy, S. Mostakim, D. Volkmer, A. Dhakshinamoorthy and S. Biswas, *Inorg. Chem.*, 2021, **60**, 4539-4550.